SCUOLA DI DOTTORATO
UNIVERSITÀ DEGLI STUDI DI MILANO-BICOCCA

School of Medicine and Surgery

PhD program in

Translational and Molecular Medicine – DIMET

XXXI Cycle

Nanoparticles for Therapy and Diagnosis of Neurodegenerative Diseases

Alysia COX

Matricola: 810670

Tutor: Prof. Massimo MASSERINI

Co-Tutor: Dr. Francesca RE

Co-ordinator: Prof. Andrea BIONDI

Academic Year: 2017/2018

You can never be overdressed or overeducated

-Oscar Wilde

Table of Contents

CHAPTER 1

General Introduction

1.1 BLOOD-BRAIN BARRIER

1.1.1 Overview

In 1885, Paul Ehrlich observed that upon intravenous (i.v.) administration of trypan blue, the brain and spinal cord were the only organs that were not stained. The term “blood-brain barrier” (BBB) was coined by Lewandowsky 15 years later upon his dicovery that certain neurotoxic agents affected central nervous system (CNS) function upon direct brain administration, but not after i.v. administration. Seventy years later, Thomas Reese attributed this barrier to brain capillary endothelial cells and their associated components [1].

The BBB is a highly selective semi-permeable blockade that separates the peripheral circulation from the CNS. It is the major limiting factor to pharmacological agents targeting the brain in neurological, neurodegenerative, and psychiatric disorders, preventing all large molecules and 98% of small molecules from passing to the CNS from the blood [2]. The BBB consists of a dense network of endothelial cells (EC), astrocytes, and pericytes, along with protein complexes that strongly restrict the crossing of molecules (Fig. 1). The BBB is essential for the maintenance of CNS homeostasis, ensuring healthy neuronal function. The tight regulation of the CNS circulation protects the brain from toxins, pathogens, and inflammatory agents, while still allowing the passage of essential nutrients and some chemicals [3].

The neurovascular unit (NVU) consists of neurons, astrocytes, BBB ECs, pericytes, myocytes, and elements of the extracellular matrix. This group of cells work together to monitor and maintain neuronal homeostasis and appropriate cerebral blood flow through

vasodilation or vasoconstriction of capillaries. Physical and/or chemical actions induced by the NVU include production of nitric oxide by ECs and contraction/relaxation of myocytes to control blood flow. Neurons communicate changes in oxygen or nutrient concentration to interneurons and/or astrocytes, thereby triggering appropriate changes to restore balance to the CNS [4].

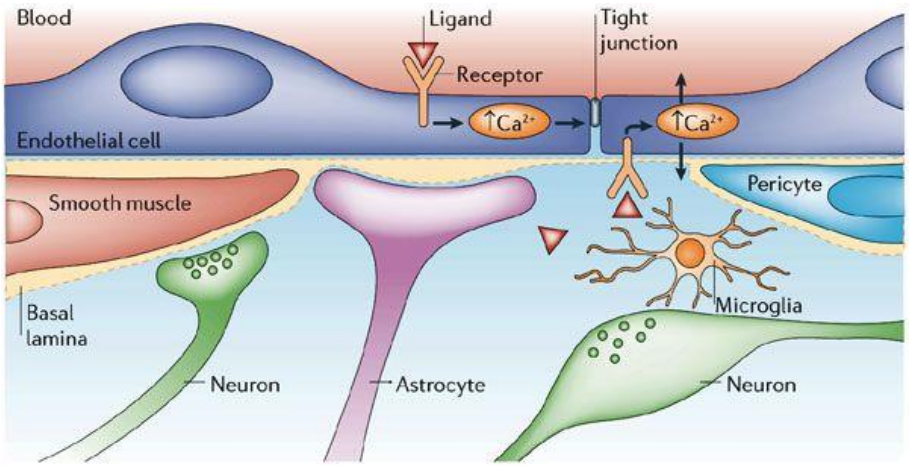

Figure 1. Representation of the cellular components of the blood-brain barrier [5].

The restrictive properties of the BBB are established mainly by ECs and strengthened or maintained by the other cells in the NVU. ECs are mesodermally-derived modified simple squamous epithelial cells that make up the blood vessel walls. ECs in the CNS differ from peripheral ECs in several ways. The polarized cells are connected by tight junctions (TJs), which limit paracellular diffusion of hydrophilic compounds and are up to 100 times tighter than those in the periphery. Brain ECs lack fenestration and contain approximately five times more mitochondria than other ECs, possibly due to the necessity for ATP to

drive ion gradients for transport. Transcytosis is highly limited in brain ECs, restricting transcellular passage. Specific transporters are expressed by ECs. Efflux transporters are polarized to the luminal surface and can transport many lipophilic molecules to the blood. Highly specific nutrient transporters move nutrients into the CNS and remove waste products from the brain into the blood. CNS ECs also have an extremely low level of leukocyte adhesion molecules (LAMs) in order to limit immune cell entry to the CNS [6].

ECs express various components that are vital to the structure of the BBB, and transport across it (Fig. 2). CNS ECs are connected by TJs, which are cellular adhesions formed on the apical side of the lateral membrane. TJs strongly prevent paracellular passage of ions and molecules. This is highly dependent on molecule size, with uncharged molecules less than 4 nm in diameter having higher paracellular permeability than larger molecules. TJs consist of transmembrane occludins, claudins, and junctional adhesion molecules (JAMs) [7]. *In vitro* data indicates that claudins are essential for TJ formation. Claudin-5 is highly expressed in CNS ECs and knockout mice display size-selective leakage through the BBB [8]. Conversely, mice lacking occludin have a fully functioning BBB, though it is believed that its enrichment in CNS ECs is important for the resistance of the BBB [9]. JAMs are part of the immunoglobin superfamily and are involved in regulating leukocyte extravasation and paracellular permeability.

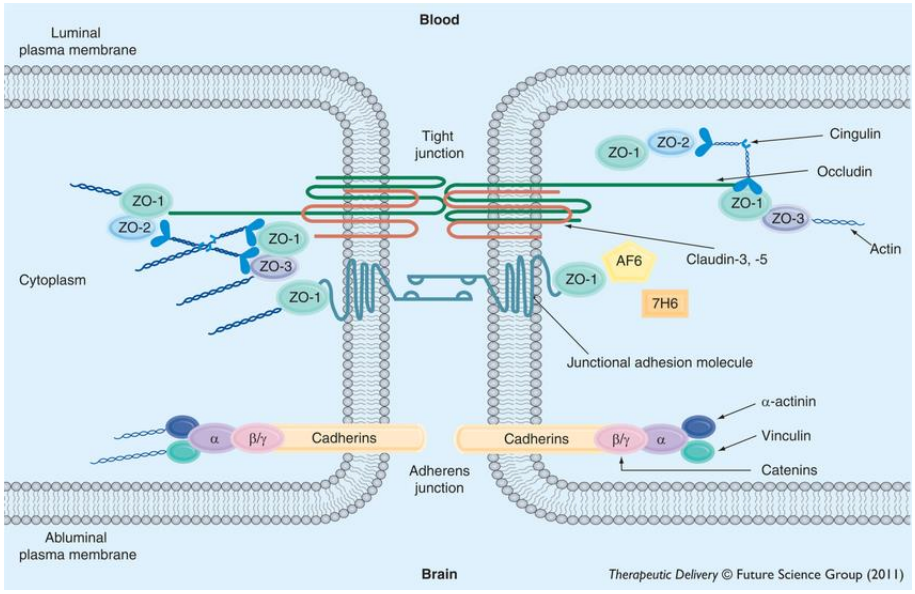

Figure 2. Basic molecular organization of tight-junction protein complexes at the blood-brain barrier [10].

The above transmembrane adhesion complexes are linked to the EC cytoskeleton by cytoplasmic adaptors, for example zonula occludens (ZO)-1, ZO-2, cingulin, jacop, MAGIs, and MPPs. Vascular endothelial (VE)-cadherin and platelet EC adhesion molecules (PECAM)-1 are the adherens junctions (AJs) that connect ECs and are linked to the cytoskeleton by catenins [6].

Pericytes extend long cellular processes across the ablumenal surface of the microvascular ECs and are embedded in the vascular basement membrane (BM). The BM prevents most of the cell body and processes from coming into direct contact with the endothelium. Instead, the cellular processes adhere to ECs at discrete points, mediated by N-cadherin. Pericytes cover approximately 20-30 % of the endothelium, and the CNS microvasculature has the highest

EC:pericyte ratio in the body, estimated to be between 1:1 and 3:1. They contain contractile proteins, which can control capillary diameter. Pericytes regulate blood flow, angiogenesis, endothelium proliferation, extracellular matrix deposition, immune cell infiltration, and wound healing in response to neural activity. They are also involved in BBB development and maintenance, including the polarization of astrocytic endfeet. Without pericytes, abnormal vasculogenesis, endothelial hyperplasia, and increased endothelial permeability is observed [11].

The neurovascular tube is surrounded by the inner vascular BM, secreted by ECs and pericytes, and the outer parenchymal BM, secreted by astrocytic processes. They contain type IV collagens, laminin, nidogen, heparin sulfate proteoglycans, and other glycoproteins, though have differing compositions. These extracellular matrices act as a base for many vascular signalling processes and as a barrier to molecules entering the brain. BM disruption, commonly by matrix metalloproteinases (MMPs), leads to BBB dysfunction and subsequent leukocyte infiltration [12].

Astrocytes are glial cells that have polarized cellular processes covering the neuronal processes or blood vessels. The endfeet of the basal processes cover almost the entire vascular tube and contain a variety of proteins such as dystrophin, dystroclycan, and aquaporin 4 [13]. Aquaporins are pore-forming molecules in the astrocytic endfeet that allow passage of water into the CNS. Reduction of aquaporin 4 can cause or exacerbate cytotoxic brain edema. It is believed that aquaporin 4 is passive, allowing water to cross along pressure gradients in order to eliminate extracellular fluid and prevent vasogenic edema [14]. The dystroglycan-dystrophin complex binds agrin, linking the endfeet

cytoskeleton to the BM, which is critical to maintain CNS water homeostasis. Astrocytes provide a cellular link between neurons and blood vessels, enabling them to regulate blood flow according to neuronal activity. They are important mediators of BBB formation and can induce barrier properties in non-CNS blood vessels. They are a source of regulatory factors such as TGF-β, GDNF, and IL-6. However, *in vivo* analysis has shown that they do not play a role in the initial BBB formation, but rather modulate and maintain the mature barrier by secreting regulatory factors [15].

1.1.2 Physiological pathways and strategies to cross the BBB

Though the major function of the BBB is to restrict passage of molecules from the blood to the brain, the entry of certain molecules is essential for the health and correct function of the CNS. A variety of mechanisms exists to facilitate this (Fig. 3).

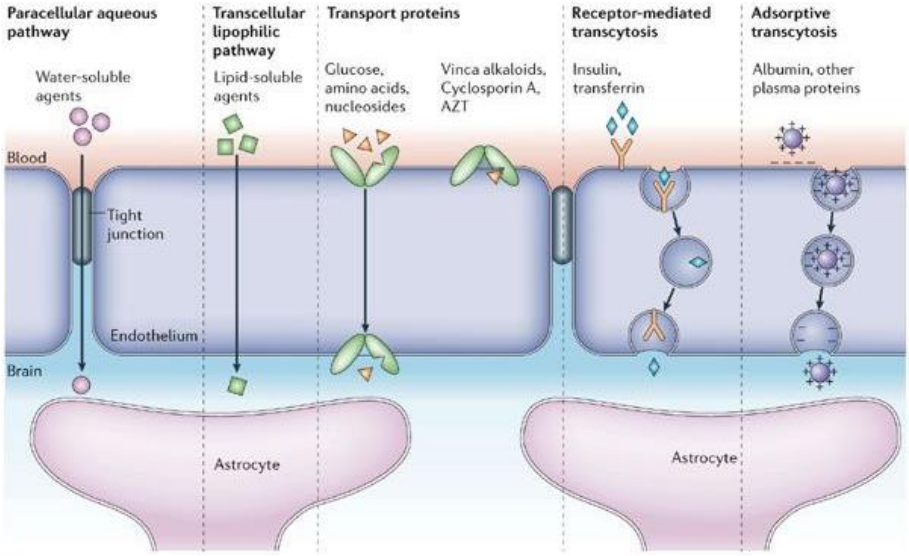

Figure 3. Pathways across the blood-brain barrier [5].

Paracellular passage is possible upon opening of the TJs, though passage is normally highly restricted to water soluble agents and limits the passage of molecules more than 4 nm in diameter [16]. TJ modulators can affect the extent of paracellular passage. Sodium caprate (C10), a clinically approved absorption enhancer for ampicillin, can reduce claudin-5 levels resulting in the transient opening of TJs [17]. RNA interference has been used to reduce TJ proteins, including organic ion transporter 3 (OAT3) and claudin-5, specifically at the BBB level in order to assist brain drug delivery [18]. A peptide targeting the

first extracellular loop of occludin at the BBB could selectively increase paracellular permeability to mannitol [19].

Molecules can pass from the blood through ECs to the brain *via* three main mechanisms: lipid-mediated free diffusion, carrier- or receptor-mediated transcytosis, or adsorptive-mediated transcytosis. As previously mentioned, the rate of transcytosis is much lower in CNS ECs compared to peripheral ECs, and is often upregulated during disease or injury, causing major BBB dysfunction [20].

The transcellular lipophilic pathway can transport some lipid-soluble, hydrophobic molecules such as O_2 and CO_2. These molecules freely diffuse across the plasma membrane following their concentration gradient. If a compound has a molecular weight less than 450 and is highly lipophilic, it has a high chance of entering the brain using this pathway. Substances with lower molecular weights will cross the BBB faster. Furthermore, if the sum of the nitrogen and oxygen atoms in the molecule is five or less, the molecule is likely to cross the BBB [21].

Brain ECs employ clathrin-coated vesicles containing adaptor protein complex-2, large fluid-engulfing macropinocytotic vesicles, and plasma membrane-derived caveolae formed from lipid raft domains, but have fewer pinocytotic vesicles than peripheral ECs [22]. In receptor-mediated transcytosis, clathrin-coated vesicles and caveolae endocytose plasma membrane receptors and their specific ligands, deliver them to the brain *via* exocytosis, and receptors are recycled back to the plasma membrane [22]. Targeting ligands to increase passage using receptors that are exclusively or over-expressed at the BBB are frequently exploited.

Nutrient transporters move specific nutrients necessary for brain health down a concentration gradient. Certain transporters are highly enriched in CNS ECs compared to peripheral ECs, for example glut1 (glucose transporter), transferrin receptor (transferrin/iron transporter), Ager (amyloid transporter) and low-density receptor-related lipoprotein (LRP)-1 and LRP-8. These transporters are often targeted as "Trojan horses". This involves targeting these transporters with a drug or drug delivery system, essentially "tricking" ECs into allowing the passage of otherwise non-permeant drugs into the CNS [23].

Specific transporter molecules and receptors are expressed on the BBB to control molecule entry to the CNS. Efflux transporters, including Mdr1, MRPs, and BCRP, move molecules against a concentration gradient using ATP hydrolysis. These transporters can bind to a wide array of substrates, but often limit the entry of small lipophilic molecules that could normally passively diffuse through the EC membrane [24]. Multidrug resistance transporter (Mdr1), also known as P-glycoprotein (Pgp), is particularly vital, as shown when knockout mouse display increased amounts of small lipophilic drugs and endogenous molecules entering the brain. This ATP-binding cassette carrier moves toxic substances from the brain to the blood, but also removes potential therapeutics. Pgp upregulation is associated with drug-resistant epilepsy, cerebral ischemia, and tumours. The development of therapeutics that can avoid efflux, or of efflux transporter inhibitors, may be useful when delivering small molecule compounds to the CNS [25].

Adsorptive-mediated transcytosis occurs when cationic molecules bind to and are taken up at the luminal surface of anionic

ECs. This process is often targeted by cationic proteins (for example, albumin) or cell-penetrating peptides (CPPs). Examples of CPPs are modified Tat-1 peptides derived from HIV, gH625 derived from Herpes simplex virus type 1, and Syn-B vectors, which can be used to deliver small molecules or proteins to the CNS [26].

Along with its function as a paracellular and transcellular barrier, the BBB can produce drug-metabolizing enzymes, such as acetylcholinesterase, alkaline phosphatase, and monoamine oxidase, which degrade many compounds that enter the CNS. This vital protective mechanism is another obstacle to be overcome when attempting to deliver pharmaceuticals to the brain [27].

Extensive research focuses on efficient ways to increase the delivery of specific therapeutic and/or diagnostic molecules to the brain. Non-invasive strategies include chemically manipulating the drug or its carrier (for example, by making it more lipophilic) so that it can cross the BBB more readily, or using alternative administration routes, such as intranasal. However intranasal administration results in very low drug delivery, in part due to extensive clearance by the mucus layer and cilia [28]. The use of nanoparticles is a promising strategy and is discussed in more detail in Chapter 1, section 1.3.6.

Invasive techniques may be more effective in delivering large quantities of drugs of varying size, charge, and chemical composition to the CNS. These techniques are associated with a much higher risk of neurotoxicity. Intracerebral implants incorporating a biodegradable polymeric matrix have been used in clinical trials. Though this allows for localized drug delivery, it is a very traumatic strategy [29]. Intracerebroventricular, intrathecal and interstitial delivery has been

successfully used to deliver anti-cancer drugs [30, 31], but come with higher rates of CNS infection.

BBB disruption strategies are perhaps the most controversial. These include convection-enhanced delivery, whereby one or more catheters are inserted in the brain through cranial burr holes, and drugs are administered by micro-infusion pump [32]. Advantages of this include the ability to load large volumes of drug at consistent concentrations, but the long infusion times and invasive procedure can once again result in infection, local toxicity, and high intracranial pressure [33].

The osmotic strategy involves the intra-arterial infusion of a hyperosmotic agent, for example mannitol, to transiently interrupt the BBB. Mannitol specifically increases BBB permeability *via* shrinkage of cerebrovascular ECs and subsequent disruption of adjoining TJs for several hours [34]. However, an unfavourable toxic/therapeutic ratio means that extra care is required with this procedure to avoid neurotoxicity.

Some vasoactive compounds, such as histamine, may selectively increase the permeability of abnormal brain capillaries, but not healthy brain capillaries, therefore making this a more specific, reliable, and possibly less neurotoxic technique [35]. Non-specific opening of the BBB could lead to the infiltration of harmful substances or destructive immune cells to the CNS, causing extensive damage to the brain.

Ultrasound-mediated BBB disruption has received much attention in recent years (Fig. 4). This involves the application of pressure waves (> 20 kHz) to focal sites of brain tissue through the skull

using large surface area phased arrays. Image guided systems, for example using magnetic resonance imaging (MRI), can ensure the opening of the BBB in very specific locations, limiting entry of harmful substances to the CNS. Ultrasound can also be combined with preformed ultrasonic microbubbles to decrease the amount of acoustic energy required, thereby decreasing the risk of overheating the skull and damaging ECs [29]. However, there are serious neurotoxicity concerns about repetitive or prolonged BBB opening. It is also important to note that most of these methods are evaluated in rodents, and may not be as effective in humans [36].

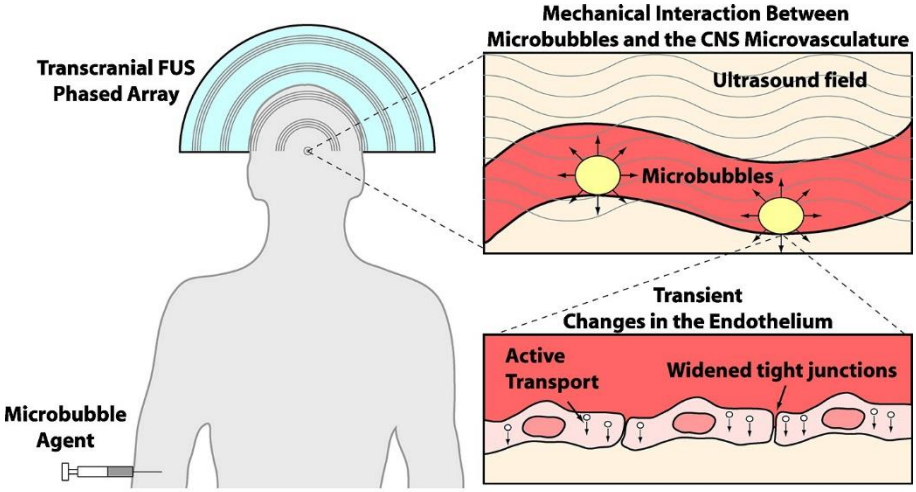

Figure 4. BBB disruption *via* focused ultrasound and microbubbles: noninvasive, transient, targeted drug delivery [36].

1.1.4 *In vitro* system to reproduce the BBB

Historically, most promising drugs that are developed for the treatment of CNS disorders fail due to their inability to penetrate the BBB. Therefore, pharmacological testing must evaluate the the permeability of drugs through the BBB using appropriate *in vitro* models. Although *in vivo* experiments are the most accurate way to measure drug delivery to the brain, these experiments are restricted by ethical and financial considerations, and access to specialized facilities and equipment. Testing using *in vivo* models should involve animals with specific pathologies, as the BBB state is affected by disease and can differ greatly from the healthy condition, as discussed in further detail in Chapter 1, section 1.2.2. However, transgenic or diseased animal models can be more expensive and time-consuming to produce, and the disease progression or presentation often does not exactly match the human disease. Therefore, these studies can be unsuitable for medium or high throughput screening. *In vitro* models offer reduced costs, strong reproducibility, and the simplicity and versatility of working conditions required in the earliest stages of drug development [37].

The most widely used *in vitro* models of the BBB have been developed using non-human mammalian brain capillary endothelial cell lines, for example mouse bEnd3 or porcine PBMEC/C1-2 cells. These models are not ideal because TJ proteins, fenestration patterns, BBB transporters, enzymes and specific receptors on ECs often vary between species. These factors could influence BBB permeability, and may limit the translational potential of models based on non-human cells. Therefore, models using human cerebral endothelial cell lines could give a more accurate representation of the *in vivo* BBB. The

hCMEC/D3 immortalized human cerebral microvascular endothelial cell line is one of the best characterized and most widely used. Polarized secretion and transport, architectural organization, and protein expression in the cells mimics the healthy human BBB. It is widely validated in over 150 studies of cerebral endothelial biology and pharmacology, easy to use, and suitable for drug screening [38].

The transwell model is the simplest *in vitro* tool for the study of the BBB [39]. Cerebral ECs are seeded on the collagenated porous filter of a transwell insert, which separates an apical compartment representing the blood and a basolateral one representing the brain (Fig. 5). A polarized monolayer forms, mimicking the BBB. The pores of the membrane allow exchange of solutes between the apical and basolateral compartments and, depending on the pore size, even cellular trafficking can be studied. The major advantage of this monoculture model is its simplicity and ease of use, allowing for relatively high throughput screenings at a moderate cost. However, the effects of other cellular components present in the neurovascular unit are not considered.

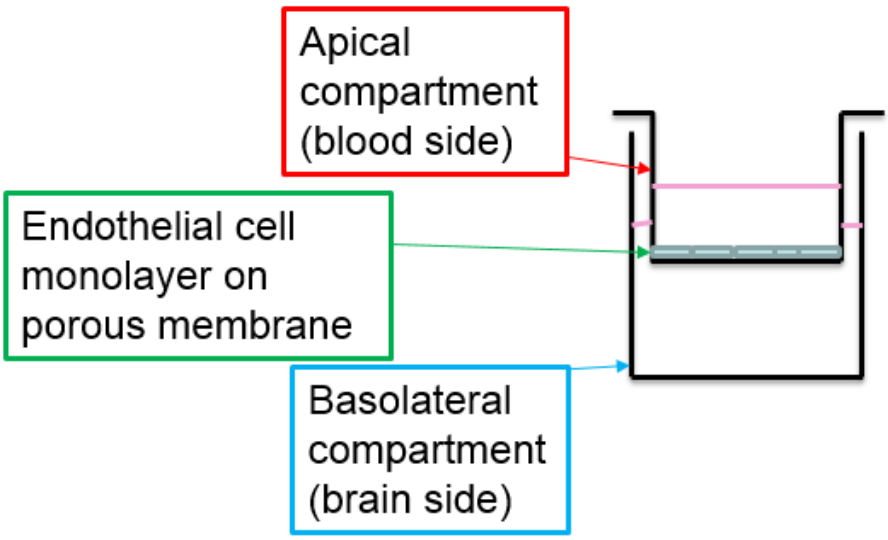

Figure 5. Transwell model of the BBB. The model consists of an apical compartment (representing the blood) separated from a basolateral compartment (representing the brain) by a monolayer of human brain microvascular endothelial cells seeded on a porous membrane.

As cell culture techniques have advanced in recent years, highly sophisticated cellular models that better reflect the *in vivo* anatomy of the neurovascular unit have been developed. Multicellular spheroid cell models have been developed to reflect the complexity of other cell types, particularly in the study of cancer [40]. Now, three-dimensional models of the midbrain and cerebral cortex offer new hope for the creation of a more complete model of the BBB [41, 42], though research is lacking. Cerebral ECs can be cultured in the presence of pericytes, astrocytes, and/or neurons in different arrangements. However, these complicated models can be relatively expensive and time-consuming to produce [43].

Dynamic BBB models have been created to reflect the fact that BBB endothelial properties are affected by shear stress induced by blood flow [44]. *In vivo* blood flow can be mimicked by culturing ECs in hollow fibers where circulating culture medium can induce tunable shear stress. Though this is more representative of the *in vivo* condition, the model is unsuitable for rapid, high throughput studies. Its development requires specific technical skills and a large number of cells to load the capillaries. Furthermore, the optical monitoring of cell morphology is impossible. Microfluidic models require less cells. The cells are cultured on a porous membrane located at the interface of two microchannels, which allows the flow of culture medium. High costs and the lack of standardization have restricted the widespread use of this model [45, 46].

A major limitation of most *in vitro* BBB models is that they represent the healthy state and not the pathological one. Considering the extensive changes that occur in the BBB in various disease states, as discussed in further detail in Chapter 1, section 1.2.2, it is reasonable to assume that permeability of drugs will be affected by neuropathology and/or aging. Just as diseased animal models must be used for *in vivo* testing, it is essential that *in vitro* models are developed that can reflect the BBB condition in different disease states. An aged cellular model has been established by isolating and culturing ECs and perivascular cells from aged animals, but is extremely difficult to produce as proliferation and the growth of appropriate intercellular contacts is limited in such aged cells [47]. Indeed, there are very few studies analyzing the differences in drug permeability depending on the disease state, and most publications use healthy cellular models for toxicity and

permeability studies.

Other limitations are based on the simplistic nature of *in vitro* BBB models. The BBB is an extremely complex network of interacting cells and proteins, and is affected by many factors in the peripheral circulation. As with any biological system, it is difficult to perfectly simulate the *in vivo* situation *in vitro*, in terms of complexity. For the BBB, the most important factor determining paracellular permeability is the expression of TJs by ECs. It is incredibly important to verify the correct formation of TJs *in vitro*, as this has been shown to affect NP uptake by cells [48]. Expression of TJs and AJs by hCMEC/D3 cells has been extensively demonstrated, making them a good candidate for permeability studies. Though other cells may be involved in the maintenance of TJs, it is the ECs that are essential for their expression and development [15].

In conjunction with experimental models of the BBB, computational models with appropriate software may offer a new way to predict the BBB permeability of novel compounds, potentially reducing the amount of time and money wasted on testing therapeutic agents that cannot be delivered to the brain [49].

1.2 NEURODEGENERATIVE DISEASES

1.2.1 Overview

Neurodegeneration is a hallmark of many diseases, including Alzhemier's disease (AD), Parkinson's disease (PD), Huntington's disease (HD), frontotemporal dementia (FTD), multiple sclerosis (MS), and amyotrophic lateral sclerosis (ALS), and is even a presenting feature in some HIV-1 positive patients [50] (Fig. 6). Though these diseases display diverse symtoms and progression, they are all defined by the progressive breakdown of neural tissue. Neuronal death is often accompanied by changes in other CNS cell types, for example an increase in glial cells that could contribute to the disease [51]. The major risk factor for several of these diseases is age. As the global elderly population increases steadily with advances in life-prolonging medicine, the prevalence of neurodegenerative diseases increases. Pathologies such as memory loss, cognitive impairment and motor skill dysfunction have a high financial burden, as patients often require constant and continuous care. In 2015, the World Health Organization estimated that the global societal cost of dementia, a disorder characterized by progressive decline of cognitive function including memory, emotion, behaviour, language, and learning, was US$818 billion, equivalent to 1.1 % of global gross domestic product. This socio-economic burden will continue to increase as aging populations rise. Dementia alone affects 50 million people worldwide, with 60-70% of cases being attributable to AD [52].

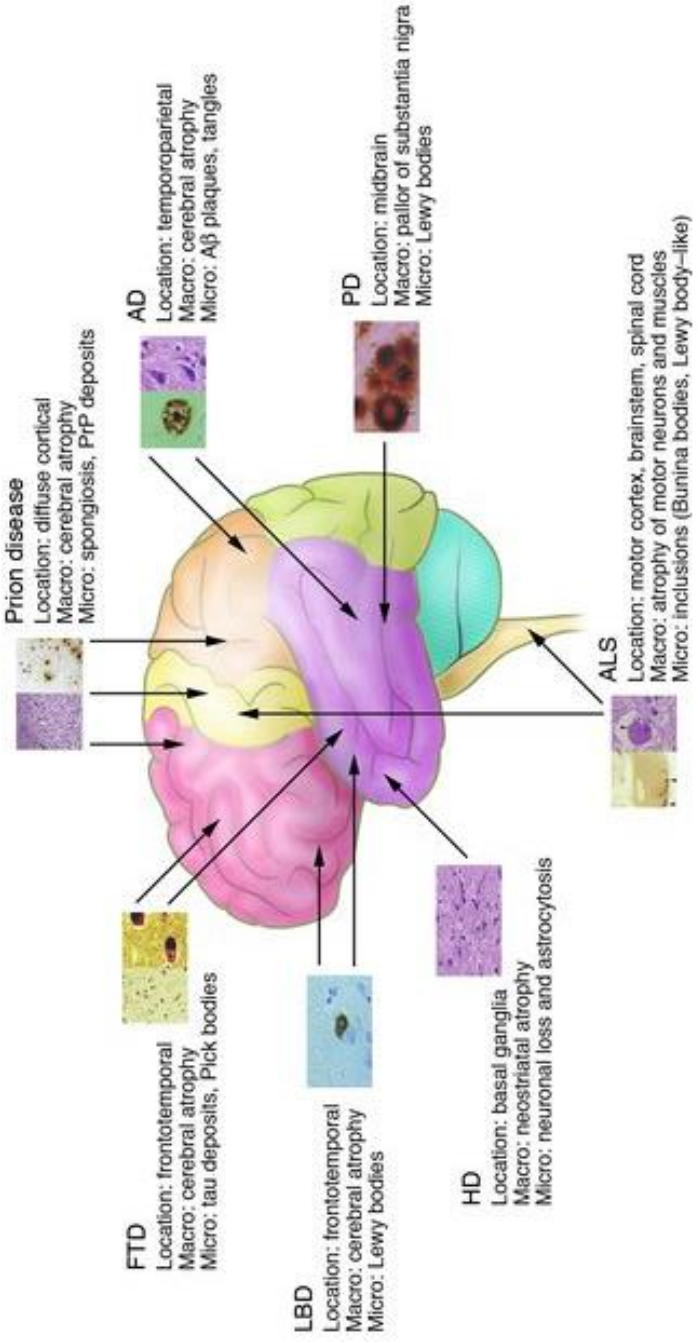

Figure 6. The anatomical location of and macroscopic and microscopic changes associated with common neurodegenerative disorders [53].

AD causes progressive and irreversible neurodegeneration with associated memory impairment and cognitive deficits. Short-term memory loss is the major symptom in the early stage of the disease. Progressive decline leads to long-term memory impairment, apathy, problems with language, executive functions, perception (agnosia), and execution of movements (apraxia), with a complete loss of autonomy. Death normally occurs within 10 years of symptomatic onset, often due to unassociated conditions such as septicemia from pneumonia [54]. The pathology includes deposition of β-amyloid (Aβ) aggregates and tau protein hyperphosphorylation, with only approximately 10% of cases linked to genetics. Apolipoprotein E4 (ApoE4) is the primary genetic risk factor for AD, causing mitochondrial dysfunction [55]. AD occurrence is widespread, and its prevalence in Europe is estimated at 5.05 %, with women having a higher risk of developing the disease [56]. With increasing lifespans, the prevalence of AD is expected to rise to 65.7 million cases by 2030 and 115.4 million by 2050 [57]. Although several curative therapeutic strategies targeting disparate aspects of AD have been proposed, only a limited number have gone through clinical trial, and all have failed to provide convincing therapeutic effects or gain clinical approval [58, 59]. Diagnosis is based on symptoms. Amyloid stains, for example thioflavin S and Congo red, and immunohistochemistry can be used to detect aggregated Aβ post-mortem for definitive diagnostic purposes in AD [60]. It was recently shown that biotinylated Tat peptide can bind amyloid deposits for *in situ* tissue labelling [61]. A preventive treatment for AD would be ideal as there is evidence that brain Aβ pathophysiological alterations leading to AD take place decades before the appearance of the first signs of

dementia, giving a broad pre-symptomatic phase for intervention with Aβ-targeted therapies [62].

PD is the second most common neurodegenerative disorder, affecting 2-3 % of the elderly population (>65 years old). It occurs upon intracellular accumulation of insoluble α-synuclein aggregates known as Lewy bodies. Dysregulated apoptosis leads to extensive loss of dopaminergic neurons, vital for motor function, in the substantia nigra of the midbrain region [63]. An early onset familial form of the disease occurs with mutations in the SNCA gene. SNCA overexpression causes excess α-synuclein to associate with the mitochondrial membrane in PD models, and induce oxidative stress [64]. Altered calcium homeostasis, axonal transport, and neuroinflammation are also implicated in the disease. Symptoms include bradykinesia, tremors, rigidity, along with cognitive impairment. With no available cure, treatment relies on dopamine substitution, deep brain stimulation, and symptom control [63].

The dominantly inherited CAG trinucleotide repeat expansion in the huntingtin gene on chromosome 4 leads to aggregation of abnormally folded huntingtin protein and development of HD. The disease causes cognitive, motor, and psychiatric disturbances. Disturbed proteostasis, transcription, mitochondrial function and protein-induced toxicity causes neuronal dysfunction and cell death. There is currently no treatment for HD, only symptomatic control. Antisense oligonucleotide therapy is being investigated as a way to lower levels of the mutant huntingtin protein [65].

FTD occurs when the frontal and temporal lobes degenerate. Depending on the location of neural damage, deficits can occur in

behavior and/or language. Mutations in MAPT mutations, the gene for tau protein linked to chromosome 17, are present in 6-11 % of FTD cases [66]. This type of dementia occurs with abnormal collections of transcative response DNA-binding protein 43 (TDP-43) and tau hyperphosphorylation. No cure is available, but symptoms can be managed using selective serotonin reuptake inhibitors (SSRI) and antipsychotics [67].

MS is an incurable disease characterized by infiltration of inflammatory cells, mainly lymphocytes, to the CNS through a leaky BBB, followed by myelin sheath destruction, axonal damage, and glial scar formation. Symptoms include paralysis, muscle spasms, neuropathic pain, and optic neuritis [68]. Neurological disability occurs episodically, lasting for days or weeks, and can be fully or partially reversible. The frequency of episodes can be reduced using pharmaceuticals, but neurodegeneration cannot be stopped or reversed [69].

ALS involves the deterioration of lower and upper motor neurons, leading to muscle atrophy, weakness, fasciculation and spasticity. Some patients also develop dementia, usually associated with focal atrophy of the frontal and temporal lobes. Markers of the disease include neuronal loss, gliosis, and TDP-43 neuronal inclusions [60].

Spinal muscular atrophy is a genetic neuromuscular disease occurring in infants with a loss-of function mutation in the SMN1 gene. An FDA approved treatment for the disease administers antisense oligonucleotides to correct a splicing defect and reinstate the SMN protein [70].

Despite the extraordinary scientific efforts dedicated to find a cure for neurodegenerative disorders, most have no disease-altering treatments and they remain one of the great challenges in medicine. The scarcity of therapeutic options is partially due to a lack in understanding of the basic mechanisms and causes of each disease, and limitations in experimental models [51]. Most of these diseases have no available diagnostic biomarkers, which means that clinicians rely on analysis of symptoms that can present late in the pathology [60]. A focus on genetic factors, despite the fact that the majority of cases are late onset sporadic forms, has also hindered progress. Considering the huge cost and burden of care associated with neurodegeneration, it is absolutely vital to develop effective treatments.

1.2.2 The BBB in disease

The BBB is altered in many neurological disorders, including amyotrophic lateral sclerosis (ALS), stroke, epilepsy, Alzheimer's disease (AD), Parkinson's disease, HIV encephalopathy, glioblastoma, bacterial meningitis, multiple sclerosis (MS), and traumatic brain injury, contributing to the progression of these pathologies [71].

BBB permeability is affected by many factors. Activated peripheral immune cells (neutrophils, T cells, and macrophages) can regulate BBB properties in response to infection, disease, or injury by releasing reactive oxygen species (ROS) that increase vascular permeability. Therefore, it is possible that inflammatory disorders that are not CNS-based can affect the BBB. There is some evidence that the BBB is damaged in rheumatoid arthritis, diabetes, eclampsia, atherosclerosis, liver failure, and hypertension [71].

Neuroinflammation is a major element of many brain disorders and has stong connections to BBB breakdown. BBB alterations have been observed in MS and stroke, allowing serum proteins to enter the CNS and damage neurons. Oxygen and nitrogen free radicals, and proteases (MMPs and cyclooxygenases) can damage the basement membranes and degrade TJ proteins [72]. Neuroinflammatory cytokines such as CCL2 (also known as MCP-1) downregulate the expression of ZO-1, occludin, and caveolin-1 [18]. TNF-α, a proinflammatory cytokine, and lipopolysaccharide (LPS), a well-known instigator of neuroinflammation, cause BBB breakdown *via* the reorganization of actin into stress fibers [73]. These two molecules are also involved in the induction of paracellular BBB permeability in HIV-1 infection and Haemophilius influenza type b [74, 75]. Another

proinflammatory cytokine, IL-1β, induces hypoxia inducible factor-1 and vascular endothelial growth factor-A (VEGF-A). VEGF-A downregulates claudin-5 and occludin mRNA and protein expression in mouse models of experimental autoimmune encephalomyelitis, a common *in vivo* model used in the study of MS [76]. A reduction in transforming growth factor (TGF)-β induced by inflammation also causes increased BBB permeability in rodents [77]. This extensive data indicates a role for anti-inflammatory therapy in restoring BBB integrity. Glucocorticosteroid treatment in MS has been shown to improve BBB function in humans, and partially reverse BBB breakdown *in vitro* [78, 79]. Furthermore, the anti-inflammatory properties of doxycycline are associated with memory recovery in an animal model of AD [80].

Interestingly, chronic sleep restriction, a form of sleep deprivation, increased BBB permeability by reducing GLUT-1 and TJ expression. This effect was reversed upon sleep recovery for 24 h [81]. Restriction of REM sleep led to similar BBB breakdown [82]. These findings highlight the widespread biological effects associated with sleep disorders.

Several clinical investigations have noted functional alterations of the BBB in AD, the leading cause of dementia. When compared to healthy controls, there is increased permeability to certain substances, altered β-amyloid peptide (Aβ) transport activity, and monocyte infiltration across the damaged BBB induced by Aβ [83]. Despite this reported increase in permeability, crossing the BBB remains a key obstacle in the pharmaceutical treatment of AD. Other changes in the AD BBB include overexpression of RAGE (receptor for advanced

glycation end-products), which transports Aβ from the blood into the brain [84], downregulation of LRP-1 and Pgp, which transport Aβ from the brain to the blood [84, 85], and overexpression of claudin-5, suggesting reduced paracellular BBB permeability [86]. These BBB modifications may affect drug performance *in vivo* and should be taken into account for the thoughtful design of targeted therapeutics and drug delivery devices.

Cerebral ischemia causes activation of MMP-2, which destroys TJ proteins leading to BBB disruption [87]. Longer ischemic events lead to more severe BBB damage, and further BBB opening can occur up to 48 h after reperfusion [88].

MS is an immune-mediated disease targeting the CNS, characterized by extensive inflammation and myelin destruction. This inflammation has been linked to BBB disruption, which allows T and B cells to enter the CNS, exacerbating symptoms [89].

SOD-1 mutant mice, a model of genetic ALS, display BBB disruption through reduced occludin, ZO-1, and claudin-5 expression [72]. *In vivo*, areas of motor neuron degeneration are associated with EC membrane and/or basement membrane damage [90].

Treatments that specifically target BBB damage are limited. High-dose methylprednisolone can reduce CSF levels of MMP-9, resulting in transient closure of the BBB in MS patients [91]. However, side effects prevent its widespread use in a clinical setting. The anti-inflammatory agent minocycline can also inhibit MMPs, reduce BBB disruption in MS and stroke patients, and is well tolerated over time in small doses [92, 93].

1.2.3 β-amyloid

Amyloids are insoluble fibrous proteins with distinct structural characteristics, such a β-sheet-rich secondary structure [60]. β-amyloid (Aβ) peptide is a 4 kDa peptide derived from the proteolytic cleavage of the amyloid precursor protein (APP), which is encoded by a gene on chromosome 21. It is composed of 37-43 amino acids, 28 of which are located at the extracellular N-terminal of APP. The remaining amino acids are located in the transmembrane domain of APP and confer hydrophobic properties that induce peptide aggregation. The two most common isoforms are $A\beta_{40}$ and $A\beta_{42}$, both of which can collect in senile plaques. Though $A\beta_{1\text{-}40}$ is more widespread, $A\beta_{42}$ is more hydrophobic, giving it a higher propensity to aggregate. Therefore, $A\beta_{42}$ is considered the primary toxic peptide in AD [94].

APP is a widely expressed integral membrane protein, abundant in neuronal synapses. Its primary function is unclear, though it has been implicated as a regulator of synapse formation, neural plasticity and iron regulation. Its proteolytic cleavage occurs *via* the non-amyloidogenic or amyloidogenic pathway (Fig. 7). In the non-amyloidogenic pathway, APP is cleaved by α-secretase and γ-secretase. The α-secretase cleavage occurs between the Lys16 and Leu17 of the Aβ region without forming Aβ peptide. The cleavage forms a soluble N-terminal fragment (sAPPα) that is secreted extracellularly, possibly to play a role in neuronal plasticity and survival. The resulting C-terminal fragment (α-CTF or C83) remains anchored to the membrane and is cleaved again by the γ-secretase complex. This second cleavage produces the APP intracellular domain (AICD) and the non-amyloidogenic fragment p3 [95]. In the amyloidogenic pathway, APP

is cleaved through β-secretase (BACE) and γ-secretase. The β-secretase releases the ectodomain of APP as a soluble fragment (sAPPβ). sAPPβ does not contain the $A\beta_{1-16}$ region at the carboxyl terminus and therefore lacks the neuroprotective properties associated with sAPPα. The resulting C-terminal fragment (βCTF or C99) remains associated to the membrane. Further γ-secretase cleavage produces AICD and Aβ peptide. Different γ-secretase cutting sites can produce Aβ peptides with different lengths, physical properties, and aggregation patterns [96].

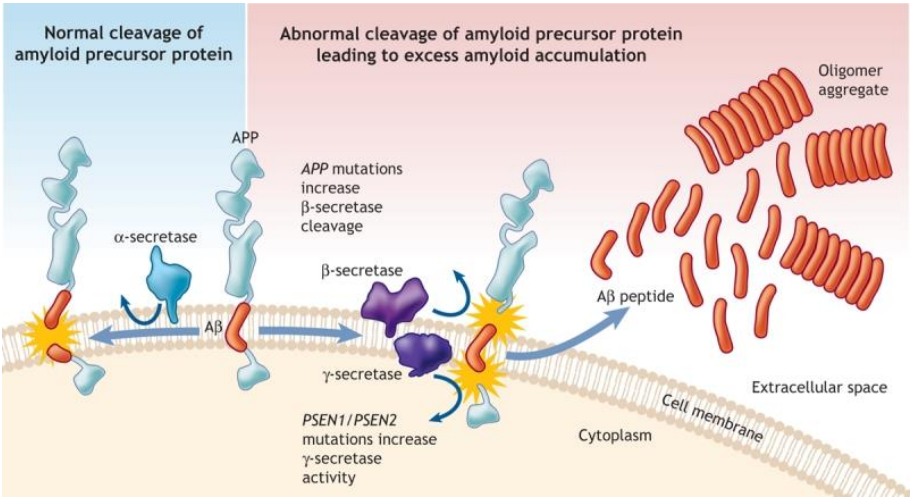

Figure 7. Processing of the amyloid precursor protein (APP) via amyloidogenic or non-amyloidogenic pathways [97].

Senile plaques are extracellular deposits containing dystrophic neurites, astroglial processes, microglia, and a dense core of insoluble aggregated protein fibrils, predominantly Aβ. These are the major biological feature of AD but are also present in a variety of neurodegenerative disorders, in healthy aged brains, or in the cerebral

arteries (cerebral amyloid angiopathy) [98]. Kinetic studies reveal a seeding or nucleation mechanism for Aβ peptides [99]. This means that the protein secondary structure changes from α-helix to β-sheet conformation, triggering peptide aggregation into soluble oligomers that act as nucleation centers for further formation of fibrils that deposit in the brain parenchyma. It is believed that the earliest amyloid plaques are diffuse, non-compact "pre-amyloid" deposits [100].

Various forms of Aβ peptides exist, with oligomers being more toxic to the brain than monomers or fibrils [101]. Aβ oligomers are the major species responsible for the neuropathological process underlying AD onset and progression, and they are the best correlates of disease severity [102]. Aβ toxicity is largely concentrated on the synapse, explaining the loss of synapses in AD and inhibition of long-term potentiation by Aβ oligomers [103]. Aβ peptides induce microglial activation, reactive astrocytosis, cytokine release, neuroinflammation, synaptic toxicity and dysfunction *in vitro* and/or in rodent brains, and may contribute to cell death [103, 104]. Butyrylcholinesterase is enriched in Aβ plaques, and its targeting with cholinesterase inhibitors may provide symptomatic relief in AD [105].

Several genetic and environmental factors have been associated with protein misfolding and aggregation, such as mutations, changes in metal ions, pathological chaperone proteins, pH or oxidative stress [106]. Many of these alterations are associated with aging, consistent with the late onset of neurodegenerative diseases. Elevated levels of $A\beta_{1-42}$ have been associated with early-onset familial forms of AD linked to the genes for APP and presenilin (PSEN1 and PSEN2) [107]. APP mutations can increase β-secretase cleavage, and PSEN1 and

PSEN2 mutations can increase γ-secretase activity, thereby increasing Aβ production.

The study of Aβ disorders is limited by the fact that spontaneous amyloidoses do not present in normal laboratory animals. Therefore, genetically engineered mouse models are essential, and are widely used for research. Several transgenic mouse models, including Tg2576, APP23, and APP_{swe}-$PS1_{dE9}$, overexpress mutant forms of APP and/or PS1, known to cause familial AD. AD hallmarks such as Aβ deposition, neuritic plaque formation, cerebral amyloid angiopathy, synaptic dysregulation, gliosis, and memory deficits are all present in these mouse models, though the tau tangles and dramatic neuronal loss seen in humans is absent [108, 109]. Triple transgenic models (APP, PS1, tau) can overexpress mutated tau. Other AD models alter expression of BACE1 or neprilysin, the main Aβ-degrading enzyme [110].

1.2.4 Sink effect

The amyloid cascade hypothesis proposes a key role of Aβ aggregates in AD [111]. According to this theory, AD is driven by increased production and/or decreased clearance of Aβ, and its subsequent aggregation in the brain. High Aβ levels lead to a series of downstream pathological events, including hyperphosphorylation of tau and neurofibrillary tangle (NFT) formation, inflammation, oxidative stress, excitotoxicity, loss of synaptic connections, neuritic injury, neuronal dysfunction, and cell death, thereby inducing the clinical symptoms of AD. NFT, the other histological hallmark of AD, are intracellular aggregates of hyperphosphorylated tau protein found in the cytoplasm of neurons, particularly in the pyramidal neurons of the hippocampus and cortex. Tau normally stabilizes the structure of microtubules in neurons. Pathogenic hyperphosphorylation causes it to separate from microtubules and aggregate into an insoluble form, with subsequent microtubule destruction and neuronal function impairment [112].

This hypothesis has inspired much research targeting Aβ aggregates by attempting to prevent Aβ peptide or plaque formation, therefore mitigating neurodegeneration and its associated symptoms. Aβ aggregation and/or fibril formation can be prevented by multiple compounds, including flavonoids, clusterin, and humanin [113-116]. Strategies targeting Aβ production include the use of inhibitors of BACE and γ-secretase. However, such inhibitors have failed clinical trials due to their limited ability to cross the BBB, and serious side effects that occur due to the involvement of these enzymes in other signalling pathways [111]. BACE1 inhibitors have been applied to the periphery in an attempt to activate the sink effect, with no success [117].

Splice-switching antisense oligonucleotides (SSO) have been used to avoid Aβ production *via* APP slicing, resulting in decreased Aβ levels *in vivo* [118]. Vaccination of transgenic AβPP mice can prevent and reduce cerebral amyloidosis by directing anti-Aβ antibodies to to the brain, where they bind to Aβ species and promote their degradation [119]. Unfortunately, clinical trials using immunization in AD patients produced unwanted side effects, and the lack of cognitive improvements was disappointing [120].

Thus, in recent years several alternative strategies have been investigated. Among them, the scavenging of the Aβ peptide and/or avoiding its aggregation and toxicity has attracted much attention and provided promising results. Behind this strategy is the so-called "sink effect" paradigm: to induce a reduction of Aβ peptide levels in the peripheral circulation by creating a steady efflux of Aβ from the brain to the blood, diminishing Aβ plaque load in the brain [121]. By removing large quantities of Aβ from the peripheral circulation with Aβ-specific binding agents, the Aβ load will dramatically decrease in the brain, thereby providing an effective treatment for AD (Fig. 8). It must be noted that large Aβ plaques and fibrils are unable to cross the BBB, so sink effect action refers to the removal of Aβ oligomers from the brain, perhaps after disaggregation of fibrils and plaques.

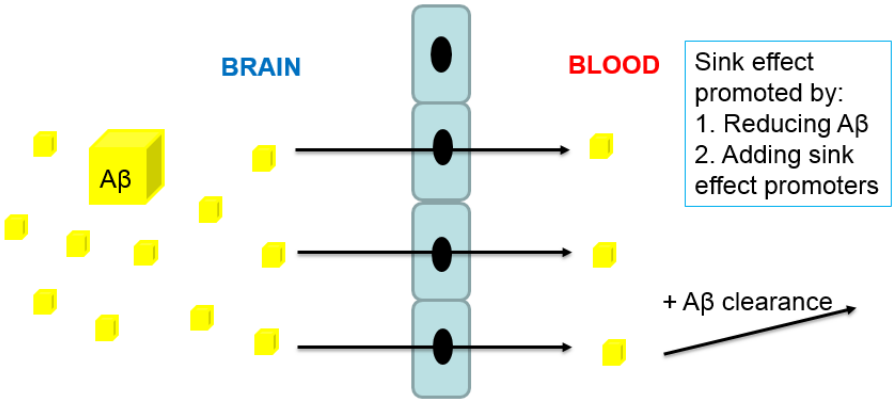

Figure 8: Schematic representation of the "sink effect" theory. A decrease in Aβ load in the blood can lead to efflux of the peptide from the brain to the blood, followed by its clearance from the periphery.

A recent study found that peritoneal dialysis in patients with chronic kidney disease reduces Aβ plasma levels in humans and can attenuate AD-associated pathology in a transgenic mouse model of AD [122]. These findings were correlated with a decrease in tau hyperphosphorylation, glial activation, neuroinflammation, neuronal loss, synaptic dysfunction, and cognitive deficits. Therefore, this method may prove useful in exploiting the sink effect theory in the treatment of AD.

1.2.5 Lipid involvement in neurodegenerative disease

The brain consists mostly of glycerolipids, sphingolipids and cholesterol, located predominantly in the neuronal membranes and myelin sheath. They have vital roles in brain structure, cell transport, signaling molecules, and modulation of transmembrane proteins [123].

Alterations in lipid homeostasis have been linked to neurodegeneration. Lipidomic analyses have shown altered lipid metabolism in the primary visual cortex of PD patients, possibly contributing to visual disturbances [124]. Statin use to lower circulating cholesterol may modestly reduce AD and PD risk [125, 126]. The involvement of membrane lipids in AD has been extensively studied, with reports that they can interact with Aβ peptide [127, 128].

The APOE ε4 allele, which increases the risk of developing AD partially by decreasing Aβ brain clearance, is also a risk factor for dyslipidemia, atherosclerosis, and coronary heart disease [129]. ApoE is the major lipoprotein in the brain, transporting cholesterol and associated proteins from astrocytes and oligodendrocytes (where it is synthesized) to neurons for cell uptake through receptor-mediated endocytosis [129]. The lipidation state of ApoE can affect lipid homeostasis and interactions with Aβ [130]. ApoE can bind and clear Aβ from the brain, with ApoE3 binding with higher affinity and than ApoE4 [131]. ApoE2 is thought to be protective against AD [132].

High serum cholesterol levels in midlife indicate a higher risk of AD [133]. Plasma apolipoproteins are associated with cholesterol, and their levels are altered in pre-demented patients displaying mild cognitive impairment [134]. Cholesterol's exact role in AD is unclear, but it may bind to APP and has been shown to stimulate BACE1

cleavage in AD and non-demented brains [135]. Cholesterol depletion reduces Aβ oligomerization in hippocampal neurons [136].

Plasma lipoproteins transport lipids between tissues, with only high-density lipoprotein (HDL) being able to cross the BBB [137]. Peripheral HDL normally removes excess cholesterol from tissues and is therefore considered protective against atherosclerosis and other cardiovascular diseases. Associated apolipoproteins act as receptor ligands and enzyme cofactors [138]. ApoA-I is the main protein component in plasma HDL, and high circulating levels have been associated with improved cognition [139]. Preferential adsorption of apoA-I can also reduce metal chelator toxicity when crossing the BBB [140]. HDL levels are inversely correlated with risk of AD. Further data relating high levels of ApoA-I or HDL with low risk of AD, and *vice versa*, has indicated that these substances may play a role in age-related cognitive deficits and pathology [141-144]. Indeed, HDL or its components may play some role in the "sink effect" but this hypothesis is underinvestigated.

1.3 NANOMEDICINE

1.3.1 Overview

Nanotechnology involves the use of particles or devices that measure in the order of billionth of meters [145]. Nanoparticles (NPs) are colloidal objects, normally measuring 1 - 100 nm in diameter. They have been widely researched as diagnostic, therapeutic, drug delivery, and tissue regeneration tools, in part because their surface can be easily manipulated and modified, and they can be loaded with drugs or contrast agents. NPs can be used for controlled drug release [146] and can be manufactured in a wide range of sizes and chemical compositions, facilitating the delivery of many types of drugs. Encapsulation can improve the solubility, pharmacokinetic, and pharmacodynamic profiles of compounds, enhance their stability by reducing their degradation in the systemic circulation, and increase their concentration at the diseased tissue through active targeting, thereby reducing toxic side effects in normal tissues. Furthermore, NPs can be administered by many routes, including oral, inhalation, parenteral, intravenous, and intraperitoneal [147].

NPs have been proposed as intriguing tools to enhance the transport of drugs across biological barriers, including the BBB, specifically by functionalizing their surface with targeting agents.

NP size is critical to avoid rapid clearance from the circulation. Renal filtration is responsible for the elimination of NPs measuring < 5 nm. NPs larger than 200 nm are removed from the peripheral circulation by the reticuloendothelial system (RES), clearing them to the liver and spleen. The avoidance of RES clearance could lead to a prolonged half-life *in vivo*. Surface functionalization of NPs with non-ionic surfactants

or polymeric macromolecules can increase half-life up to 24 h in rodents and 45 h in humans [148]. It has been demonstrated that neutral or negatively charged NPs have longer circulation half-lives compared to positively charged NPs because the latter have a higher affinity for serum proteins, which promote RES clearance [149]. Furthermore, surface functionalization can affect the extent of opsonization, complement activation and subsequent leukocyte uptake of NPs [150, 151].

NP shape affects interactions with vessel walls, which is essential for endothelial receptor recognition [149]. Blood flow dynamic simulations demonstrate that discoidal NPs are more prone to adhere to the vascular wall compared to spherical NPs [152].

1.3.2 Types of NPs

The great interest in researching NPs as medical devices has resulted in the production of a wide variety of NPs (Fig. 9). Natural or synthetic polymers or lipids are often used to synthesize biocompatible and biodegradable NPs. Liposomes, solid lipid NPs (SLN), polymeric NPs, and gold NPs are the most studied NPs for brain drug delivery, due to their common features of biocompatibility, stability, biodegradability, limited antigenicity and suitability for surface functionalization. Moreover, they can incorporate both hydrophobic and hydrophilic drugs and controlled drug release can be achieved.

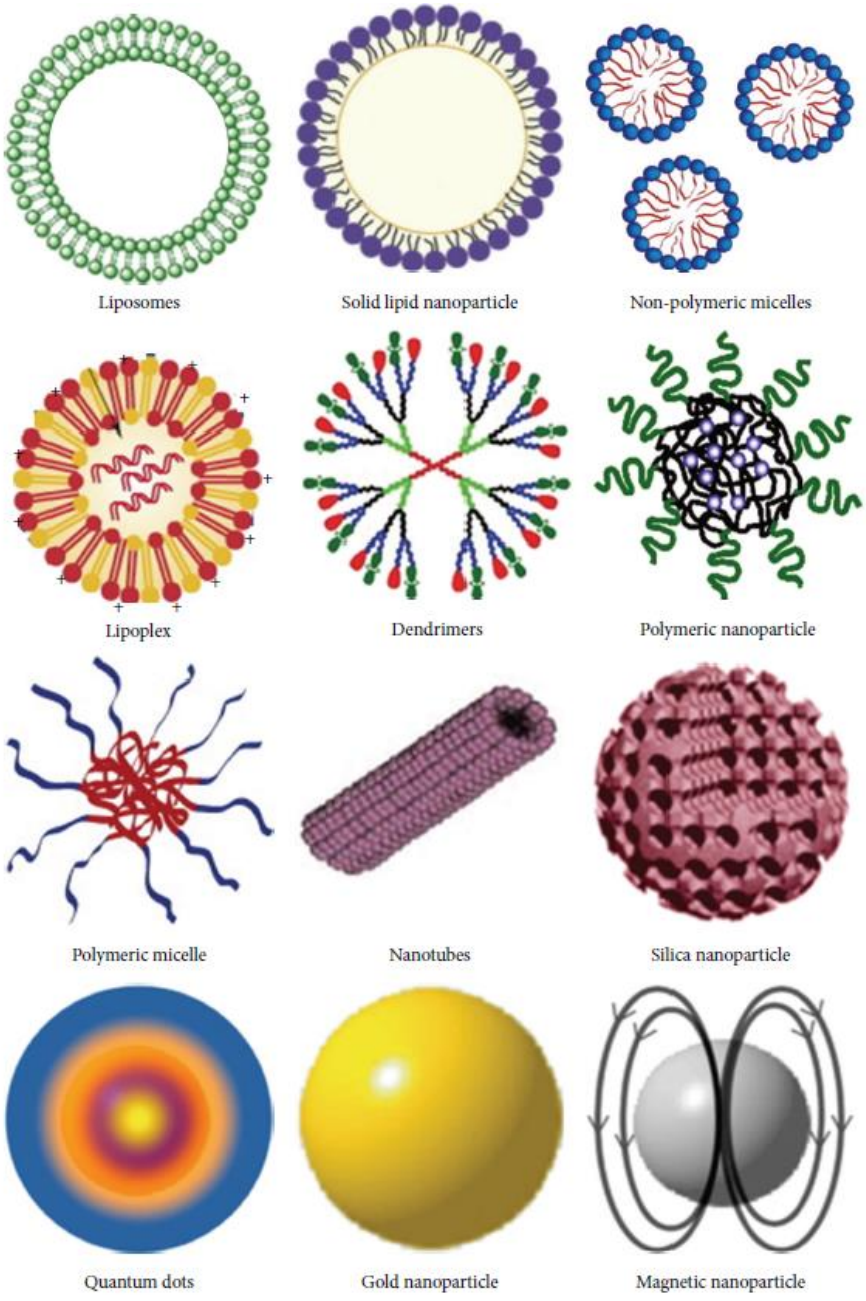

Figure 9. Types of NPs. The most commonly used NPs for biomedical applications, typically less than 100 nm in diameter [153].

Liposomes are spherical vesicles containing an aqueous inner core enclosed by one or more phospholipid bilayers, normally composed of naturally occurring amphiphilic physiological phospholipids, such as sphingomyelin, phosphatidylcholine, glycerophospholipids, and cholesterol [154]. The use of physiological lipids can decrease bilayer permeability and increase liposome stability *in vivo* [153]. Multilamellar vesicles (MLV), measuring several μm, are composed of multiple concentric lipid bilayers. Large unilamellar vesicles (LUV) consist of a single lamella (or bilayer) and are > 100 nm. Small unilamellar vesicles (SUV) have one bilayer and measure up to 100 nm [153]. Liposomes can be adapted for a specific target by altering the lipid composition, size and charge of the vesicle, and/or adding surface coatings and ligands to improve efficacy, reduce RES clearance, and minimize toxicity. Liposomes are extensively used as molecule carriers in the cosmetic, food, farming, and pharmaceutical industries. Thery are particularly attractive tools in biomedical applications due to their biocompatibility, non-immunogenicity, non-toxicity, biodegradability and high physical stability [155].

Liposomes composed of an equimolar sphingomyelin-cholesterol matrix have been repeatedly applied *in vivo* for therapeutic purposes, displaying good circulation times in blood, biocompatibility, resistance to hydrolysis, and low ion permeability [156, 157]. Moreover, these bilayers can form raft-like or liquid-ordered domains that are representative of a native cellular membrane where Aβ accumulates [158]. Cholesterol in particular can strengthen the Aβ-membrane interaction [159].

Liposome encapsulation is used to improve pharmacokinetics

and protect drugs from degradation, enhancing their circulation half-lives. Additionally, the surface of liposomes can be easily functionalized in order to obtain site specific targeting of the enclosed drug, thereby reducing peripheral side effects. Liposomes are amphiphilic, so hydrophilic compounds can be encapsulated in the aqueous core and lipophilic compounds can be dissolved in the lipid bilayer without alteration of the encapsulated molecules. This makes these NPs particularly attractive for the delivery of peptides, proteins, RNA, or DNA variants [155].

SLN are nanospheres made of lipids that are solid at physiological temperature, stabilized by physiologically compatible emulsifiers. SLN are very stable and can be produced easily on a large scale [160]. SLN are generally considered to have low toxicity and are non-toxic to N2a neuroblastoma cells when coupled with a neuroprotective co-drug [161].

Polymeric NPs are nanosized carriers synthesized using natural or synthetic polymers. Advantages of polymer-based systems include the ability to control drug release, combine therapy and imaging for "theranostic" purposes, and drug targeting [162]. The prodrug approach, where a drug is covalently linked to a polymeric scaffold, can prove very useful in avoiding "burst release" and any subsequent systemic toxicity of NP-delivered drugs [163].

Polymeric NP characteristics are affected by the preparation method and the composition of the organic phase used. Nanocapsules, consisting of a polymer shell containing an aqueous cavity, and nanospheres, consisting of drugs and polymers dispersed in a matrix-like structure, can be easily formulated. Drug release is controlled by

altering polymer biodegradation rates or diffusion out of the polymer matrix. Natural polymers are popular in formulation due to their general biocompatibility, though they can be mildly immunogenic. Synthetic polymers have a chemical composition that can be controlled more easily, but can vary in terms of biocompatibility [164]. Polyisoprene has favorable properties such as good degradability and biocompatibility, due to its similarity to natural terpenoid, and therefore is a suitable candidate for NP formulation [165].

Gold NPs are the most stable metal NPs with unique optical, electronic, physicochemical, and magnetic properties. Their high X-ray absorption coefficient, strong binding affinity to thiols, disulfides and amines, and the ability to easily change their synthetic properties make them useful tools in nanomedicine [166]. The stability and ease of use of gold NPs make them perfect to study NP-protein interactions *in vitro*.

1.3.3 NP-based strategies to cross the BBB

NPs are used for many targets, often in the study of cancer, but NPs designed for BBB crossing require specific features. It is estimated that the extracellular spaces in human brain tissue have very few pores over 200 nm and that ~25 % of all pores are ≥ 100 nm [153]. Therefore, NPs should be less than 200 nm in diameter to facilitate diffusion in the brain. The ability of NPs to overcome biological barriers, particularly the BBB, and their general biodistribution depends on parameters such as NP shape, size, composition, surface charge and functionalization [149, 167].

Polymeric NPs have been extensively tested as the basis for drug delivery systems to the CNS, and surface modification with various ligands has been explored to enhance their permeability through the BBB [168]. PEG-PLA NPs are commonly used, and are non-toxic to immortalized mouse brain endothelial cells [169].

Magnetic NPs can be focused in a specific tissue or region by using an externally applied magnet. Magnetite chitosan microparticles have been used to deliver the drug tacrine to the brain, by keeping a magnet at the target region upon i.v. injection in healthy rats. This system caused caused a five-fold increase in tacrine concentration in the brain when compared to the free drug [170].

Furthermore, gold NPs have been shown to cross the BBB with or without functionalization [171, 172], with surface coating affecting cell uptake and processing [173].

Although most brain targeting with pharmaceuticals focuses on crossing the BBB, this is not always necessary. Squalene nanoparticles loaded with adenosine were unable to cross the BBB, but still exerted

neuroprotective effects in an *in vivo* model of stroke when delivered to BBB ECs [174]. Therefore, promoting BBB cell targeting may be just as effective as BBB crossing in neurodegenerative disease treatment. This is most prominently seen with particles, either synthetic ones or physiological ones such as plasma lipoproteins, or other agents that promote the "sink effect" in Alzheimer's disease, a phenomenon that is further discussed in Chapter 1, section 1.2.4. Several studies have described the development of injectable scavenging systems, such as liposomes or polymeric NPs, to reduce blood and therefore brain Aβ [121, 175, 176]. For example, liposomes bi-functionalized with modified apolipoprotein E (mApoE) and phosphatidic acid (PA) can strongly bind to Aβ (K_d = 0.6 μM), inhibit peptide aggregation, and trigger disaggregation of preformed Aβ aggregates [177]. Molecular dynamics simulation studies suggest that negatively charged PA phosphate groups can interact with positively charged residues on Aβ peptide, while the positively charged mApoE can interact with negatively charged residues present on Aβ peptide at physiological pH [178]. This could explain the synergic activity of the two elements used for functionalization. In both acute and long-term treatments using *in vivo* mouse models of AD, the reduction of brain Aβ was associated with its increase in peripheral organs, liver and spleen. Therefore, it was speculated that a small proportion of mApoE-PA-LIP liposomes cross the BBB and destabilize or inhibit deposition of brain Aβ aggregates. The generated lower MW Aβ species are then able to cross the BBB from the brain to the blood, and can be peripherally cleared by the liver and spleen *via* the sink effect, which is mediated by the majority of the mApoE-PA-LIP that remain in the circulation [179]. This strategy is a

promising one and requires two steps: (i) crossing the BBB with even a small number of NPs, either synthetic ones or physiological ones such as plasma lipoproteins, or other Aβ destabilizing agents that can disrupt large toxic Aβ aggregates that are normally sequestered in the brain due to their inability to cross the BBB. (ii) The majority of administered NPs, which remain in the circulation, then promote the sink effect, enhancing efflux of lower smaller Aβ peptides from the brain to the blood, thereby decreasing Aβ load in the CNS and ameliorating AD symptoms. Therefore, it is important to note that BBB-crossing ability may not be the only necessary factor to exploit the sink effect using NPs.

PEGylated NPs functionalized with an antibody directed towards $A\beta_{1-42}$ have been shown to reduce Aβ oligomer levels in the brain, increase Aβ plasma levels, and reverse memory deficits in a transgenic model of AD, possibly through the sink effect [180].

Nevertheless, this strategy has strong weaknesses. The low systemic half-life of NPs after i.v. administration, in the region of hours, limits BBB crossing and the elimination capacity of amyloid and may require multiple injections. Furthermore, the distribution and elimination of NPs after binding to the Aβ peptide is often uncertain.

It is important to note that the ability of NPs to cross the BBB may be different in the disease state compared to the healthy one. Changes in permeability and receptor expression, as detailed in Chapter 1, section 1.2.2, may alter BBB-NP interactions positively or negatively, emphasizing the need to choose relevant *in vitro* and *in vivo* models for research.

1.3.4 NP functionalization to cross the BBB

NP functionalization involves the attachment of one or more targeting ligands for a specific molecule, pathway, cells, or tissue, or to encourage the crossing of biological barriers (Fig. 10). Though NPs offer a promising approach to surpass the BBB, modifications are necessary to maximize drug delivery to the CNS. Due to the large surface area to volume ratio of NPs, multiple copies of ligands can be attached, dramatically increasing their binding affinity *via* multivalent interactions [181]. Synthetic and physiological peptides and proteins have extensively been used to functionalize NPs for BBB targeting, identified using various techniques including peptide phage display and computer-assisted design [182].

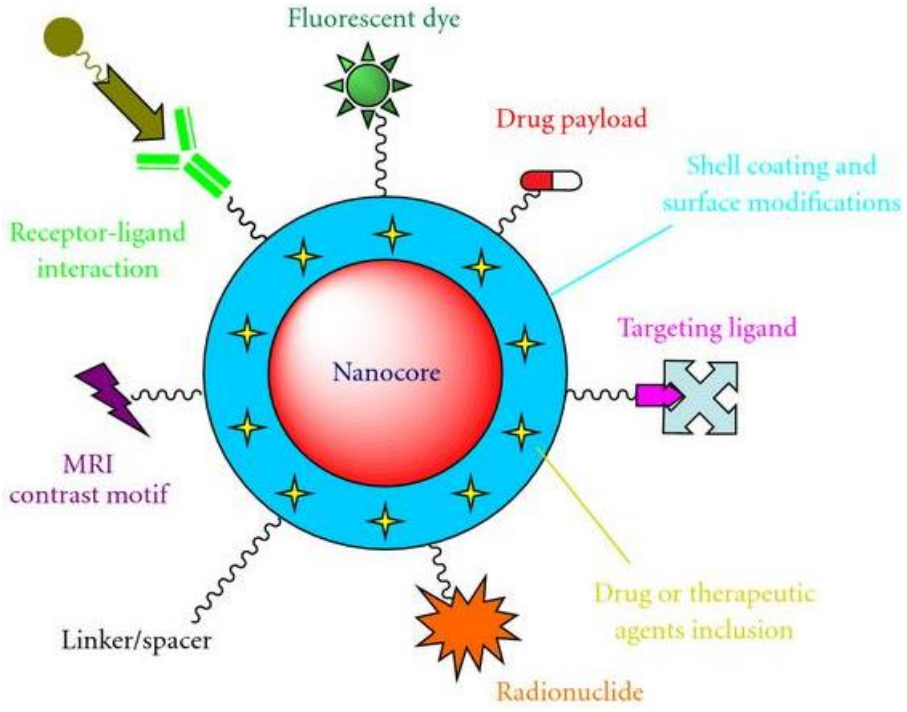

Figure 10. Scheme of multifunctional NP for molecular imaging, drug delivery, and therapy [183].

The most common approach to enhance NP passage from the peripheral circulation to the brain is to exploit existing physiological mechanisms of transport, for example, receptor-mediated or adsorptive-mediated endocytosis. In this case, choosing appropriate ligands is essential.

BBB crossing may be facilitated by conjugation of positively charged ligands to the NP surface, exploiting adsorptive-mediated endocytosis triggered by electrostatic interactions of the ligand with the negatively charged endothelial cell surface. For example, sphingomyelin/cholesterol-based liposomes with a high affinity for Aβ have been functionalized with a modified cell-penetrating trans-activating transcriptor (TAT)-peptide to enhance BBB passage. The functionalization led to an increase in endothelial permeability across a hCMEC/D3 cell-based BBB model [184]. TAT-conjugated NPs have also been used to efficiently deliver ritonavir to the CNS [185].

NPs composed of or coated with chitosan, a biocompatible and biodegradable polymer that enhances positive charge density on the NP surface at physiological pH, may increase BBB passage [186]. Surface-adsorbed chitosan promotes the transcytosis of PLGA NPs functionalized with an anti-Aβ Abs (IgG4.1) across the BBB in a polarized canine kidney cell monolayer [187]. In mice, brain uptake of an Aβ fragment is higher when it is loaded on chitosan NPs [188]. Although chitosan is a generally considered non-toxic and biocompatible, various forms can differ in size and degree of deacetylation. Therefore, specific biocompatibility studies are essential when using this material.

Different coupling reactions have been used to link peptides or

antibodies (Abs) to NPs, in an attempt to bind specific receptors on BBB cell surfaces. These ligands can be linked *via* covalent bond between a free thiol (either already present or generated by thiolation on its primary amines) and a maleimide group present on the NP surface [189]. Maleimide is known to easily react with free cysteines on proteins and is often added to NP surfaces specifically for protein functionalization [190]. For gold NPs, the thiol group may form a stable S-Au bond with the NP core [191]. Immunoliposomes can be prepared by activating free carboxyl groups on the NP surface with ethylcarbodiimide and N-hydroxysuccinimide, and covalently conjugating Abs through displacement of N-hydroxysuccinimide groups by antibody amines [192].

NP functionalization using non-covalent binding is also widely implemented by taking advantage of the high affinity between biotin and streptavidin [193]. It has been extensively shown that a wide array of proteins are easily adsorbed *via* strong electrostatic interactions with the surface of NPs [194]. However, there are several advantages of choosing covalent binding over the simple adsorption of proteins on the surface of NPs, including improved selectivity of protein binding and higher binding capacity. Furthermore, as covalent bonds are stronger than electrostatic forces this may possibly prevent the displacement of functionalized proteins by serum proteins upon *in vivo* administration, or their removal in the purification process [195]. RI7217, an anti-TfR Ab, covalently bound to liposomes is more effective than biotin/streptavidin ligation in traversing a human BBB cellular model [39]. It has been shown that continuous protein layers form on polymer films for both adsorbed and covalently bound proteins [195]. However,

it is not unusual that there is slightly less protein bound in the presence of maleimide, as the arrangement of proteins on the NP surface will differ depending on the location of binding and orientation of the proteins on the NP surface. Moreover, covalent binding gives a fixed position to the bound protein, making the attachment of subsequent proteins more difficult due to steric hindrance, whereas the layer formed by absorbed proteins is likely more fluid.

NPs increase in size upon protein functionalization *in vitro* and physiological protein binding *in vivo,* which can affect their biological processing [196]. Some non—biological substrates can denature physiological proteins, which may affect the biological activity of the protein or affect its binding capabilities [195]. The packing and orientation of some proteins on substrates is highly dependent on the substrate surface characteristics [197]. It has been theorized that flexible surfaces may facilitate better maintenance of protein structure [198]. Indeed, the use of proteins for NP functionalization may be limited by competition with endogenous proteins, which may restrict the amount of protein-functionalized NPs that traverse the BBB by receptor-mediated pathways.

Functionalization can be carried out using ligands that trigger receptor-mediated endocytosis, particularly through transferrin receptor (TfR), lactoferrin receptor (LacR), and low-density lipoprotein receptor (LDLr) [199]. Unfortunately, these three receptors are not specific to the BBB, meaning that targeted NPs to these receptors could be taken up by other organs before reaching the brain.

Ligands for TfR include peptides selected from the phage display technique [200] and anti-TfR Abs [39, 201]. Poly(ethylene

glycol)-poly(lactic acid) block copolymer (PEG-PLA) NPs have been functionalized with a phage display-derived peptide (CGHKAKGPRK), named B6, demonstrating high affinity for TfR. Functionalization enhanced NP brain accumulation *in vivo* in BALB/c nude mice [200]. Transferrin antibody chimeras have been used in *in vivo* models of Parkinson's disease, AD, and stroke to enhance brain accumulation of therapeutic proteins [202].

Lactoferrin is the endogenous ligand for LacR and has been used to increase brain delivery of PEG-polylactide-co-glycolide (PEG-PLGA) polymersomes in mice [203].

LDLr is present on the capillary endothelial cells of several species, and its expression is upregulated in the BBB compared to other endothelia [204]. Apolipoprotein E (ApoE) is a physiological ligand for LDLr. Liposome functionalization with the monomeric fragment 141–150 of human ApoE peptide, named mApoE, modified with the attachment of the CWG sequence CWG-LRKLRKRLLR, enhanced *in vitro* BBB permeability and *in vivo* brain delivery in healthy mice *via* transcytosis, bypassing lysosomal degradation [177, 189]. Thiol-maleimide covalent coupling was used to functionalize NPs [39]. Multifunctionalization of LUV liposomes with ligands targeting both TfR and LDLr has been used to enhance brain targeting for AD treatment [205].

A particularly strong advantage of using NPs for biomedical purposes is the ability for multi-functionalization. An example of this involves the use of phosphatidic acid (PA), which can bind Aβ binding and the above described mApoE to cross the BBB. Bi-functionalized liposomes (mApoE-PA-LIP) increased BBB passage *in vitro* five-fold

compared to PA-LIP, showed higher brain accumulation *in vivo* [177], and efficient hCMEC/D3 cell targeting. However, there is decreased uptake of mApoE-PA-LIP and other synthetic peptides mimetic of human ApoE, in the presence of free mApoE peptide. This suggests that a saturable receptor-mediated pathway is involved, highlighting the complexities of using physiologically derived NP ligands.

Functionalization must be tailored to the specific administration route intended. Several compounds, such as cyclodextrins, phosphatidylcholines, and fusidic acid derivatives, have been investigated as nasal absorption enhancers [206]. Albumin NPs carrying cyclodextrin and tacrine show good adhesion to the nasal mucosa *in vitro* but had lower drug permeation than free tacrine in *ex vivo* permeation studies across sheep nasal mucosa [207]. Similarly, PEG-PLGA NPs entrapping fibroblast growth factor for AD treatment have been decorated with Solanum tuberosum lectin, which selectively binds to N-acetylglucosamine on the nasal epithelial membrane. The brain content of growth factor increased almost two-fold following intranasal administration of targeted NPs compared with i.v. administration of the same dose of free drug. Moreover, spatial learning and memory of AD rats were improved [208].

1.3.5 Identifying targeting ligands for NP functionalization

Phage display is a rapid high-throughput screening method for protein or peptide interactions (Fig. 11). The concept utilizes genetically engineered libraries of filamentous bacteriophages, for example M13, containing surface protein genes expressing a specific peptide (or polypeptide) on its surface, with each library carrying a huge variety of peptides. The biopanning process involves administering phages intravenously *in vivo* or incubating them with a specific cell type or other target *in vitro.* After isolating the target tissue of interest *in vivo* or washing the free phage away from the *in vitro* setting, the attached phages are eluted. This leaves an enriched pool of phages, which theoretically express peptides that are target-specific. The isolated phage is amplified using bacteria and the process is repeated, usually three times, to isolate a highly specific phage library. The genetic material in the bacteriophage is sequenced and the linked peptides can be synthesized for further validation in experimental models. These peptides are frequently used as ligands for NPs to improve targeting [209]. The physical link between the genetic material inside the phage and its corresponding displayed peptide provides comprehensive knowledge about the specific peptide chosen. This promising technique, the discoverers of which were awarded the Nobel Prize for chemistry in 2018, may hold the key to finding NP ligands that can target the BBB.

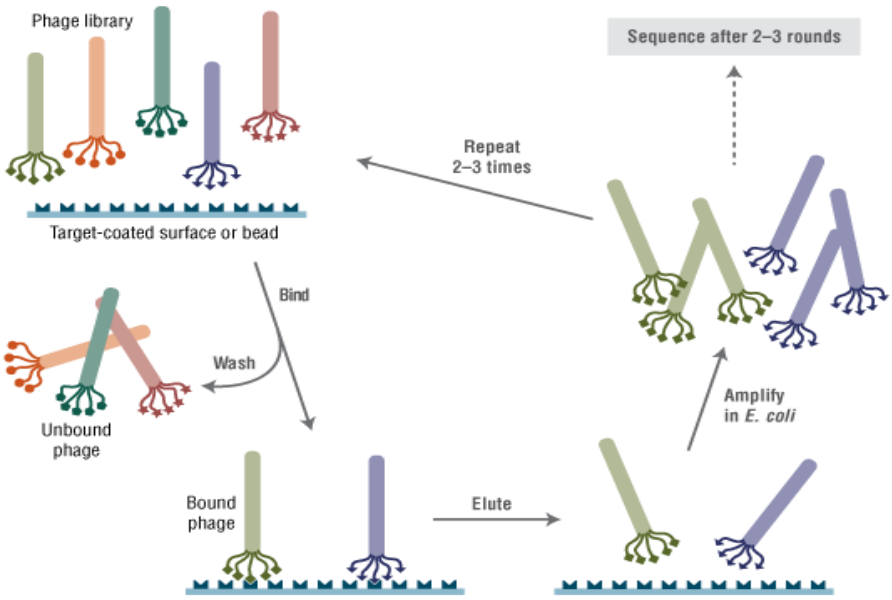

Figure 11. Scheme displaying phage-display process *in vitro* [210].

Targeting agents for Aβ have been identified with phage display technology, facilitating the delivery of neuroprotective agents, amyloid-destroying agents, or molecules that prevent plaque formation. They may also be used as diagnostic agents, elucidating the extent of plaque formation in AD patients. Two 20-mer peptides were synthesized following phage display discovery, and were shown to specifically bind to $A\beta_{1\text{-}40}$ [211]. A similar study discovered two peptides that were able to inhibit amyloid fiber formation in brain sections from an APP/PS1 transgenic mouse model of AD as measured by the thioflavin T aggregation assay [212]. These peptides were non-toxic to neurons and able to cross the BBB when attached to an MRI contrast agent, indicating their potential successful use as a NP ligand to target AD pathology.

Phage display can be exploited for diagnostic purposes, in order to track changes in the AD brain. *In vivo* phage display was used to identify molecular markers of cerebrovascular changes in mouse models of AD [213]. A 9-mer cyclic peptide was shown to accumulate in the hippocampus of hAPP-J20 mice at different ages. Upon i.v. administration in AD mouse models, the peptide gathers in neurovascular endothelial cells and reactive astrocytes. Its specific target is connective tissue growth factor, a matricellular protein that is highly expressed in the AD brain. Therefore, the peptide may be useful as a theranostic tool, potentially delivering drugs and/or imaging agents to sites of vascular change within the AD brain, or indeed any neuroinflammatory disorder.

Immunostaining studies have also been used to identify Aβ ligands that could be incorporated into NPs. Phosphatidic acid (PA), an anionic phospholipid, was identified *via* this method. Molecular dynamics simulations showed that negatively charged phospholipids facilitate the liposome-Aβ interactions, as the peptide is positively charged. However, Aβ also contains negatively charged amino acids, meaning that small amounts of these lipids in the bilayer can decrease mutual repulsion [178]. PA was integrated into a liposome bilayer and displayed high affinity for Aβ in all its aggregation forms, including oligomers and fibrils. The high binding affinity was likely due to multivalent interactions, which also resulted in an extremely low dissociation rate constant [214].

1.3.6 Protein corona

NP half-life in the circulation is strongly affected by the adsorption of serum proteins on their surface, forming the "protein corona". The protein corona is a continuous layer of proteins that rapidly adheres to the NP surface upon biological administration, normally in the blood, and consists of two parts. The inner "hard" corona consists of proteins directly adhered to the NP surface and is relatively stable. An outer "soft" corona consists of protein-protein interactions, whereby a second layer of proteins forms around the hard corona. This layer is more dynamic and loosely bound (Fig. 12). The protein corona is the true interface with which NPs interact with biological systems, and its quantitative and qualitative composition changes over time [215].

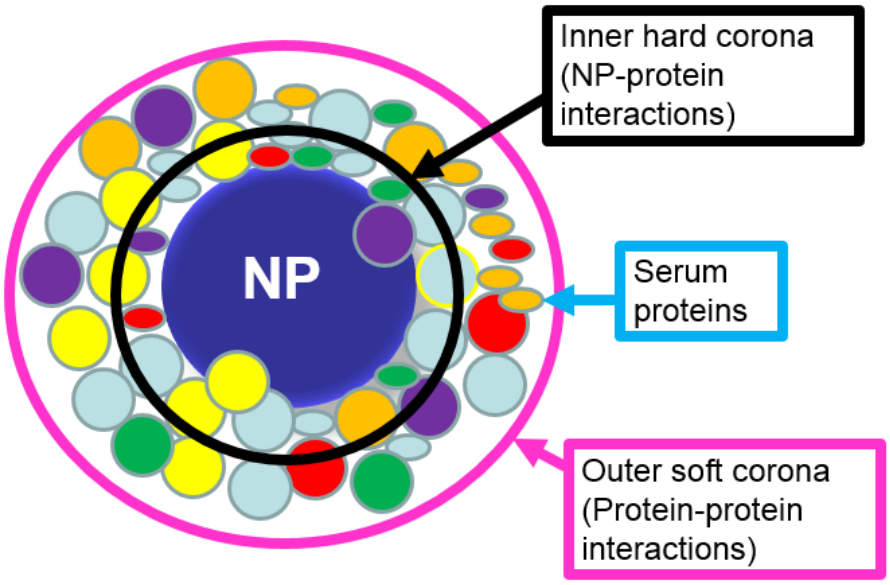

Figure 12. Protein corona on NPs. The protein corona consists of an inner stable hard corona, and outer dynamic soft corona.

The protein corona, and in particular the binding of opsonins (IgG, complement components and fibrinogen) to NPs causes their clearance to the liver and spleen by RES, thereby reducing their half-lives in the bloodstream. The corona can also affect the bioavailability, biodistribution, BBB permeability, cell uptake, targeting capacity, size, surface charge, and toxicity of NPs [216]. Controlling corona formation could help reduce some of these negative effects.

The corona composition itself depends on many factors, including the route of administration *in vivo*, temperature, pH, shear stress, time of exposure, serum concentration *in vitro*, and the physicochemical properties of the NPs [149, 153]. Plasma protein changes linked to specific disease or lifestyle patterns has been shown to affect the protein corona composition, indicating a role for personalized protein coronas in research for biomedical application [217]. The corona is unique to each type of NP. The most abundant proteins in the serum or biological medium will bind to the NP surface first, and will then be replaced by proteins with a higher affinity for the NP, a concept known as the Vroman effect [215]. Therefore, the composition and quantity of proteins bound to NPs is not always representative of the protein composition of the serum. Furthermore, attachment to NPs can lead to alterations in protein conformation, possibly affecting their function or ability to be recognized by endogenous receptors [218].

The protein corona has been shown to affect NP crossing of the BBB in several ways. The attachment of biological proteins to the NP surface can hide surface ligands used for functionalization and therefore inhibit effective targeting. Protein aggregation can also inhibit targeting

and cause detrimental side effects in the bloodstream. Furthermore, the binding of complement components in the protein corona can cause complement activation and influence coagulation [219].

PEGylation is the most common method to avoid rapid NP clearance due to corona formation. This involves coating the NP surface with polyethylene glycol (PEG), a hydrophilic surfactant that forms a tight association with water molecules, reducing opsonization and therefore strongly extending their circulation time [149]. NP coating with leukocyte or erythrocyte-derived cell membranes can also increase NP half-life in the circulation [149, 220, 221]. Similar work has been carried out using platelet membranes to coat NPs, though its efficacy in avoiding immune system activation is debatable [222].

Manipulation of the protein corona or selective binding of specific physiological proteins to NPs in the bloodstream can improve targeting. For example, NPs coated with polysorbate 80 selectively adsorb apolipoproteins, including apolipoprotein E, from the blood, subsequently facilitating their uptake by brain capillary endothelial cells by receptor-mediated endocytosis [223] or by peripheral tissues such as the liver.

1.3.7 Neurotoxicity of NPs

Though brain targeting is essential for the treatment of neurodegenerative diseases, the brain is one of the most delicate organs in the body, requiring the maintenance of strict parameters for normal neurological function. The exposure of the brain to nanomaterials raises concerns about potential neurotoxicity.

There are a limited number of clinical studies measuring toxicity of NPs. Considering the ease with which certain NPs can enter cells and come into contact with the cytoplasm and subcellular organelles, the neurotoxic and immunogenic effects of these NPs must be thoroughly investigated. In particular, NPs have been shown to induce inflammation, oxidative stress, DNA damage, cardiovascular toxicity and coagulation, a particularly potent problem when NPs are not targeted to specific cells or organs [224]. It is well established that the size, shape, composition, reactivity, and surface properties can have major effects on NP biocompatibility [225, 226]. For example, smaller sized NPs exhibit higher toxic effects due to increased surface area [227], and NPs composed of one chemical are less toxic than those containing multiple chemicals [228].

NPs that are not biodegradable, for example gold NPs, or cannot be cleared effectively from the CNS pose a particularly high risk, as their accumulation in the brain with prolonged treatment may cause increased toxicity [169]. Some metal-based NPs [229, 230] and mesoporous silica NPs [231] are toxic to neuronal cells due to high bioaccumulation, and can even contribute to Aβ fibrillation mediated AD progression. Cationic amine group dendrimers can cause severe damage to lipid-rich cell membranes [232, 233]. Chronic exposure to

aluminium and iron NPs has been linked to AD [234], and manganese NPs cause psychiatric and motor disturbances [235].

Many NPs have been widely studied and are now considered generally safe for *in vivo* use, often because they are formed from biological materials and are easily degraded in the body. Different gold NPs have no short-term toxicity in mouse models [236], no effect on BBB integrity in Sprague-Dawley rats [237], and do not affect cell viability *in vitro* when tested on murine microglial cells and human neuroblastoma cells [238]. However, the surface coating or ligands can affect the adsorption of ions and biomolecules and therefore influence biological processes and induce toxicity of otherwise safe NPs [239, 240]. For example, 11 organic surface coating agents that are commonly used were tested on multiple cell lines, and six of them were found to be cytotoxic [241]. Cationic albumin has been successfully used to functionalize NPs and enhance their passage through the BBB [242, 243]. However, i.v. injection of cationic proteins in large quantities causes an increase in vascular permeability and the destruction of BBB permeability [26].

Conversely, a coating can block the action of some neurotoxic NPs. For example, quantum dots are often synthesized using toxic semiconductor materials such as cadmium selenide or cadmium sulfate. Such NPs have been coated in polymers, including phospholipids, to successfully reduce their toxicity *in vivo* [244].

NPs can reduce the peripheral toxicity of drugs, focusing their action on the specific disease site, for example Aβ plaques in the AD brain. Rivastigmine is a promising drug for the treatment of AD, reversibly inhibiting butrylcholinestrase and acetylcholinesterase.

However, its hydrophilicity means it has low bioavailability and low penetration to the brain. Targeted delivery of the drug has been successful using PLGA NPs, and PBCA-80 NPs, reducing peripheral toxicity and improving brain delivery [245]. NPs may actually decrease the toxicity of their attached or incorporated drugs. For example, it has been extensively demonstrated that zinc, copper, and iron are enriched in Aβ plaques, leading to the use of metal chelators as inhibitors of Aβ aggregation. However, metal chelators are neurotoxic and their passage is severely limited by the BBB. When iron chelators targeting Aβ are conjugated to NPs to cross the BBB, their toxicity decreases, possibly by decreasing the lipophilicity of the chelators, and they can enter the CNS and inhibit Aβ aggregation [246, 247].

Considering that one of the major advantages of nanomedicine is the possibility of multifunctionalization, the attachment of neuroprotective ligands to NPs could combat any potential neurotoxicity. CL protects SK-N-MC cells from neurotoxicity, and has been successfully attached to liposomes to rescue apoptotic neurons in AD [248].

As most NPs are unable to cross the BBB, or only cross in very small quantities, the interactions between the brain and NPs can be difficult to determine. NPs or their ligands can trigger inflammation and induce oxidative stress through ROS production [249]. ROS toxicity may be more dramatic in the CNS due to the high content of unsaturated fatty acids, which are particularly susceptible to peroxidation [250]. In particular, Ag-25 NPs cause oxidative DNA damage in the brain through ROS production [251]. Manganese oxide and anionic magnetic NPs decrease PC-12 neuronal cell viability *in vitro*, depleting dopamine

levels and increasing ROS production [252, 253]. Similar effects are found when immortalized mouse microglial cells (BV2) are exposed to NPs [254]. NPs can disrupt gene expression in the dopamine system, disturb the cell cycle, and induce apoptosis and the p53 mediated signalling pathway [255]. Considering that there is some degree of neuroinflammation in most neurodegenerative diseases, further pro-inflammatory responses induced by NPs may actually worsen the conditions. *In vitro* research has shown that microglial cells can internalize gold NPs with different coatings (cetyl trimethylammonium bromide or PEG) and shapes (urchin, spherical, rod) without inducing cytotoxicity, though *in vivo* administration caused transient activation of microglia [256], highlighting the need for more sophisticated cell models. Microglial activation occurs in many neurogenerative disorders, including AD, and leads to the production of neurotoxic compounds such as superoxide radicals, nitric oxide, and glutamate [257]. Therefore, further activation of these cells must be avoided when designing brain-targeting NPs.

A major aspect of neurotoxicity is complement system (CS) activation, and is affected by a variety of factors, including the surface oxidation state of administered materials [258]. Glial cells and neurons can release complement components in healthy brains, as well as during infection or following injury. In AD, senile plaques have been shown to activate the CS, upregulating classical pathway components in the cortex [259]. Further CS activation by NPs could be detrimental to brain health. Liposomes may activate CS through naturally occurring antibodies targeting phospholipid head groups, cholesterol binding, or anionic phospholipid interaction with C1q, which is positively charged

[260, 261]. Liposomes measuring more than 200 nm are particularly strong CS activators when compared to smaller liposomes of identical composition [262]. It has been shown that subtle physicochemical differences between four different FDA-approved drug-loaded liposomes and liposomes batches, specifically in terms of particle numbers and vesicular population aspect ratios, can alter the complement response [263]. However, these studies concern complement activation in the blood, highlighting how vital it is to carry out studies specific to the CNS. Though NPs often activate the CS after i.v. administration, this affect can be attenuated by using functionalization or stabilizing molecules such as citrem [264].

Another potential neurotoxic effect of NPs is the breakdown of the BBB. Some NPs, including Cu and Ag NPs, can damage the brain vasculature and increase BBB permeability, potentially allowing toxic substances or microorganisms into the CNS [265]. Liposomes that were bi-functionalized with transferrin and cereport, and then used to encapsulate NFG, increased BBB permeability by increasing the width of intercellular TJs and opening endothelial pores [266]. Though this BBB alteration allowed NPs and attached drugs to enter the brain in larger quantities, it also opens the possibility of pathogens entering the brain and causing severe side effects, particularly if the increase in permeability is not transient.

A major problem with NP toxicity studies is that most are carried out *in vitro* using relatively simple cell models and techniques, such as MTT (measuring mitochondrial function) or LDH (measuring cell membrane integrity) assays. These studies do not necessarily translate to the *in vivo* situation. There is an urgent need for *in vivo*

neurotoxicity analysis, as *in vitro* models are extremely limited in their complexity and translation potential. Some promising NPs, including quantum dots and carbon nanotubes, were abandoned because they induced toxicity *in vivo* despite no indications of toxicity *in vitro* [254]. Even *in vivo* models have their disadvantages, as mouse models do not perfectly mimic the disease state in humans [267]. Most toxicity studies are carried out in healthy rats and mice, or transgenic mouse models, with rare examples of NP testing in Cynomolgus monkeys [268]. It is clearly essential to analyze the potential risk of neurotoxicity when designing NPs to target the CNS, including any materials used for functionalization, and evaluate if the therapeutic benefit outweighs any side effects on the brain. Neurotoxicology and biodistribution studies must use appropriate cell and animal models that have neurodegenerated brains with any associated changes in the BBB, specific to the disease being studied.

A new approach for the toxicity screening of NPs involves using Xenopus embryo analysis, which correlates with cell based *in vitro* assays, in order to carry out rapid screening. Such tests should be combined with mammalian cytotoxicity data for a more thorough approach to toxicity evaluation [269].

Currently there is no standard technique to definitively quantify the toxicity of NPs in the brain. It is vital that comprehensive toxicity studies include pharmacokinetic studies, biodistribution, and both acute and chronic toxicological testing of all NPs, considering the unique and varying characteristics of different formulations and their ligands. Formulating NPs using organic and degradable materials could minimize potential toxicity. Furthermore, specificity in their delivery,

in terms of targeting the CNS and specific regions or cells of the brain will limit unwanted side effects.

1.4 SCOPE OF THE THESIS

Overcoming the BBB remains one of the major requirements in pharmaceutical development for neurological disorders. NPs may be a viable tool to approach this problem, but their complex biological interactions, particularly with the BBB, are still unclear. The identification of appropriate and effective ligands targeting the BBB is also a challenge in NP design.

My contribution in this research field has been the identification of new ligands to target and cross the BBB addressing the unanswered question of how to optimize NP passage across the BBB. Two different approaches were used to address this research question. The first involved proteomic analysis of the protein corona formed on gold NPs surface in order to analyze the changes in its composition during the passage across the *in vitro* BBB, with the final aim to identify physiological plasma proteins that could be exploited to boost passage of NPs through the BBB (Chapter 2: Cox *et al*, 2018, ACS Nano). Here I address the question of what happens to the NP protein corona following passage through an *in vitro* model of the BBB and if any identified changes could offer useful insight into effective functionalization of BBB-targeting NPs. Gold NPs were used due to their ease of use and manipulation in terms of corona formation and isolation, and also because they are able to cross the *in vitro* BBB even in the absence of functionalization. A transwell model of the BBB was established using immortalized cerebral microvascular endothelial cells (hCMEC/D3) as it is relatively simple to produce and characterize and produces the tight junctions that are responsible for preventing the paracellular passage of most NPs through the BBB. The second

approach was to study the ability of physiological NPs present in human plasma, i.e. high-density lipoproteins (HDL), to cross the BBB. The crucial features of HDL that contribute to its BBB crossing were identified so that they can then be used to generate biomimetic NPs with the ability to overcome the BBB (Chapter 3: Dal Magro *et al*, submitted).

However, as already discussed, the fact that the BBB is altered in pathological conditions is often overlooked. The question of how NP crossing of the BBB is affected by pathological changes was the final research topic addressed. I focused my attention on analyzing the ability of brain targeting NPs to cross the BBB in a diseased or aged state, in comparison to healthy conditions (Chapter 4: Dal Magro *et al*, 2018, Nanomedicine (Lond)). Well-characterized liposomes were used as their ability to target the brain has previously been published. *In vivo* models of Alzheimer's disease were used as this is one of the most impactful neurodegenerative diseases that currently has no effective treatment, partially due to the inability of therapeutics to penetrate the BBB. The information derived from this research could be useful in identifying new BBB ligands with targets that are differentially expressed in normal versus diseased conditions.

References

[1] N.R. Saunders, J.J. Dreifuss, K.M. Dziegielewska, P.A. Johansson, M.D. Habgood, K. Møllgård, H.C. Bauer, The rights and wrongs of blood-brain barrier permeability studies: a walk through 100 years of history, Front Neurosci 8 (2014) 404.

[2] J.L. Mikitsh, A.M. Chacko, Pathways for small molecule delivery to the central nervous system across the blood-brain barrier, Perspect Medicin Chem 6 (2014) 11-24.

[3] H. Wolburg, S. Noell, A. Mack, K. Wolburg-Buchholz, P. Fallier-Becker, Brain endothelial cells and the glio-vascular complex, Cell Tissue Res 335(1) (2009) 75-96.

[4] V. Muoio, P.B. Persson, M.M. Sendeski, The neurovascular unit - concept review, Acta Physiol (Oxf) 210(4) (2014) 790-8.

[5] N.J. Abbott, L. Rönnbäck, E. Hansson, Astrocyte-endothelial interactions at the blood-brain barrier, Nat Rev Neurosci 7(1) (2006) 41-53.

[6] R. Daneman, A. Prat, The blood-brain barrier, Cold Spring Harb Perspect Biol 7(1) (2015) a020412.

[7] J.M. Anderson, C.M. Van Itallie, Physiology and function of the tight junction, Cold Spring Harb Perspect Biol 1(2) (2009) a002584.

[8] T. Nitta, M. Hata, S. Gotoh, Y. Seo, H. Sasaki, N. Hashimoto, M. Furuse, S. Tsukita, Size-selective loosening of the blood-brain barrier in claudin-5-deficient mice, J Cell Biol 161(3) (2003) 653-60.

[9] M. Saitou, M. Furuse, H. Sasaki, J.D. Schulzke, M. Fromm, H. Takano, T. Noda, S. Tsukita, Complex phenotype of mice lacking occludin, a component of tight junction strands, Mol Biol Cell 11(12) (2000) 4131-42.

[10] P.T. Ronaldson, T.P. Davis, Targeting blood-brain barrier changes during inflammatory pain: an opportunity for optimizing CNS drug delivery, Ther Deliv 2(8) (2011) 1015-41.
[11] A. Armulik, M. Mäe, C. Betsholtz, Pericytes and the blood-brain barrier: recent advances and implications for the delivery of CNS therapy, Ther Deliv 2(4) (2011) 419-22.
[12] M.S. Thomsen, L.J. Routhe, T. Moos, The vascular basement membrane in the healthy and pathological brain, J Cereb Blood Flow Metab 37(10) (2017) 3300-3317.
[13] C.Y. Liu, Y. Yang, W.N. Ju, X. Wang, H.L. Zhang, Emerging Roles of Astrocytes in Neuro-Vascular Unit and the Tripartite Synapse With Emphasis on Reactive Gliosis in the Context of Alzheimer's Disease, Front Cell Neurosci 12 (2018) 193.
[14] Z. Zador, O. Bloch, X. Yao, G.T. Manley, Aquaporins: role in cerebral edema and brain water balance, Prog Brain Res 161 (2007) 185-94.
[15] M. Blanchette, R. Daneman, Formation and maintenance of the BBB, Mech Dev 138 Pt 1 (2015) 8-16.
[16] D.J. Begley, Delivery of therapeutic agents to the central nervous system: the problems and the possibilities, Pharmacol Ther 104(1) (2004) 29-45.
[17] G. Del Vecchio, C. Tscheik, K. Tenz, H.C. Helms, L. Winkler, R. Blasig, I.E. Blasig, Sodium caprate transiently opens claudin-5-containing barriers at tight junctions of epithelial and endothelial cells, Mol Pharm 9(9) (2012) 2523-33.

[18] C. Greene, M. Campbell, Tight junction modulation of the blood brain barrier: CNS delivery of small molecules, Tissue Barriers 4(1) (2016) e1138017.

[19] S. Tavelin, K. Hashimoto, J. Malkinson, L. Lazorova, I. Toth, P. Artursson, A new principle for tight junction modulation based on occludin peptides, Mol Pharmacol 64(6) (2003) 1530-40.

[20] I. Mäger, A.H. Meyer, J. Li, M. Lenter, T. Hildebrandt, G. Leparc, M.J.A. Wood, Targeting blood-brain-barrier transcytosis - perspectives for drug delivery, Neuropharmacology 120 (2017) 4-7.

[21] B.M. Fu, Experimental methods and transport models for drug delivery across the blood-brain barrier, Curr Pharm Biotechnol 13(7) (2012) 1346-59.

[22] J.E. Preston, N. Joan Abbott, D.J. Begley, Transcytosis of macromolecules at the blood-brain barrier, Adv Pharmacol 71 (2014) 147-63.

[23] L. Sanchez-Covarrubias, L.M. Slosky, B.J. Thompson, T.P. Davis, P.T. Ronaldson, Transporters at CNS barrier sites: obstacles or opportunities for drug delivery?, Curr Pharm Des 20(10) (2014) 1422-49.

[24] N. Strazielle, J.F. Ghersi-Egea, Efflux transporters in blood-brain interfaces of the developing brain, Front Neurosci 9 (2015) 21.

[25] A. Spudich, E. Kilic, H. Xing, U. Kilic, K.M. Rentsch, H. Wunderli-Allenspach, C.L. Bassetti, D.M. Hermann, Inhibition of multidrug resistance transporter-1 facilitates neuroprotective therapies after focal cerebral ischemia, Nat Neurosci 9(4) (2006) 487-8.

[26] F. Hervé, N. Ghinea, J.M. Scherrmann, CNS delivery via adsorptive transcytosis, AAPS J 10(3) (2008) 455-72.

[27] Q. Wang, Z. Zuo, Impact of transporters and enzymes from blood-cerebrospinal fluid barrier and brain parenchyma on CNS drug uptake, Expert Opin Drug Metab Toxicol 14(9) (2018) 961-972.
[28] C.D. Chapman, W.H. Frey, S. Craft, L. Danielyan, M. Hallschmid, H.B. Schiöth, C. Benedict, Intranasal treatment of central nervous system dysfunction in humans, Pharm Res 30(10) (2013) 2475-84.
[29] C.T. Lu, Y.Z. Zhao, H.L. Wong, J. Cai, L. Peng, X.Q. Tian, Current approaches to enhance CNS delivery of drugs across the brain barriers, Int J Nanomedicine 9 (2014) 2241-57.
[30] N.H. Greig, Optimizing drug delivery to brain tumors, Cancer Treat Rev 14(1) (1987) 1-28.
[31] R.E. Harbaugh, R.L. Saunders, R.F. Reeder, Use of implantable pumps for central nervous system drug infusions to treat neurological disease, Neurosurgery 23(6) (1988) 693-8.
[32] J. Cunningham, P. Pivirotto, J. Bringas, B. Suzuki, S. Vijay, L. Sanftner, M. Kitamura, C. Chan, K.S. Bankiewicz, Biodistribution of adeno-associated virus type-2 in nonhuman primates after convection-enhanced delivery to brain, Mol Ther 16(7) (2008) 1267-75.
[33] E.A. Neuwelt, Mechanisms of disease: the blood-brain barrier, Neurosurgery 54(1) (2004) 131-40; discussion 141-2.
[34] S.I. Rapoport, P.J. Robinson, Tight-junctional modification as the basis of osmotic opening of the blood-brain barrier, Ann N Y Acad Sci 481 (1986) 250-67.
[35] T.F. Cloughesy, K.L. Black, Pharmacological blood-brain barrier modification for selective drug delivery, J Neurooncol 26(2) (1995) 125-32.

[36] M. Aryal, C.D. Arvanitis, P.M. Alexander, N. McDannold, Ultrasound-mediated blood-brain barrier disruption for targeted drug delivery in the central nervous system, Adv Drug Deliv Rev 72 (2014) 94-109.
[37] I. Wilhelm, I.A. Krizbai, In vitro models of the blood-brain barrier for the study of drug delivery to the brain, Mol Pharm 11(7) (2014) 1949-63.
[38] B. Weksler, I.A. Romero, P.O. Couraud, The hCMEC/D3 cell line as a model of the human blood brain barrier, Fluids Barriers CNS 10(1) (2013) 16.
[39] E. Salvati, F. Re, S. Sesana, I. Cambianica, G. Sancini, M. Masserini, M. Gregori, Liposomes functionalized to overcome the blood-brain barrier and to target amyloid-β peptide: the chemical design affects the permeability across an in vitro model, Int J Nanomedicine 8 (2013) 1749-58.
[40] G. Lazzari, V. Nicolas, M. Matsusaki, M. Akashi, P. Couvreur, S. Mura, Multicellular spheroid based on a triple co-culture: A novel 3D model to mimic pancreatic tumor complexity, Acta Biomater 78 (2018) 296-307.
[41] R.M. Marton, S.P. Paşca, Neural Differentiation in the Third Dimension: Generating a Human Midbrain, Cell Stem Cell 19(2) (2016) 145-146.
[42] A.M. Paşca, S.A. Sloan, L.E. Clarke, Y. Tian, C.D. Makinson, N. Huber, C.H. Kim, J.Y. Park, N.A. O'Rourke, K.D. Nguyen, S.J. Smith, J.R. Huguenard, D.H. Geschwind, B.A. Barres, S.P. Paşca, Functional cortical neurons and astrocytes from human pluripotent stem cells in 3D culture, Nat Methods 12(7) (2015) 671-8.

[43] E.D. Osipova, Y.K. Komleva, A.V. Morgun, O.L. Lopatina, Y.A. Panina, R.Y. Olovyannikova, E.F. Vais, V.V. Salmin, A.B. Salmina, Designing, Front Aging Neurosci 10 (2018) 234.
[44] L. Cucullo, M. Hossain, V. Puvenna, N. Marchi, D. Janigro, The role of shear stress in Blood-Brain Barrier endothelial physiology, BMC Neurosci 12 (2011) 40.
[45] M.W. van der Helm, A.D. van der Meer, J.C. Eijkel, A. van den Berg, L.I. Segerink, Microfluidic organ-on-chip technology for blood-brain barrier research, Tissue Barriers 4(1) (2016) e1142493.
[46] M. Bonakdar, P.M. Graybill, R.V. Davalos, A microfluidic model of the blood-brain barrier to study permeabilization by pulsed electric fields, RSC Adv 7(68) (2017) 42811-42818.
[47] V.V. Salmin, Y.K. Komleva, N.V. Kuvacheva, A.V. Morgun, E.D. Khilazheva, O.L. Lopatina, E.A. Pozhilenkova, K.A. Shapovalov, Y.A. Uspenskaya, A.B. Salmina, Differential Roles of Environmental Enrichment in Alzheimer's Type of Neurodegeneration and Physiological Aging, Front Aging Neurosci 9 (2017) 245.
[48] V. Francia, A. Aliyandi, A. Salvati, Effect of the development of a cell barrier on nanoparticle uptake in endothelial cells, Nanoscale 10(35) (2018) 16645-16656.
[49] A.A. Toropov, A.P. Toropova, M. Beeg, M. Gobbi, M. Salmona, QSAR model for blood-brain barrier permeation, J Pharmacol Toxicol Methods 88(Pt 1) (2017) 7-18.
[50] Y. Zeinolabediny, F. Caccuri, L. Colombo, F. Morelli, M. Romeo, A. Rossi, S. Schiarea, C. Ciaramelli, C. Airoldi, R. Weston, L. Donghui, J. Krupinski, R. Corpas, E. García-Lara, S. Sarroca, C. Sanfeliu, M. Slevin, A. Caruso, M. Salmona, L. Diomede, HIV-1 matrix protein p17

misfolding forms toxic amyloidogenic assemblies that induce neurocognitive disorders, Sci Rep 7(1) (2017) 10313.

[51] A.D. Gitler, P. Dhillon, J. Shorter, Neurodegenerative disease: models, mechanisms, and a new hope, Dis Model Mech 10(5) (2017) 499-502.

[52] Fact Sheet Dementia, 2017. http://www.who.int/news-room/fact-sheets/detail/dementia. (Accessed 03/10/18 2018).

[53] L. Bertram, R.E. Tanzi, The genetic epidemiology of neurodegenerative disease, J Clin Invest 115(6) (2005) 1449-57.

[54] S. Weintraub, A.H. Wicklund, D.P. Salmon, The neuropsychological profile of Alzheimer disease, Cold Spring Harb Perspect Med 2(4) (2012) a006171.

[55] V.K. Ramanan, A.J. Saykin, Pathways to neurodegeneration: mechanistic insights from GWAS in Alzheimer's disease, Parkinson's disease, and related disorders, Am J Neurodegener Dis 2(3) (2013) 145-75.

[56] H. Niu, I. Álvarez-Álvarez, F. Guillén-Grima, I. Aguinaga-Ontoso, Prevalence and incidence of Alzheimer's disease in Europe: A meta-analysis, Neurologia 32(8) (2017) 523-532.

[57] A. Wimo, L. Jönsson, A. Gustavsson, D. McDaid, K. Ersek, J. Georges, L. Gulácsi, K. Karpati, P. Kenigsberg, H. Valtonen, The economic impact of dementia in Europe in 2008-cost estimates from the Eurocode project, Int J Geriatr Psychiatry 26(8) (2011) 825-32.

[58] S.Y. Hung, W.M. Fu, Drug candidates in clinical trials for Alzheimer's disease, J Biomed Sci 24(1) (2017) 47.

[59] G. Di Fede, G. Giaccone, M. Salmona, F. Tagliavini, Translational Research in Alzheimer's and Prion Diseases, J Alzheimers Dis 62(3) (2018) 1247-1259.
[60] B.N. Dugger, D.W. Dickson, Pathology of Neurodegenerative Diseases, Cold Spring Harb Perspect Biol 9(7) (2017).
[61] E. Maderna, L. Colombo, A. Cagnotto, G. Di Fede, A. Indaco, F. Tagliavini, M. Salmona, G. Giaccone, In Situ Tissue Labeling of Cerebral Amyloid Using HIV-Related Tat Peptide, Mol Neurobiol 55(8) (2018) 6834-6840.
[62] R.A. Sperling, J. Karlawish, K.A. Johnson, Preclinical Alzheimer disease-the challenges ahead, Nat Rev Neurol 9(1) (2013) 54-8.
[63] W. Poewe, K. Seppi, C.M. Tanner, G.M. Halliday, P. Brundin, J. Volkmann, A.E. Schrag, A.E. Lang, Parkinson disease, Nat Rev Dis Primers 3 (2017) 17013.
[64] C. Henchcliffe, M.F. Beal, Mitochondrial biology and oxidative stress in Parkinson disease pathogenesis, Nat Clin Pract Neurol 4(11) (2008) 600-9.
[65] P. McColgan, S.J. Tabrizi, Huntington's disease: a clinical review, European Journal of Neurology 25(1) (2018) 24-34.
[66] M. Hutton, C.L. Lendon, P. Rizzu, M. Baker, S. Froelich, H. Houlden, S. Pickering-Brown, S. Chakraverty, A. Isaacs, A. Grover, J. Hackett, J. Adamson, S. Lincoln, D. Dickson, P. Davies, R.C. Petersen, M. Stevens, E. de Graaff, E. Wauters, J. van Baren, M. Hillebrand, M. Joosse, J.M. Kwon, P. Nowotny, L.K. Che, J. Norton, J.C. Morris, L.A. Reed, J. Trojanowski, H. Basun, L. Lannfelt, M. Neystat, S. Fahn, F. Dark, T. Tannenberg, P.R. Dodd, N. Hayward, J.B. Kwok, P.R. Schofield, A. Andreadis, J. Snowden, D. Craufurd, D. Neary, F. Owen,

B.A. Oostra, J. Hardy, A. Goate, J. van Swieten, D. Mann, T. Lynch, P. Heutink, Association of missense and 5'-splice-site mutations in tau with the inherited dementia FTDP-17, Nature 393(6686) (1998) 702-5.
[67] J.J. Young, M. Lavakumar, D. Tampi, S. Balachandran, R.R. Tampi, Frontotemporal dementia: latest evidence and clinical implications, Ther Adv Psychopharmacol 8(1) (2018) 33-48.
[68] W.W. Chen, X. Zhang, W.J. Huang, Role of neuroinflammation in neurodegenerative diseases (Review), Mol Med Rep 13(4) (2016) 3391-6.
[69] D.S. Reich, C.F. Lucchinetti, P.A. Calabresi, Multiple Sclerosis, N Engl J Med 378(2) (2018) 169-180.
[70] R.S. Finkel, C.A. Chiriboga, J. Vajsar, J.W. Day, J. Montes, D.C. De Vivo, M. Yamashita, F. Rigo, G. Hung, E. Schneider, D.A. Norris, S. Xia, C.F. Bennett, K.M. Bishop, Treatment of infantile-onset spinal muscular atrophy with nusinersen: a phase 2, open-label, dose-escalation study, Lancet 388(10063) (2016) 3017-3026.
[71] P.K. Pandey, A.K. Sharma, U. Gupta, Blood brain barrier: An overview on strategies in drug delivery, realistic in vitro modeling and in vivo live tracking, Tissue Barriers 4(1) (2016) e1129476.
[72] G.A. Rosenberg, Neurological diseases in relation to the blood-brain barrier, J Cereb Blood Flow Metab 32(7) (2012) 1139-51.
[73] W.A. Banks, A.M. Gray, M.A. Erickson, T.S. Salameh, M. Damodarasamy, N. Sheibani, J.S. Meabon, E.E. Wing, Y. Morofuji, D.G. Cook, M.J. Reed, Lipopolysaccharide-induced blood-brain barrier disruption: roles of cyclooxygenase, oxidative stress, neuroinflammation, and elements of the neurovascular unit, J Neuroinflammation 12 (2015) 223.

[74] M. Fiala, D.J. Looney, M. Stins, D.D. Way, L. Zhang, X. Gan, F. Chiappelli, E.S. Schweitzer, P. Shapshak, M. Weinand, M.C. Graves, M. Witte, K.S. Kim, TNF-alpha opens a paracellular route for HIV-1 invasion across the blood-brain barrier, Mol Med 3(8) (1997) 553-64.

[75] B. Wispelwey, A.J. Lesse, E.J. Hansen, W.M. Scheld, Haemophilus influenzae lipopolysaccharide-induced blood brain barrier permeability during experimental meningitis in the rat, J Clin Invest 82(4) (1988) 1339-46.

[76] A.T. Argaw, L. Asp, J. Zhang, K. Navrazhina, T. Pham, J.N. Mariani, S. Mahase, D.J. Dutta, J. Seto, E.G. Kramer, N. Ferrara, M.V. Sofroniew, G.R. John, Astrocyte-derived VEGF-A drives blood-brain barrier disruption in CNS inflammatory disease, J Clin Invest 122(7) (2012) 2454-68.

[77] P.T. Ronaldson, K.M. Demarco, L. Sanchez-Covarrubias, C.M. Solinsky, T.P. Davis, Transforming growth factor-beta signaling alters substrate permeability and tight junction protein expression at the blood-brain barrier during inflammatory pain, J Cereb Blood Flow Metab 29(6) (2009) 1084-98.

[78] D.H. Miller, A.J. Thompson, S.P. Morrissey, D.G. MacManus, S.G. Moore, B.E. Kendall, I.F. Moseley, W.I. McDonald, High dose steroids in acute relapses of multiple sclerosis: MRI evidence for a possible mechanism of therapeutic effect, J Neurol Neurosurg Psychiatry 55(6) (1992) 450-3.

[79] K.G. Blecharz, A. Haghikia, M. Stasiolek, N. Kruse, D. Drenckhahn, R. Gold, N. Roewer, A. Chan, C.Y. Förster, Glucocorticoid effects on endothelial barrier function in the murine

brain endothelial cell line cEND incubated with sera from patients with multiple sclerosis, Mult Scler 16(3) (2010) 293-302.
[80] C. Balducci, G. Santamaria, P. La Vitola, E. Brandi, F. Grandi, A.R. Viscomi, M. Beeg, M. Gobbi, M. Salmona, S. Ottonello, G. Forloni, Doxycycline counteracts neuroinflammation restoring memory in Alzheimer's disease mouse models, Neurobiol Aging 70 (2018) 128-139.
[81] J. He, H. Hsuchou, Y. He, A.J. Kastin, Y. Wang, W. Pan, Sleep restriction impairs blood-brain barrier function, J Neurosci 34(44) (2014) 14697-706.
[82] B. Gómez-González, G. Hurtado-Alvarado, E. Esqueda-León, R. Santana-Miranda, J. Rojas-Zamorano, J. Velázquez-Moctezuma, REM sleep loss and recovery regulates blood-brain barrier function, Curr Neurovasc Res 10(3) (2013) 197-207.
[83] N. Weiss, F. Miller, S. Cazaubon, P.O. Couraud, The blood-brain barrier in brain homeostasis and neurological diseases, Biochim Biophys Acta 1788(4) (2009) 842-57.
[84] R.D. Bell, The imbalance of vascular molecules in Alzheimer's disease, J Alzheimers Dis 32(3) (2012) 699-709.
[85] D.M. van Assema, M. Lubberink, P. Rizzu, J.C. van Swieten, R.C. Schuit, J. Eriksson, P. Scheltens, M. Koepp, A.A. Lammertsma, B.N. van Berckel, Blood-brain barrier P-glycoprotein function in healthy subjects and Alzheimer's disease patients: effect of polymorphisms in the ABCB1 gene, EJNMMI Res 2(1) (2012) 57.
[86] M.O. Romanitan, B.O. Popescu, S. Spulber, O. Băjenaru, L.M. Popescu, B. Winblad, N. Bogdanovic, Altered expression of claudin

family proteins in Alzheimer's disease and vascular dementia brains, J Cell Mol Med 14(5) (2010) 1088-100.
[87] Y. Yang, E.Y. Estrada, J.F. Thompson, W. Liu, G.A. Rosenberg, Matrix metalloproteinase-mediated disruption of tight junction proteins in cerebral vessels is reversed by synthetic matrix metalloproteinase inhibitor in focal ischemia in rat, J Cereb Blood Flow Metab 27(4) (2007) 697-709.
[88] G.A. Rosenberg, E.Y. Estrada, J.E. Dencoff, Matrix metalloproteinases and TIMPs are associated with blood-brain barrier opening after reperfusion in rat brain, Stroke 29(10) (1998) 2189-95.
[89] D.H. Miller, O.A. Khan, W.A. Sheremata, L.D. Blumhardt, G.P. Rice, M.A. Libonati, A.J. Willmer-Hulme, C.M. Dalton, K.A. Miszkiel, P.W. O'Connor, I.N.M.S.T. Group, A controlled trial of natalizumab for relapsing multiple sclerosis, N Engl J Med 348(1) (2003) 15-23.
[90] S. Garbuzova-Davis, E. Haller, S. Saporta, I. Kolomey, S.V. Nicosia, P.R. Sanberg, Ultrastructure of blood-brain barrier and blood-spinal cord barrier in SOD1 mice modeling ALS, Brain Res 1157 (2007) 126-37.
[91] G.A. Rosenberg, J.E. Dencoff, N. Correa, M. Reiners, C.C. Ford, Effect of steroids on CSF matrix metalloproteinases in multiple sclerosis: relation to blood-brain barrier injury, Neurology 46(6) (1996) 1626-32.
[92] N. Matsukawa, T. Yasuhara, K. Hara, L. Xu, M. Maki, G. Yu, Y. Kaneko, K. Ojika, D.C. Hess, C.V. Borlongan, Therapeutic targets and limits of minocycline neuroprotection in experimental ischemic stroke, BMC Neurosci 10 (2009) 126.

[93] S.C. Fagan, J.L. Waller, F.T. Nichols, D.J. Edwards, L.C. Pettigrew, W.M. Clark, C.E. Hall, J.A. Switzer, A. Ergul, D.C. Hess, Minocycline to improve neurologic outcome in stroke (MINOS): a dose-finding study, Stroke 41(10) (2010) 2283-7.
[94] C.R. Harrington, The molecular pathology of Alzheimer's disease, Neuroimaging Clin N Am 22(1) (2012) 11-22, vii.
[95] D.J. Selkoe, Cell biology of the amyloid beta-protein precursor and the mechanism of Alzheimer's disease, Annu Rev Cell Biol 10 (1994) 373-403.
[96] Y. Lu, P. Derreumaux, Z. Guo, N. Mousseau, G. Wei, Thermodynamics and dynamics of amyloid peptide oligomerization are sequence dependent, Proteins 75(4) (2009) 954-63.
[97] C. Patterson, J.W. Feightner, A. Garcia, G.Y.R. Hsiung, C. MacKnight, A.D. Sadovnick, Diagnosis and treatment of dementia: 1. Risk assessment and primary prevention of Alzheimer disease, CMAJ : Canadian Medical Association Journal 178(5) (2008) 548-556.
[98] A.A. Rensink, R.M. de Waal, B. Kremer, M.M. Verbeek, Pathogenesis of cerebral amyloid angiopathy, Brain Res Brain Res Rev 43(2) (2003) 207-23.
[99] M. Bartolini, C. Bertucci, M.L. Bolognesi, A. Cavalli, C. Melchiorre, V. Andrisano, Insight into the kinetic of amyloid beta (1-42) peptide self-aggregation: elucidation of inhibitors' mechanism of action, Chembiochem 8(17) (2007) 2152-61.
[100] F. Tagliavini, G. Giaccone, B. Frangione, O. Bugiani, Preamyloid deposits in the cerebral cortex of patients with Alzheimer's disease and nondemented individuals, Neurosci Lett 93(2-3) (1988) 191-6.

[101] K. Ono, M.M. Condron, D.B. Teplow, Structure-neurotoxicity relationships of amyloid beta-protein oligomers, Proc Natl Acad Sci U S A 106(35) (2009) 14745-50.
[102] C.A. McLean, R.A. Cherny, F.W. Fraser, S.J. Fuller, M.J. Smith, K. Beyreuther, A.I. Bush, C.L. Masters, Soluble pool of Abeta amyloid as a determinant of severity of neurodegeneration in Alzheimer's disease, Ann Neurol 46(6) (1999) 860-6.
[103] G.M. Shankar, D.M. Walsh, Alzheimer's disease: synaptic dysfunction and Abeta, Mol Neurodegener 4 (2009) 48.
[104] C. Balducci, A. Frasca, M. Zotti, P. La Vitola, E. Mhillaj, E. Grigoli, M. Iacobellis, F. Grandi, M. Messa, L. Colombo, M. Molteni, L. Trabace, C. Rossetti, M. Salmona, G. Forloni, Toll-like receptor 4-dependent glial cell activation mediates the impairment in memory establishment induced by β-amyloid oligomers in an acute mouse model of Alzheimer's disease, Brain Behav Immun 60 (2017) 188-197.
[105] M.R. Farlow, M.L. Miller, V. Pejovic, Treatment options in Alzheimer's disease: maximizing benefit, managing expectations, Dement Geriatr Cogn Disord 25(5) (2008) 408-22.
[106] C. Soto, Unfolding the role of protein misfolding in neurodegenerative diseases, Nat Rev Neurosci 4(1) (2003) 49-60.
[107] D. Scheuner, C. Eckman, M. Jensen, X. Song, M. Citron, N. Suzuki, T.D. Bird, J. Hardy, M. Hutton, W. Kukull, E. Larson, E. Levy-Lahad, M. Viitanen, E. Peskind, P. Poorkaj, G. Schellenberg, R. Tanzi, W. Wasco, L. Lannfelt, D. Selkoe, S. Younkin, Secreted amyloid beta-protein similar to that in the senile plaques of Alzheimer's disease is increased in vivo by the presenilin 1 and 2 and APP mutations linked to familial Alzheimer's disease, Nat Med 2(8) (1996) 864-70.

[108] A. Snellman, F.R. López-Picón, J. Rokka, M. Salmona, G. Forloni, M. Scheinin, O. Solin, J.O. Rinne, M. Haaparanta-Solin, Longitudinal amyloid imaging in mouse brain with 11C-PIB: comparison of APP23, Tg2576, and APPswe-PS1dE9 mouse models of Alzheimer disease, J Nucl Med 54(8) (2013) 1434-41.
[109] J.C. Dodart, C. Mathis, K.R. Bales, S.M. Paul, Does my mouse have Alzheimer's disease?, Genes Brain Behav 1(3) (2002) 142-55.
[110] C. Duyckaerts, M.C. Potier, B. Delatour, Alzheimer disease models and human neuropathology: similarities and differences, Acta Neuropathol 115(1) (2008) 5-38.
[111] S.H. Barage, K.D. Sonawane, Amyloid cascade hypothesis: Pathogenesis and therapeutic strategies in Alzheimer's disease, Neuropeptides 52 (2015) 1-18.
[112] Y. Cheng, F. Bai, The Association of Tau With Mitochondrial Dysfunction in Alzheimer's Disease, Front Neurosci 12 (2018) 163.
[113] C. Guzzi, L. Colombo, A. Luigi, M. Salmona, F. Nicotra, C. Airoldi, Flavonoids and Their Glycosides as Anti-amyloidogenic Compounds: Aβ1-42 Interaction Studies to Gain New Insights into Their Potential for Alzheimer's Disease Prevention and Therapy, Chem Asian J 12(1) (2017) 67-75.
[114] M. Romeo, M. Stravalaci, M. Beeg, A. Rossi, F. Fiordaliso, A. Corbelli, M. Salmona, M. Gobbi, A. Cagnotto, L. Diomede, Humanin Specifically Interacts with Amyloid-β Oligomers and Counteracts Their in vivo Toxicity, J Alzheimers Dis 57(3) (2017) 857-871.
[115] M. Beeg, M. Stravalaci, M. Romeo, A.D. Carrá, A. Cagnotto, A. Rossi, L. Diomede, M. Salmona, M. Gobbi, Clusterin Binds to Aβ1-42 Oligomers with High Affinity and Interferes with Peptide Aggregation

by Inhibiting Primary and Secondary Nucleation, J Biol Chem 291(13) (2016) 6958-66.

[116] M.F.M. Sciacca, V. Romanucci, A. Zarrelli, I. Monaco, F. Lolicato, N. Spinella, C. Galati, G. Grasso, L. D'Urso, M. Romeo, L. Diomede, M. Salmona, C. Bongiorno, G. Di Fabio, C. La Rosa, D. Milardi, Inhibition of Aβ Amyloid Growth and Toxicity by Silybins: The Crucial Role of Stereochemistry, ACS Chem Neurosci 8(8) (2017) 1767-1778.

[117] B. Georgievska, S. Gustavsson, J. Lundkvist, J. Neelissen, S. Eketjäll, V. Ramberg, T. Bueters, K. Agerman, A. Juréus, S. Svensson, S. Berg, J. Fälting, U. Lendahl, Revisiting the peripheral sink hypothesis: inhibiting BACE1 activity in the periphery does not alter β-amyloid levels in the CNS, J Neurochem 132(4) (2015) 477-86.

[118] J.L. Chang, A.J. Hinrich, B. Roman, M. Norrbom, F. Rigo, R.A. Marr, E.M. Norstrom, M.L. Hastings, Targeting Amyloid-β Precursor Protein, APP, Splicing with Antisense Oligonucleotides Reduces Toxic Amyloid-β Production, Mol Ther 26(6) (2018) 1539-1551.

[119] D.L. Brody, D.M. Holtzman, Active and passive immunotherapy for neurodegenerative disorders, Annu Rev Neurosci 31 (2008) 175-93.

[120] D.J. Selkoe, Resolving controversies on the path to Alzheimer's therapeutics, Nat Med 17(9) (2011) 1060-5.

[121] S. Mancini, S. Minniti, M. Gregori, G. Sancini, A. Cagnotto, P.O. Couraud, L. Ordóñez-Gutiérrez, F. Wandosell, M. Salmona, F. Re, The hunt for brain Aβ oligomers by peripherally circulating multi-functional nanoparticles: Potential therapeutic approach for Alzheimer disease, Nanomedicine 12(1) (2016) 43-52.

[122] W.S. Jin, L.L. Shen, X.L. Bu, W.W. Zhang, S.H. Chen, Z.L. Huang, J.X. Xiong, C.Y. Gao, Z. Dong, Y.N. He, Z.A. Hu, H.D. Zhou, W. Song, X.F. Zhou, Y.Z. Wang, Y.J. Wang, Peritoneal dialysis reduces amyloid-beta plasma levels in humans and attenuates Alzheimer-associated phenotypes in an APP/PS1 mouse model, Acta Neuropathol 134(2) (2017) 207-220.
[123] M.W. Wong, N. Braidy, A. Poljak, R. Pickford, M. Thambisetty, P.S. Sachdev, Dysregulation of lipids in Alzheimer's disease and their role as potential biomarkers, Alzheimers Dement 13(7) (2017) 810-827.
[124] D. Cheng, A.M. Jenner, G. Shui, W.F. Cheong, T.W. Mitchell, J.R. Nealon, W.S. Kim, H. McCann, M.R. Wenk, G.M. Halliday, B. Garner, Lipid pathway alterations in Parkinson's disease primary visual cortex, PLoS One 6(2) (2011) e17299.
[125] D.L. Sparks, Alzheimer disease: statins in the treatment of Alzheimer disease, Nat Rev Neurol 7(12) (2011) 662-3.
[126] X. Gao, K.C. Simon, M.A. Schwarzschild, A. Ascherio, Prospective study of statin use and risk of Parkinson disease, Arch Neurol 69(3) (2012) 380-4.
[127] K. Matsuzaki, Physicochemical interactions of amyloid beta-peptide with lipid bilayers, Biochim Biophys Acta 1768(8) (2007) 1935-42.
[128] V. Rondelli, P. Brocca, S. Motta, M. Messa, L. Colombo, M. Salmona, G. Fragneto, L. Cantù, E. Del Favero, Amyloid-β peptides in interaction with raft-mime model membranes: a neutron reflectivity insight, Sci Rep 6 (2016) 20997.
[129] I.J. Martins, E. Hone, J.K. Foster, S.I. Sünram-Lea, A. Gnjec, S.J. Fuller, D. Nolan, S.E. Gandy, R.N. Martins, Apolipoprotein E,

cholesterol metabolism, diabetes, and the convergence of risk factors for Alzheimer's disease and cardiovascular disease, Mol Psychiatry 11(8) (2006) 721-36.

[130] D.M. Holtzman, J. Herz, G. Bu, Apolipoprotein E and apolipoprotein E receptors: normal biology and roles in Alzheimer disease, Cold Spring Harb Perspect Med 2(3) (2012) a006312.

[131] J.M. Castellano, J. Kim, F.R. Stewart, H. Jiang, R.B. DeMattos, B.W. Patterson, A.M. Fagan, J.C. Morris, K.G. Mawuenyega, C. Cruchaga, A.M. Goate, K.R. Bales, S.M. Paul, R.J. Bateman, D.M. Holtzman, Human apoE isoforms differentially regulate brain amyloid-β peptide clearance, Sci Transl Med 3(89) (2011) 89ra57.

[132] C. Conejero-Goldberg, J.J. Gomar, T. Bobes-Bascaran, T.M. Hyde, J.E. Kleinman, M.M. Herman, S. Chen, P. Davies, T.E. Goldberg, APOE2 enhances neuroprotection against Alzheimer's disease through multiple molecular mechanisms, Mol Psychiatry 19(11) (2014) 1243-50.

[133] M. Kivipelto, E.L. Helkala, M.P. Laakso, T. Hänninen, M. Hallikainen, K. Alhainen, S. Iivonen, A. Mannermaa, J. Tuomilehto, A. Nissinen, H. Soininen, Apolipoprotein E epsilon4 allele, elevated midlife total cholesterol level, and high midlife systolic blood pressure are independent risk factors for late-life Alzheimer disease, Ann Intern Med 137(3) (2002) 149-55.

[134] F. Song, A. Poljak, J. Crawford, N.A. Kochan, W. Wen, B. Cameron, O. Lux, H. Brodaty, K. Mather, G.A. Smythe, P.S. Sachdev, Plasma apolipoprotein levels are associated with cognitive status and decline in a community cohort of older individuals, PLoS One 7(6) (2012) e34078.

[135] H. Xiong, D. Callaghan, A. Jones, D.G. Walker, L.F. Lue, T.G. Beach, L.I. Sue, J. Woulfe, H. Xu, D.B. Stanimirovic, W. Zhang, Cholesterol retention in Alzheimer's brain is responsible for high beta- and gamma-secretase activities and Abeta production, Neurobiol Dis 29(3) (2008) 422-37.
[136] A. Schneider, W. Schulz-Schaeffer, T. Hartmann, J.B. Schulz, M. Simons, Cholesterol depletion reduces aggregation of amyloid-beta peptide in hippocampal neurons, Neurobiol Dis 23(3) (2006) 573-7.
[137] H. Wang, R.H. Eckel, What are lipoproteins doing in the brain?, Trends Endocrinol Metab 25(1) (2014) 8-14.
[138] C. Vitali, C.L. Wellington, L. Calabresi, HDL and cholesterol handling in the brain, Cardiovasc Res 103(3) (2014) 405-13.
[139] A. Merched, Y. Xia, S. Visvikis, J.M. Serot, G. Siest, Decreased high-density lipoprotein cholesterol and serum apolipoprotein AI concentrations are highly correlated with the severity of Alzheimer's disease, Neurobiol Aging 21(1) (2000) 27-30.
[140] G. Liu, M.R. Garrett, P. Men, X. Zhu, G. Perry, M.A. Smith, Nanoparticle and other metal chelation therapeutics in Alzheimer disease, Biochim Biophys Acta 1741(3) (2005) 246-52.
[141] A. Hye, J. Riddoch-Contreras, A.L. Baird, N.J. Ashton, C. Bazenet, R. Leung, E. Westman, A. Simmons, R. Dobson, M. Sattlecker, M. Lupton, K. Lunnon, A. Keohane, M. Ward, I. Pike, H.D. Zucht, D. Pepin, W. Zheng, A. Tunnicliffe, J. Richardson, S. Gauthier, H. Soininen, I. Kłoszewska, P. Mecocci, M. Tsolaki, B. Vellas, S. Lovestone, Plasma proteins predict conversion to dementia from prodromal disease, Alzheimers Dement 10(6) (2014) 799-807.e2.

[142] Y.H. Shih, K.J. Tsai, C.W. Lee, S.C. Shiesh, W.T. Chen, M.C. Pai, Y.M. Kuo, Apolipoprotein C-III is an amyloid-β-binding protein and an early marker for Alzheimer's disease, J Alzheimers Dis 41(3) (2014) 855-65.
[143] D.A. Elliott, C.S. Weickert, B. Garner, Apolipoproteins in the brain: implications for neurological and psychiatric disorders, Clin Lipidol 51(4) (2010) 555-573.
[144] H.C. Liu, C.J. Hu, J.G. Chang, S.M. Sung, L.S. Lee, R.Y. Yuan, S.J. Leu, Proteomic identification of lower apolipoprotein A-I in Alzheimer's disease, Dement Geriatr Cogn Disord 21(3) (2006) 155-61.
[145] S.M. Moghimi, A.C. Hunter, J.C. Murray, Nanomedicine: current status and future prospects, FASEB J 19(3) (2005) 311-30.
[146] R. Ferrari, L. Talamini, M.B. Violatto, P. Giangregorio, M. Sponchioni, M. Morbidelli, M. Salmona, P. Bigini, D. Moscatelli, Biocompatible Polymer Nanoformulation To Improve the Release and Safety of a Drug Mimic Molecule Detectable via ICP-MS, Mol Pharm 14(1) (2017) 124-134.
[147] K.C. Petkar, S.S. Chavhan, S. Agatonovik-Kustrin, K.K. Sawant, Nanostructured materials in drug and gene delivery: a review of the state of the art, Crit Rev Ther Drug Carrier Syst 28(2) (2011) 101-64.
[148] S.M. Moghimi, J. Szebeni, Stealth liposomes and long circulating nanoparticles: critical issues in pharmacokinetics, opsonization and protein-binding properties, Prog Lipid Res 42(6) (2003) 463-78.
[149] E. Blanco, H. Shen, M. Ferrari, Principles of nanoparticle design for overcoming biological barriers to drug delivery, Nat Biotechnol 33(9) (2015) 941-51.

[150] G. Wang, J.I. Griffin, S. Inturi, B. Brenneman, N.K. Banda, V.M. Holers, S.M. Moghimi, D. Simberg, and, Front Immunol 8 (2017) 151.
[151] S. Inturi, G. Wang, F. Chen, N.K. Banda, V.M. Holers, L. Wu, S.M. Moghimi, D. Simberg, Modulatory Role of Surface Coating of Superparamagnetic Iron Oxide Nanoworms in Complement Opsonization and Leukocyte Uptake, ACS Nano 9(11) (2015) 10758-68.
[152] K. Vahidkhah, P. Bagchi, Microparticle shape effects on margination, near-wall dynamics and adhesion in a three-dimensional simulation of red blood cell suspension, Soft Matter 11(11) (2015) 2097-109.
[153] M. Masserini, Nanoparticles for brain drug delivery, ISRN Biochem 2013 (2013) 238428.
[154] H. Hillaireau, P. Couvreur, Nanocarriers' entry into the cell: relevance to drug delivery, Cell Mol Life Sci 66(17) (2009) 2873-96.
[155] G. Bozzuto, A. Molinari, Liposomes as nanomedical devices, Int J Nanomedicine 10 (2015) 975-99.
[156] M.S. Webb, T.O. Harasym, D. Masin, M.B. Bally, L.D. Mayer, Sphingomyelin-cholesterol liposomes significantly enhance the pharmacokinetic and therapeutic properties of vincristine in murine and human tumour models, Br J Cancer 72(4) (1995) 896-904.
[157] D.A. Thomas, A.H. Sarris, J. Cortes, S. Faderl, S. O'Brien, F.J. Giles, G. Garcia-Manero, M.A. Rodriguez, F. Cabanillas, H. Kantarjian, Phase II study of sphingosomal vincristine in patients with recurrent or refractory adult acute lymphocytic leukemia, Cancer 106(1) (2006) 120-7.

[158] A. Choucair, M. Chakrapani, B. Chakravarthy, J. Katsaras, L.J. Johnston, Preferential accumulation of Abeta(1-42) on gel phase domains of lipid bilayers: an AFM and fluorescence study, Biochim Biophys Acta 1768(1) (2007) 146-54.

[159] L. Qiu, A. Lewis, J. Como, M.W. Vaughn, J. Huang, P. Somerharju, J. Virtanen, K.H. Cheng, Cholesterol modulates the interaction of beta-amyloid peptide with lipid bilayers, Biophys J 96(10) (2009) 4299-307.

[160] L. Gastaldi, L. Battaglia, E. Peira, D. Chirio, E. Muntoni, I. Solazzi, M. Gallarate, F. Dosio, Solid lipid nanoparticles as vehicles of drugs to the brain: current state of the art, Eur J Pharm Biopharm 87(3) (2014) 433-44.

[161] S. Laserra, A. Basit, P. Sozio, L. Marinelli, E. Fornasari, I. Cacciatore, M. Ciulla, H. Türkez, F. Geyikoglu, A. Di Stefano, Solid lipid nanoparticles loaded with lipoyl-memantine codrug: preparation and characterization, Int J Pharm 485(1-2) (2015) 183-91.

[162] S. Mura, P. Couvreur, Nanotheranostics for personalized medicine, Adv Drug Deliv Rev 64(13) (2012) 1394-416.

[163] V. Delplace, P. Couvreur, J. Nicolas, Recent trends in the design of anticancer polymer prodrug nanocarriers, Polymer Chemistry 5(5) (2014) 1529-1544.

[164] C.I.C. Crucho, M.T. Barros, Polymeric nanoparticles: A study on the preparation variables and characterization methods, Mater Sci Eng C Mater Biol Appl 80 (2017) 771-784.

[165] D. Vinciguerra, S. Denis, J. Mougin, M. Jacobs, Y. Guillaneuf, S. Mura, P. Couvreur, J. Nicolas, A facile route to heterotelechelic

polymer prodrug nanoparticles for imaging, drug delivery and combination therapy, J Control Release 286 (2018) 425-438.
[166] N. Elahi, M. Kamali, M.H. Baghersad, Recent biomedical applications of gold nanoparticles: A review, Talanta 184 (2018) 537-556.
[167] L. Talamini, M.B. Violatto, Q. Cai, M.P. Monopoli, K. Kantner, Ž. Krpetić, A. Perez-Potti, J. Cookman, D. Garry, C. P Silveira, L. Boselli, B. Pelaz, T. Serchi, S. Cambier, A.C. Gutleb, N. Feliu, Y. Yan, M. Salmona, W.J. Parak, K.A. Dawson, P. Bigini, Influence of Size and Shape on the Anatomical Distribution of Endotoxin-Free Gold Nanoparticles, ACS Nano 11(6) (2017) 5519-5529.
[168] J. Kreuter, Drug delivery to the central nervous system by polymeric nanoparticles: what do we know?, Adv Drug Deliv Rev 71 (2014) 2-14.
[169] Y.L. Hu, J.Q. Gao, Potential neurotoxicity of nanoparticles, Int J Pharm 394(1-2) (2010) 115-21.
[170] B. Wilson, M.K. Samanta, K. Santhi, K.P. Sampath Kumar, M. Ramasamy, B. Suresh, Significant delivery of tacrine into the brain using magnetic chitosan microparticles for treating Alzheimer's disease, J Neurosci Methods 177(2) (2009) 427-33.
[171] Y. Cheng, Q. Dai, R.A. Morshed, X. Fan, M.L. Wegscheid, D.A. Wainwright, Y. Han, L. Zhang, B. Auffinger, A.L. Tobias, E. Rincón, B. Thaci, A.U. Ahmed, P.C. Warnke, C. He, M.S. Lesniak, Blood-brain barrier permeable gold nanoparticles: an efficient delivery platform for enhanced malignant glioma therapy and imaging, Small 10(24) (2014) 5137-50.

[172] F. Sousa, S. Mandal, C. Garrovo, A. Astolfo, A. Bonifacio, D. Latawiec, R.H. Menk, F. Arfelli, S. Huewel, G. Legname, H.J. Galla, S. Krol, Functionalized gold nanoparticles: a detailed in vivo multimodal microscopic brain distribution study, Nanoscale 2(12) (2010) 2826-34.

[173] A. Verma, O. Uzun, Y. Hu, H.S. Han, N. Watson, S. Chen, D.J. Irvine, F. Stellacci, Surface-structure-regulated cell-membrane penetration by monolayer-protected nanoparticles, Nat Mater 7(7) (2008) 588-95.

[174] A. Gaudin, M. Yemisci, H. Eroglu, S. Lepetre-Mouelhi, O.F. Turkoglu, B. Dönmez-Demir, S. Caban, M.F. Sargon, S. Garcia-Argote, G. Pieters, O. Loreau, B. Rousseau, O. Tagit, N. Hildebrandt, Y. Le Dantec, J. Mougin, S. Valetti, H. Chacun, V. Nicolas, D. Desmaële, K. Andrieux, Y. Capan, T. Dalkara, P. Couvreur, Squalenoyl adenosine nanoparticles provide neuroprotection after stroke and spinal cord injury, Nat Nanotechnol 9(12) (2014) 1054-1062.

[175] D. Brambilla, R. Verpillot, B. Le Droumaguet, J. Nicolas, M. Taverna, J. Kóňa, B. Lettiero, S.H. Hashemi, L. De Kimpe, M. Canovi, M. Gobbi, V. Nicolas, W. Scheper, S.M. Moghimi, I. Tvaroška, P. Couvreur, K. Andrieux, PEGylated nanoparticles bind to and alter amyloid-beta peptide conformation: toward engineering of functional nanomedicines for Alzheimer's disease, ACS Nano 6(7) (2012) 5897-908.

[176] L. Ordóñez-Gutiérrez, F. Re, E. Bereczki, E. Ioja, M. Gregori, A.J. Andersen, M. Antón, S.M. Moghimi, J.J. Pei, M. Masserini, F. Wandosell, Repeated intraperitoneal injections of liposomes containing

phosphatidic acid and cardiolipin reduce amyloid-β levels in APP/PS1 transgenic mice, Nanomedicine 11(2) (2015) 421-30.
[177] L. Bana, S. Minniti, E. Salvati, S. Sesana, V. Zambelli, A. Cagnotto, A. Orlando, E. Cazzaniga, R. Zwart, W. Scheper, M. Masserini, F. Re, Liposomes bi-functionalized with phosphatidic acid and an ApoE-derived peptide affect Aβ aggregation features and cross the blood-brain-barrier: implications for therapy of Alzheimer disease, Nanomedicine 10(7) (2014) 1583-90.
[178] H. Ahyayauch, M. Raab, J.V. Busto, N. Andraka, J.L. Arrondo, M. Masserini, I. Tvaroska, F.M. Goñi, Binding of β-amyloid (1-42) peptide to negatively charged phospholipid membranes in the liquid-ordered state: modeling and experimental studies, Biophys J 103(3) (2012) 453-63.
[179] J.G. Sutcliffe, P.B. Hedlund, E.A. Thomas, F.E. Bloom, B.S. Hilbush, Peripheral reduction of β-amyloid is sufficient to reduce brain β-amyloid: implications for Alzheimer's disease, J Neurosci Res 89(6) (2011) 808-14.
[180] D. Carradori, C. Balducci, F. Re, D. Brambilla, B. Le Droumaguet, O. Flores, A. Gaudin, S. Mura, G. Forloni, L. Ordoñez-Gutierrez, F. Wandosell, M. Masserini, P. Couvreur, J. Nicolas, K. Andrieux, Antibody-functionalized polymer nanoparticle leading to memory recovery in Alzheimer's disease-like transgenic mouse model, Nanomedicine 14(2) (2018) 609-618.
[181] X. Montet, M. Funovics, K. Montet-Abou, R. Weissleder, L. Josephson, Multivalent effects of RGD peptides obtained by nanoparticle display, J Med Chem 49(20) (2006) 6087-93.

[182] H. Gao, Progress and perspectives on targeting nanoparticles for brain drug delivery, Acta Pharm Sin B 6(4) (2016) 268-86.
[183] Z. Liu, F. Kiessling, J. Gätjens, Advanced Nanomaterials in Multimodal Imaging: Design, Functionalization, and Biomedical Applications, Journal of Nanomaterials 2010 (2010) 15.
[184] M. Gregori, G. Sancini, M. Gregori, E. Salvati, I. Cambianica, F. Re, F. Ornaghi, M. Canovi, C. Fracasso, A. Cagnotto, M. Colombo, C. Zona, M. Gobbi, M. Salmona, B. La Ferla, F. Nicotra, M. Masserini, Functionalization with TAT-Peptide Enhances Blood-Brain Barrier Crossing In vitro of Nanoliposomes Carrying a Curcumin-Derivative to Bind Amyloid-b Peptide, 2013.
[185] K.S. Rao, M.K. Reddy, J.L. Horning, V. Labhasetwar, TAT-conjugated nanoparticles for the CNS delivery of anti-HIV drugs, Biomaterials 29(33) (2008) 4429-38.
[186] H. Elmizadeh, M. Khanmohammadi, K. Ghasemi, G. Hassanzadeh, M. Nassiri-Asl, A.B. Garmarudi, Preparation and optimization of chitosan nanoparticles and magnetic chitosan nanoparticles as delivery systems using Box-Behnken statistical design, J Pharm Biomed Anal 80 (2013) 141-6.
[187] K.M. Jaruszewski, S. Ramakrishnan, J.F. Poduslo, K.K. Kandimalla, Chitosan enhances the stability and targeting of immuno-nanovehicles to cerebro-vascular deposits of Alzheimer's disease amyloid protein, Nanomedicine 8(2) (2012) 250-60.
[188] Z. Songjiang, W. Lixiang, Amyloid-beta associated with chitosan nano-carrier has favorable immunogenicity and permeates the BBB, AAPS PharmSciTech 10(3) (2009) 900-5.

[189] F. Re, I. Cambianica, C. Zona, S. Sesana, M. Gregori, R. Rigolio, B. La Ferla, F. Nicotra, G. Forloni, A. Cagnotto, M. Salmona, M. Masserini, G. Sancini, Functionalization of liposomes with ApoE-derived peptides at different density affects cellular uptake and drug transport across a blood-brain barrier model, Nanomedicine 7(5) (2011) 551-9.

[190] J. Nicolas, G. Mantovani, D.M. Haddleton, Living Radical Polymerization as a Tool for the Synthesis of Polymer-Protein/Peptide Bioconjugates, Macromolecular Rapid Communications 28(10) (2007) 1083-1111.

[191] R. Prades, S. Guerrero, E. Araya, C. Molina, E. Salas, E. Zurita, J. Selva, G. Egea, C. López-Iglesias, M. Teixidó, M.J. Kogan, E. Giralt, Delivery of gold nanoparticles to the brain by conjugation with a peptide that recognizes the transferrin receptor, Biomaterials 33(29) (2012) 7194-205.

[192] A. Mathew, T. Fukuda, Y. Nagaoka, T. Hasumura, H. Morimoto, Y. Yoshida, T. Maekawa, K. Venugopal, D.S. Kumar, Curcumin loaded-PLGA nanoparticles conjugated with Tet-1 peptide for potential use in Alzheimer's disease, PLoS One 7(3) (2012) e32616.

[193] A. Jain, K. Cheng, The principles and applications of avidin-based nanoparticles in drug delivery and diagnosis, J Control Release 245 (2017) 27-40.

[194] N. Sathyamoorthy, D.D. Magharla, S.D. Vankayalu, Effect of Surface Modification on the, J Pharm Bioallied Sci 9(2) (2017) 135-143.

[195] E.P. Ivanova, J.P. Wright, D.K. Pham, N. Brack, P. Pigram, Y.V. Alekseeva, G.M. Demyashev, D.V. Nicolau, A comparative study

between the adsorption and covalent binding of human immunoglobulin and lysozyme on surface-modified poly(tert-butyl methacrylate), Biomed Mater 1(1) (2006) 24-32.
[196] N.V. Konduru, R.M. Molina, A. Swami, F. Damiani, G. Pyrgiotakis, P. Lin, P. Andreozzi, T.C. Donaghey, P. Demokritou, S. Krol, W. Kreyling, J.D. Brain, Protein corona: implications for nanoparticle interactions with pulmonary cells, Part Fibre Toxicol 14(1) (2017) 42.
[197] R.A. Vijayendran, D.E. Leckband, A quantitative assessment of heterogeneity for surface-immobilized proteins, Anal Chem 73(3) (2001) 471-80.
[198] S. Petrash, T. Cregger, B. Zhao, E. Pokidysheva, M.D. Foster, W.J. Brittain, V. Sevastianov, C.F. Majkrzak, Changes in Protein Adsorption on Self-Assembled Monolayers with Monolayer Order: Comparison of Human Serum Albumin and Human Gamma Globulin, Langmuir 17(24) (2001) 7645-7651.
[199] S. Krol, Challenges in drug delivery to the brain: nature is against us, J Control Release 164(2) (2012) 145-55.
[200] Z. Liu, X. Gao, T. Kang, M. Jiang, D. Miao, G. Gu, Q. Hu, Q. Song, L. Yao, Y. Tu, H. Chen, X. Jiang, J. Chen, B6 peptide-modified PEG-PLA nanoparticles for enhanced brain delivery of neuroprotective peptide, Bioconjug Chem 24(6) (2013) 997-1007.
[201] S. Mourtas, A.N. Lazar, E. Markoutsa, C. Duyckaerts, S.G. Antimisiaris, Multifunctional nanoliposomes with curcumin-lipid derivative and brain targeting functionality with potential applications for Alzheimer disease, Eur J Med Chem 80 (2014) 175-83.

[202] W.M. Pardridge, Blood-brain barrier endogenous transporters as therapeutic targets: a new model for small molecule CNS drug discovery, Expert Opin Ther Targets 19(8) (2015) 1059-72.
[203] K. Hu, J. Li, Y. Shen, W. Lu, X. Gao, Q. Zhang, X. Jiang, Lactoferrin-conjugated PEG-PLA nanoparticles with improved brain delivery: in vitro and in vivo evaluations, J Control Release 134(1) (2009) 55-61.
[204] B. Dehouck, M.P. Dehouck, J.C. Fruchart, R. Cecchelli, Upregulation of the low density lipoprotein receptor at the blood-brain barrier: intercommunications between brain capillary endothelial cells and astrocytes, J Cell Biol 126(2) (1994) 465-73.
[205] K. Papadia, E. Markoutsa, S. Mourtas, A.D. Giannou, B. La Ferla, F. Nicotra, M. Salmona, P. Klepetsanis, G.T. Stathopoulos, S.G. Antimisiaris, Multifunctional LUV liposomes decorated for BBB and amyloid targeting. A. In vitro proof-of-concept, Eur J Pharm Sci 101 (2017) 140-148.
[206] S. Türker, E. Onur, Y. Ozer, Nasal route and drug delivery systems, Pharm World Sci 26(3) (2004) 137-42.
[207] B. Luppi, F. Bigucci, G. Corace, A. Delucca, T. Cerchiara, M. Sorrenti, L. Catenacci, A.M. Di Pietra, V. Zecchi, Albumin nanoparticles carrying cyclodextrins for nasal delivery of the anti-Alzheimer drug tacrine, Eur J Pharm Sci 44(4) (2011) 559-65.
[208] C. Zhang, J. Chen, C. Feng, X. Shao, Q. Liu, Q. Zhang, Z. Pang, X. Jiang, Intranasal nanoparticles of basic fibroblast growth factor for brain delivery to treat Alzheimer's disease, Int J Pharm 461(1-2) (2014) 192-202.

[209] A. Rami, M. Behdani, N. Yardehnavi, M. Habibi-Anbouhi, F. Kazemi-Lomedasht, An overview on application of phage display technique in immunological studies, Asian Pacific Journal of Tropical Biomedicine 7(7) (2017) 599-602.

[210] N.E. Biolabs, Phage Display Peptide Library Kit. https://international.neb.com/products/e8110-phd-12-phage-display-peptide-library-kit#Product%20Information.

[211] C.K. Kang, V. Jayasinha, P.T. Martin, Identification of peptides that specifically bind Abeta1-40 amyloid in vitro and amyloid plaques in Alzheimer's disease brain using phage display, Neurobiol Dis 14(1) (2003) 146-56.

[212] L. Larbanoix, C. Burtea, E. Ansciaux, S. Laurent, I. Mahieu, L. Vander Elst, R.N. Muller, Design and evaluation of a 6-mer amyloid-beta protein derived phage display library for molecular targeting of amyloid plaques in Alzheimer's disease: Comparison with two cyclic heptapeptides derived from a randomized phage display library, Peptides 32(6) (2011) 1232-43.

[213] A.P. Mann, P. Scodeller, S. Hussain, G.B. Braun, T. Mölder, K. Toome, R. Ambasudhan, T. Teesalu, S.A. Lipton, E. Ruoslahti, Identification of a peptide recognizing cerebrovascular changes in mouse models of Alzheimer's disease, Nat Commun 8(1) (2017) 1403.

[214] M. Gobbi, F. Re, M. Canovi, M. Beeg, M. Gregori, S. Sesana, S. Sonnino, D. Brogioli, C. Musicanti, P. Gasco, M. Salmona, M.E. Masserini, Lipid-based nanoparticles with high binding affinity for amyloid-beta1-42 peptide, Biomaterials 31(25) (2010) 6519-29.

[215] V.H. Nguyen, B.J. Lee, Protein corona: a new approach for nanomedicine design, Int J Nanomedicine 12 (2017) 3137-3151.

[216] F. Bertoli, D. Garry, M.P. Monopoli, A. Salvati, K.A. Dawson, The Intracellular Destiny of the Protein Corona: A Study on its Cellular Internalization and Evolution, ACS Nano 10(11) (2016) 10471-10479.
[217] M.J. Hajipour, J. Raheb, O. Akhavan, S. Arjmand, O. Mashinchian, M. Rahman, M. Abdolahad, V. Serpooshan, S. Laurent, M. Mahmoudi, Personalized disease-specific protein corona influences the therapeutic impact of graphene oxide, Nanoscale 7(19) (2015) 8978-94.
[218] I. Lynch, K.A. Dawson, Protein-nanoparticle interactions, Nano Today 3(1) (2008) 40-47.
[219] A. Åkesson, M. Cárdenas, G. Elia, M.P. Monopoli, K.A. Dawson, The protein corona of dendrimers: PAMAM binds and activates complement proteins in human plasma in a generation dependent manner, RSC Advances 2(30) (2012) 11245-11248.
[220] A. Parodi, N. Quattrocchi, A.L. van de Ven, C. Chiappini, M. Evangelopoulos, J.O. Martinez, B.S. Brown, S.Z. Khaled, I.K. Yazdi, M.V. Enzo, L. Isenhart, M. Ferrari, E. Tasciotti, Synthetic nanoparticles functionalized with biomimetic leukocyte membranes possess cell-like functions, Nat Nanotechnol 8(1) (2013) 61-8.
[221] C.M. Hu, L. Zhang, S. Aryal, C. Cheung, R.H. Fang, Erythrocyte membrane-camouflaged polymeric nanoparticles as a biomimetic delivery platform, Proc Natl Acad Sci U S A 108(27) (2011) 10980-5.
[222] S.M. Moghimi, A.C. Hunter, D. Peer, Platelet mimicry: The emperor's new clothes?, Nanomedicine 12(1) (2016) 245-8.
[223] J. Kreuter, D. Shamenkov, V. Petrov, P. Ramge, K. Cychutek, C. Koch-Brandt, R. Alyautdin, Apolipoprotein-mediated transport of

nanoparticle-bound drugs across the blood-brain barrier, J Drug Target 10(4) (2002) 317-25.
[224] H.E. Gendelman, V. Anantharam, T. Bronich, S. Ghaisas, H. Jin, A.G. Kanthasamy, X. Liu, J. McMillan, R.L. Mosley, B. Narasimhan, S.K. Mallapragada, Nanoneuromedicines for degenerative, inflammatory, and infectious nervous system diseases, Nanomedicine 11(3) (2015) 751-67.
[225] M. Gregori, M. Masserini, S. Mancini, Nanomedicine for the treatment of Alzheimer's disease, Nanomedicine (Lond) 10(7) (2015) 1203-18.
[226] S. Mura, H. Hillaireau, J. Nicolas, B. Le Droumaguet, C. Gueutin, S. Zanna, N. Tsapis, E. Fattal, Influence of surface charge on the potential toxicity of PLGA nanoparticles towards Calu-3 cells, Int J Nanomedicine 6 (2011) 2591-605.
[227] G. Oberdörster, E. Oberdörster, J. Oberdörster, Nanotoxicology: an emerging discipline evolving from studies of ultrafine particles, Environ Health Perspect 113(7) (2005) 823-39.
[228] K. Donaldson, V. Stone, A. Clouter, L. Renwick, W. MacNee, Ultrafine particles, Occup Environ Med 58(3) (2001) 211-6, 199.
[229] W.H. Wu, X. Sun, Y.P. Yu, J. Hu, L. Zhao, Q. Liu, Y.F. Zhao, Y.M. Li, TiO2 nanoparticles promote beta-amyloid fibrillation in vitro, Biochem Biophys Res Commun 373(2) (2008) 315-8.
[230] X. Feng, A. Chen, Y. Zhang, J. Wang, L. Shao, L. Wei, Central nervous system toxicity of metallic nanoparticles, Int J Nanomedicine 10 (2015) 4321-40.
[231] G. Karthivashan, P. Ganesan, S.Y. Park, J.S. Kim, D.K. Choi, Therapeutic strategies and nano-drug delivery applications in

management of ageing Alzheimer's disease, Drug Deliv 25(1) (2018) 307-320.
[232] T.P. Thomas, I. Majoros, A. Kotlyar, D. Mullen, M.M. Holl, J.R. Baker, Cationic poly(amidoamine) dendrimer induces lysosomal apoptotic pathway at therapeutically relevant concentrations, Biomacromolecules 10(12) (2009) 3207-14.
[233] F. Vidal, L. Guzman, Dendrimer nanocarriers drug action: perspective for neuronal pharmacology, Neural Regen Res 10(7) (2015) 1029-31.
[234] J.R. Cannon, J.T. Greenamyre, The role of environmental exposures in neurodegeneration and neurodegenerative diseases, Toxicol Sci 124(2) (2011) 225-50.
[235] M. Aschner, B. Lukey, A. Tremblay, The Manganese Health Research Program (MHRP): status report and future research needs and directions, Neurotoxicology 27(5) (2006) 733-6.
[236] C. Lasagna-Reeves, D. Gonzalez-Romero, M.A. Barria, I. Olmedo, A. Clos, V.M. Sadagopa Ramanujam, A. Urayama, L. Vergara, M.J. Kogan, C. Soto, Bioaccumulation and toxicity of gold nanoparticles after repeated administration in mice, Biochem Biophys Res Commun 393(4) (2010) 649-55.
[237] S. Guerrero, E. Araya, J.L. Fiedler, J.I. Arias, C. Adura, F. Albericio, E. Giralt, J.L. Arias, M.S. Fernández, M.J. Kogan, Improving the brain delivery of gold nanoparticles by conjugation with an amphipathic peptide, Nanomedicine (Lond) 5(6) (2010) 897-913.
[238] F. Koch, A.M. Möller, M. Frenz, U. Pieles, K. Kuehni-Boghenbor, M. Mevissen, An in vitro toxicity evaluation of gold-, PLLA- and PCL-coated silica nanoparticles in neuronal cells for

nanoparticle-assisted laser-tissue soldering, Toxicol In Vitro 28(5) (2014) 990-8.
[239] C.J. Rivet, Y. Yuan, D.A. Borca-Tasciuc, R.J. Gilbert, Altering iron oxide nanoparticle surface properties induce cortical neuron cytotoxicity, Chem Res Toxicol 25(1) (2012) 153-61.
[240] X. Li, W. Liu, L. Sun, K.E. Aifantis, B. Yu, Y. Fan, Q. Feng, F. Cui, F. Watari, Effects of physicochemical properties of nanomaterials on their toxicity, J Biomed Mater Res A 103(7) (2015) 2499-507.
[241] Y. Zhang, B. Newton, E. Lewis, P.P. Fu, R. Kafoury, P.C. Ray, H. Yu, Cytotoxicity of organic surface coating agents used for nanoparticles synthesis and stability, Toxicol In Vitro 29(4) (2015) 762-8.
[242] T. Parikh, M.M. Bommana, E. Squillante, Efficacy of surface charge in targeting pegylated nanoparticles of sulpiride to the brain, Eur J Pharm Biopharm 74(3) (2010) 442-50.
[243] X. Liu, C. An, P. Jin, L. Wang, Protective effects of cationic bovine serum albumin-conjugated PEGylated tanshinone IIA nanoparticles on cerebral ischemia, Biomaterials 34(3) (2013) 817-30.
[244] B. Dubertret, P. Skourides, D.J. Norris, V. Noireaux, A.H. Brivanlou, A. Libchaber, In vivo imaging of quantum dots encapsulated in phospholipid micelles, Science 298(5599) (2002) 1759-62.
[245] S. Hernando, O. Gartziandia, E. Herran, J.L. Pedraz, M. Igartua, R.M. Hernandez, Advances in nanomedicine for the treatment of Alzheimer's and Parkinson's diseases, Nanomedicine (Lond) 11(10) (2016) 1267-85.
[246] G. Liu, P. Men, W. Kudo, G. Perry, M.A. Smith, Nanoparticle-chelator conjugates as inhibitors of amyloid-beta aggregation and

neurotoxicity: a novel therapeutic approach for Alzheimer disease, Neurosci Lett 455(3) (2009) 187-90.
[247] M.S. Mufamadi, Y.E. Choonara, P. Kumar, G. Modi, D. Naidoo, V.M. Ndesendo, L.C. du Toit, S.E. Iyuke, V. Pillay, Surface-engineered nanoliposomes by chelating ligands for modulating the neurotoxicity associated with β-amyloid aggregates of Alzheimer's disease, Pharm Res 29(11) (2012) 3075-89.
[248] Y.C. Kuo, C.C. Lin, Rescuing apoptotic neurons in Alzheimer's disease using wheat germ agglutinin-conjugated and cardiolipin-conjugated liposomes with encapsulated nerve growth factor and curcumin, Int J Nanomedicine 10 (2015) 2653-72.
[249] A. Nel, T. Xia, L. Mädler, N. Li, Toxic potential of materials at the nanolevel, Science 311(5761) (2006) 622-7.
[250] S. Sharifi, S. Behzadi, S. Laurent, M.L. Forrest, P. Stroeve, M. Mahmoudi, Toxicity of nanomaterials, Chem Soc Rev 41(6) (2012) 2323-43.
[251] M.F. Rahman, J. Wang, T.A. Patterson, U.T. Saini, B.L. Robinson, G.D. Newport, R.C. Murdock, J.J. Schlager, S.M. Hussain, S.F. Ali, Expression of genes related to oxidative stress in the mouse brain after exposure to silver-25 nanoparticles, Toxicol Lett 187(1) (2009) 15-21.
[252] S.M. Hussain, A.K. Javorina, A.M. Schrand, H.M. Duhart, S.F. Ali, J.J. Schlager, The interaction of manganese nanoparticles with PC-12 cells induces dopamine depletion, Toxicol Sci 92(2) (2006) 456-63.
[253] C. Grabinski, S. Hussain, K. Lafdi, L. Braydich-Stolle, J. Schlager, Effect of particle dimension on biocompatibility of carbon nanomaterials, Carbon 45(14) (2007) 2828-2835.

[254] T.T. Win-Shwe, H. Fujimaki, Nanoparticles and neurotoxicity, Int J Mol Sci 12(9) (2011) 6267-80.
[255] J. Wu, C. Wang, J. Sun, Y. Xue, Neurotoxicity of silica nanoparticles: brain localization and dopaminergic neurons damage pathways, ACS Nano 5(6) (2011) 4476-89.
[256] E. Hutter, S. Boridy, S. Labrecque, M. Lalancette-Hébert, J. Kriz, F.M. Winnik, D. Maysinger, Microglial response to gold nanoparticles, ACS Nano 4(5) (2010) 2595-606.
[257] B. Fonseca-Santos, M.P. Gremião, M. Chorilli, Nanotechnology-based drug delivery systems for the treatment of Alzheimer's disease, Int J Nanomedicine 10 (2015) 4981-5003.
[258] P.P. Wibroe, S.V. Petersen, N. Bovet, B.W. Laursen, S.M. Moghimi, Soluble and immobilized graphene oxide activates complement system differently dependent on surface oxidation state, Biomaterials 78 (2016) 20-6.
[259] K. Yasojima, C. Schwab, E.G. McGeer, P.L. McGeer, Up-regulated production and activation of the complement system in Alzheimer's disease brain, Am J Pathol 154(3) (1999) 927-36.
[260] C.R. Alving, Natural antibodies against phospholipids and liposomes in humans, Biochem Soc Trans 12(2) (1984) 342-4.
[261] A.J. Bradley, E. Maurer-Spurej, D.E. Brooks, D.V. Devine, Unusual electrostatic effects on binding of C1q to anionic liposomes: role of anionic phospholipid domains and their line tension, Biochemistry 38(25) (1999) 8112-23.
[262] D.V. Devine, K. Wong, K. Serrano, A. Chonn, P.R. Cullis, Liposome-complement interactions in rat serum: implications for

liposome survival studies, Biochim Biophys Acta 1191(1) (1994) 43-51.

[263] P.P. Wibroe, D. Ahmadvand, M.A. Oghabian, A. Yaghmur, S.M. Moghimi, An integrated assessment of morphology, size, and complement activation of the PEGylated liposomal doxorubicin products Doxil®, Caelyx®, DOXOrubicin, and SinaDoxosome, J Control Release 221 (2016) 1-8.

[264] P.P. Wibroe, I.D. Mat Azmi, C. Nilsson, A. Yaghmur, S.M. Moghimi, Citrem modulates internal nanostructure of glyceryl monooleate dispersions and bypasses complement activation: Towards development of safe tunable intravenous lipid nanocarriers, Nanomedicine 11(8) (2015) 1909-14.

[265] H.S. Sharma, A. Sharma, Nanoparticles aggravate heat stress induced cognitive deficits, blood-brain barrier disruption, edema formation and brain pathology, Prog Brain Res 162 (2007) 245-73.

[266] Y.C. Kuo, P.R. Chou, Neuroprotection against degeneration of sk-N-mc cells using neuron growth factor-encapsulated liposomes with surface cereport and transferrin, J Pharm Sci 103(8) (2014) 2484-97.

[267] F.M. LaFerla, K.N. Green, Animal models of Alzheimer disease, Cold Spring Harb Perspect Med 2(11) (2012).

[268] J. Tian, G. Du, L. Ye, X. Yu, J. Zhang, H. Wang, P. Yu, F. Fu, W. Liu, Y. Li, X. Cen, X. Guan, Three-month subchronic intramuscular toxicity study of rotigotine-loaded microspheres in Cynomolgus monkeys, Food Chem Toxicol 52 (2013) 143-52.

[269] C.A. Webster, D. Di Silvio, A. Devarajan, P. Bigini, E. Micotti, C. Giudice, M. Salmona, G.N. Wheeler, V. Sherwood, F.B. Bombelli, An early developmental vertebrate model for nanomaterial safety:

bridging cell-based and mammalian toxicity assessment, Nanomedicine (Lond) 11(6) (2016) 643-56.

CHAPTER 2

Evolution of Nanoparticle Protein Corona Across the Blood-Brain Barrier

Alysia Cox, Patrizia Andreozzi, Roberta Dal Magro, Fabio Fiordaliso, Alessandro Corbelli, Laura Talamini, Clizia Chinello, Francesca Raimondo, Fulvio Magni, Maria Tringali, Silke Krol, Paulo Jacob Silva, Francesco Stellacci, Massimo Masserini, Francesca Re

ACS Nano, 2018; 12(7):7292-7300

Highlights

For the first time, changes in the quantitative and qualitative composition of the protein corona are examined after passage through the BBB *in vitro*, using gold NPs that can traverse the BBB even in the absence of functionalization. There is ample information about the protein corona composition on different nanomaterials under different conditions, but how and if the corona changes upon BBB crossing has never been investigated. This exploration is vital in order to efficiently target the BBB using NPs. Furthermore, the brain-permeant corona may indicate specific proteins that could be used for NP functionalization and BBB targeting.

2.1 ABSTRACT

Engineered nanoparticles offer the chance to improve drug transport and delivery through biological barriers, exploiting the possibility to leave the blood circulation and traverse the endothelial vascular bed, blood-brain barrier (BBB) included, to reach their target. It is known that nanoparticles gather molecules on their surface upon contact with biological fluids, forming the "protein corona", which can affect their fate and therapeutic/diagnostic performance, yet no information on its evolution across the barrier has been gathered so far. Using a cellular model of the BBB and gold nanoparticles, we show that the composition of the corona undergoes dramatic quantitative and qualitative molecular modifications during passage from the "blood" to the "brain" side, while it is stable once beyond the BBB. Thus, we demonstrate that the nanoparticle corona dynamically and drastically evolves upon crossing the BBB, and that its initial composition is not predictive of nanoparticle fate and performance once beyond the barrier at the target organ.

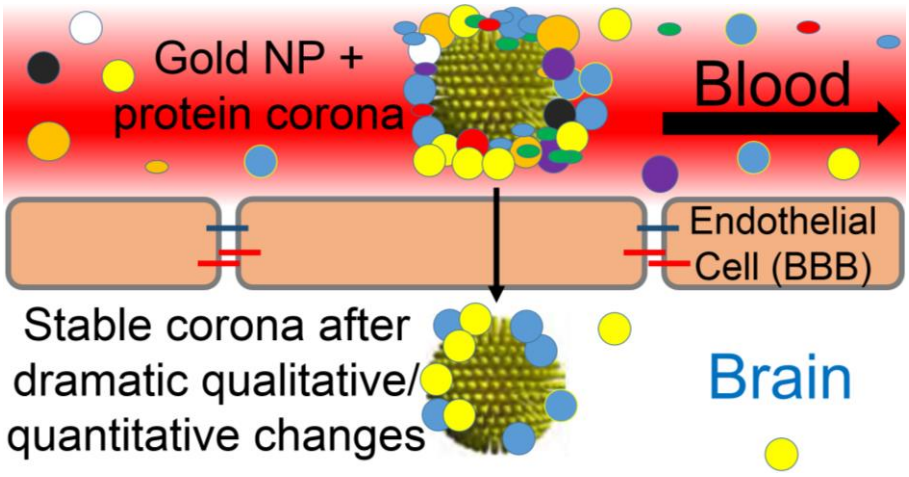

2.2 INTRODUCTION

The use of nanoparticles (NP) is an interesting approach to overcome the problem of delivering therapeutic and/or diagnostic molecules through the blood-brain barrier (BBB) to the brain, particularly due to the possibility of multi-functionalization.[1-5] However, when NP designed for medical purposes enter into contact with biological fluids, a series of interactions leads to the assembly of biomolecules gathered from the biological environment onto their surface, named the "corona". This biomolecular coating confers a biological identity to NP, determining how they are recognized by and interact with cells, and likely defines their biological fate, including their biodistribution, cell internalization, intracellular trafficking and subsequent cellular processing.[6, 7]

A major challenge and disadvantage with NP-based therapeutic design is rapid phagocytosis and reticuloendothelial (RES)-based clearance which limits NP bioavailability. Thus, the study of protein corona in context with bio-physicochemical features of nanoparticulate systems for drug delivery may allow for its fine-tuning to disguise biomolecular recognition of NP by immune cells and prevent phagocytosis.[8-10]

NP designed to treat neurological, psychiatric, and neurodegenerative disorders must traverse the BBB, which allows the passage of essential nutrients for the brain while also protecting the most delicate cells of the body from harmful substances and invading micro-organisms from the bloodstream.[11, 12] While it is likely that the corona governs the interaction of NP with the barrier, whether and how the corona changes after crossing the BBB, what of the original corona

is retained or lost, and what is collected during the passage is unknown. The importance of this issue is clear: the corona composition beyond the barrier should be taken into account in order to design more efficient therapeutic and/or diagnostic devices. Additionally, since the BBB limits the transport of macromolecules from the blood,[13] the possible arrival of otherwise non-permeant proteins with the corona from the blood may affect, either positively or negatively, the metabolism of the central nervous system.

Within this frame, the present research aims to study the protein corona evolution across an *in vitro* BBB cellular transwell model[14] using gold NP coated with 11-mercapto-1-undecanesulfonate (MUS) (All MUS NP), whose synthesis and characterization has been previously reported,[15-17] as an investigative tool.

2.3 MATERIALS AND METHODS

Materials

Chemical reagents and FITC-dextran 40kDa were purchased from Sigma-Aldrich, Milan, Italy. [^{14}C]-sucrose and [^{3}H]-propranolol were purchased from PerkinElmer. Media and supplements for cell culture and rat type I collagen were from Invitrogen Srl, Milan, Italy. EBM-2 medium was purchased from Lonza, Basel, Switzerland. The hCMEC/D3 cell line was obtained under license from Institut National de la Santé et de la Recherché Medicale (INSERM, Paris, France). Polystyrene transwell 12-well plates (0.4 µm sized pores, 1.12 cm^2 inserts) were from Euroclone. Mouse anti-ZO-1, AlexaFluor 488 goat anti-mouse and ProLog Gold antifade reagent were purchased from ThermoFisher Scientific. Mouse anti-β-catenin was from BD Biosciences. NuPAGE LDS sample buffer, reducing agent, MOPS SDS running buffer and NuPAGE 4-12% Bis-Tris Mini Gels (10 and 15 wells) for SDS-PAGE were purchased from ThermoFisher Scientific.

All MUS NP preparation and cell biocompatibility

1.2 mmol of gold salt ($HAuCl_4$) were dissolved in 200 ml of ethanol, and 1.2 mmol of the hydrophilic 11-mercapto-1-undecanesulfonate (MUS) thiol ligand was added while stirring the reaction solution. MUS was synthesized as described previously[15]. A saturated ethanol solution of sodium borohydride ($NaBH_4$) was added drop-wise over 2 h. The solution was stirred for 3 h and the reaction flask was then placed in a refrigerator overnight. The product was washed 3-5 times by suspending and centrifuging (5,500 rpm) it in methanol, ethanol and then acetone. Finally, the product was washed 5 times with DI-water

using Amicon® Ultra-15 centrifugal filter devices (10k NMWL). All solvents were reagent grade and purged with nitrogen gas for more than 30 min prior to the reaction. NP were suspended in MilliQ water and stored at RT. Before use, they were sonicated for 10 min at RT and sterile filtered (0.22 µm). A Zeta Nanosizer unit, Malvern NZ (Malvern, UK) was used to perform dynamic light scattering and zeta potential measurements, with laser set at 633 nm wavelength, operating in back scattering mode (BSM) at an angle of 173°. Measurements were run for a minimum of 5 min (5 measurements per sample, 15 runs, 5 sec each) at 25°C in water. TEM images were taken using a Philips/FEI CM12 operating at 120 kV and analyzed with ImageJ software.

To test All MUS NP biocompatibility with immortalized human cerebral microvascular endothelial (hCMEC/D3) cells, cells were grown for 2 days in collagenated 96-well plates (1 x 10^4 cells/well) and then treated with All MUS NP suspended in hCMEC/D3 cell medium for 3 h at 37°C at concentrations up to 0.2 mg/ml. LDH assays were carried out as described previously.[43] Five replicates were used for each condition.

In vitro cellular model of the blood-brain barrier

hCMEC/D3 cells were seeded between passages 25 and 35 at a concentration of 7 x 10^4 cells per well on the apical side of transwell inserts treated with 4 µg/cm^2 rat tail collagen type I, that separate the apical (representative of the blood) side from the basolateral (representative of the brain) side. EBM-2 medium supplemented with 5% fetal bovine serum, 1.4 µM hydrocortisone, 1% penicillin-streptomycin, 10 mM HEPES, 1 ng/ml basic FGF, 5 µg/ml ascorbic

acid, and 1/100 lipid concentrate was changed every 2 - 3 days. The apical and basolateral compartments contained 0.5 and 1 ml of medium respectively. Cells were maintained at 37°C, 5% CO_2, and saturated humidity.

Monolayer formation (approximately 14 days after seeding) was monitored by microscopy, and the trans-endothelial electrical resistance (TEER) was measured every day using an STX2 electrode Epithelial Volt-Ohm meter (World Precision Instruments, Florida). Formation of tight junctions was assessed by tracking the passage of radioactively labelled transcellular ([^{3}H]-propranolol) and paracellular ([^{14}C]-sucrose) probes from the apical to the basolateral compartment. 0.5 µCi of each probe was added to the apical compartment for 120 min. Every 30 min, 60 µl was taken from the basolateral compartment and replaced with fresh medium. The probes present in both compartments were quantified by liquid scintillation counting and endothelial permeability (EP) calculated as previously described.[44] The transwell system was used for experiments when TEER reached the maximum value and tight junction formation was assessed by confocal microscopy, which occurred around day 14 *in vitro*.

Paracellular tight (ZO-1) and adherens (β-catenin) junctions were detected by immunofluorescence labelling followed by confocal microscopy, performed directly on the cell monolayer attached to the transwell membrane. Cells were grown to confluence on transwell inserts for 14 days. The inserts were then mounted on glass slides, and cells were fixed for 20 min with 10% formalin solution. To stain the cells for β-catenin, permeabilization and blocking were performed with 3% BSA and 0.5% Triton for 1 h at RT, followed by incubation with

the primary antibody mouse anti-β-catenin (1:300) in 1% BSA overnight at 4°C. ZO-1 staining was performed after cell permeabilization and blocking with 10% normal goat serum (NGS) and 0.1% Triton for 30 min at RT. Mouse anti-ZO-1 (1:50) in 1% NGS and 0.1% BSA was incubated overnight at 4°C. Subsequently, cells were washed with PBS and incubated with the secondary antibody Alexa Fluor 488 goat anti-mouse (1:200) in BSA 0.1% for 1 h at RT. After washing with PBS, nuclei were stained with 4',6-diamidino-2-phenylindole (DAPI) in PBS (1:5,000) for 10 min at RT. Finally, the transwell membranes were cut out of the insert, mounted on glass slides using ProLong Antifade Reagent (Thermo Fisher Scientific), and incubated with mouse anti-ZO-1 (1:50 in 0.1% BSA) or mouse anti-β-catenin (1:300 in 1% BSA) antibodies overnight at 4 °C. Confocal laser scanning microscopy images were taken using an inverted confocal laser scanning microscope equipped with a Plan-Neofluar 63×/1.4 oil objective (LSM710, Carl Zeiss, Oberkochen, Germany). Excitation was performed using two ultraviolet–visible-laser diode 25 mV (405–488 nm). The pinhole was set to 1 AU. Image acquisition was conducted sequentially to minimize cross-talk between the fluorophores.

For all experiments where EP was calculated, gold (All MUS NP) was quantified in both transwell compartments by using an inductively coupled plasma-optical emission mass spectrophotometer (ICP-OES Optima 7000 DV Perkin Elmer).[45] All samples were prepared according to the following procedure: NP pellets were placed in a PTFE vessel and digested in a Milestone Ethos TC Microwave digestion system by adding 4 ml of aqua regia (HNO_3 65% and HCl 37%) in a closed system to reduce the risk of contamination. The system

was programmed to use up to 1000 W of power to increase the detected temperature to 220°C, at which time the temperature was maintained for 15 min. After digestion, samples were made up to a total of 10 ml and analyzed by ICP-OES. A certified standard reference material of Au 1000 mg/l (PerkinElmer Pure) was used for calibration and quality control. The operating parameters of ICP-OES instrument were set up using emission line at 242.795 nm in Axial View and samples solutions were measured in triplicate. The instruments detection limit is 0.1-1 µg/l.

Endothelial permeability of All MUS NP and FITC-dextran, and cellular uptake of All MUS NP by hCMEC/D3 cells

To assess their EP across the BBB, All MUS NP were added to the apical compartment of the transwell model in 500 µl cell medium at a concentration of 0.1 mg/ml, which was determined to be non-toxic by LDH assay. To assess the EP of FITC-dextran (40 kDa), 1 mg/ml was added to the apical compartment in 500 µl PBS. The basolateral compartment in both cases contained hCMEC/D3 medium with no serum (1 ml). Control wells contained no cells (filter only). After 3 h incubation, the medium in the apical and basolateral compartments were collected separately. Gold (All MUS NP) and FITC-dextran were quantified using ICP-OES and fluorescence spectroscopy respectively. For FITC-dextran, excitation was set at 496 nm and emission at 518 nm. EP was calculated as described above. Cellular uptake of All MUS NP was calculated by subtracting the amount of gold present in the apical and basolateral compartments after 3 h from the amount of gold added to the apical compartment at the beginning of the experiment.

Cellular uptake of All MUS NP by hCMEC/D3 cells visualized by TEM

hCMEC/D3 cells were seeded on collagenated 3 cm Petri dishes (250,000 cells per dish) and grown to confluence. Cells were incubated for 3 h with All MUS NP suspended in cell medium. Medium was removed, and cells were washed 3 times with 0.12 M phosphate buffer. Cells, attached to the bottom of Petri dishes, were fixed in 4% paraformaldehyde and 2% glutaraldehyde in 0.12 M phosphate buffer for 1 h at RT, and incubated for 1 h with osmium 1% in 0.05 M phosphate buffer pH 6.8-7.4 on ice. Cells were then incubated for 5 min at RT with a saturated solution of thiocarbohydrazide, followed by 1.5% ferrocianide and 1% osmium for 30 min. Cells, still adhered to the Petri dishes, were dehydrated in a graded series of ethanol. Epoxy resin (Epon 812 Fluka) was poured in the dishes, and polymerized at 60 °C for 72 h. The bottom of the Petri dishes was then removed with liquid nitrogen and small blocks of epoxy resin containing cells oriented in an axial or a coronal plane were trimmed to obtain ultrathin (55 - 60 nm thick) sections with a Leica EM UC6 ultramicrotome. Sections were then collected on 100 mesh formvar carbon-coated grids, counterstained with uranyl acetate and lead citrate, and examined with an EFTEM equipped with a YAG scintillator slow scan CCD camera (Zeiss).

Identifying the number of different proteins present in the protein corona

To analyze the number of different proteins present in the protein corona, All MUS NP (0.1 mg/ml) were incubated in hCMEC/D3 cell

medium for 3 h at 37°C. NP were washed twice with MilliQ to remove residual medium, but not attached proteins. Each step was followed by ultracentrifugation at 200,000 xg at 4°C for 40 min. A further ultracentrifugation step at 200,000 xg at 4°C for 40 min in 50% Acetonitrile with 0.05% (v/v) trifluoroacetic acid was performed to isolate a supernatant containing the loosely bound soft corona. The supernatants and related pellets containing NP coated with a hard corona were kept separate and subjected to in-solution trypsin digestion. Briefly, an equal volume of NH_4HCO_3 50mM was added to each sample. Disulfide bonds were reduced with dithiothreitol 10mM for 45 min at 56°C and then alkylated using iodoacetamide 55mM incubated in the dark for 30 min. Each sample was digested overnight using approximately 1 µg of trypsin from porcine pancreas (Proteomics Grade) and the enzymatic reaction was stopped by adding formic acid (0.1% v/v). Protein identification of trypsinized samples was carried out by nano-LC coupled online with tandem mass spectrometry (MS) as previously described.[45]

Isolation and analysis of protein corona on All MUS NP before and after passage through the *in vitro* BBB, and investigation of corona stability after passage

All MUS NP (0.1 mg/ml) were added to the apical compartment of a transwell containing 500 µl hCMEC/D3 medium, and incubated for 3 h at 37°C. The basolateral compartment contained 1 ml hCMEC/D3 medium with no serum. Samples from the apical and basolateral compartments of 18 wells were collected and pooled separately. Ultracentrifugation was carried out at 200,000 xg, 4°C, 40 min

(Beckman L90K Optima). The pellet containing protein corona-coated NP was washed and ultracentrifuged 3 times with 1 ml MilliQ water, and finally resuspended in 60 µl MilliQ water. ICP-OES was carried out on the apical and basolateral compartments from 3 wells, and EP was calculated. BCA assay was used to quantify protein in the hard corona before and after passage through the BBB. The experiment was repeated with 5% serum present in the basolateral compartment to assess the stability of the protein corona following passage through the *in vitro* BBB.

Qualitative analysis of the hard corona was completed using SDS-PAGE. 19.5 µl of sample, 7.5 µl LDS, and 3 µl reducing agent was incubated at 70°C for 10 min. Samples were loaded on a 10 or 15 well NuPAGE 4-12% Bis-Tris gels in MOPS buffer and electrophoresis was carried out at 200 V for 30 min. The gel was stained with EZBlue for 30 min in the dark at RT, washed with water, and visualized using a LasQuant 4000 instrument. Individual bands were excised and semi-quantitatively analyzed by MS as described.[46] The number and types of proteins present in the hard corona (pellet following ultracentrifugation) was calculated.

A series of experiments was carried out to ensure that the corona present in the basolateral side is actually an evolution of the corona from the apical side. First, the amount of proteins that cross the BBB in the absence of NPs was evaluated. FBS (5%) was added to the apical compartment of a transwell model and incubated for 3 h at 37°C. The media ("conditioned medium") in basolateral compartments of 15 wells were collected. BCA assay and SDS-PAGE analysis, as described above, were carried out.

Next, All MUS NP (50 µg) were added to a tube containing 15 ml of the conditioned medium recovered from the basolateral compartment. After 3 h incubation at 37°C, the sample was ultracentrifuged at 200,000 xg, 4°C, 40 min. The pellet was resuspended in 60 µl MilliQ water and SDS-PAGE analysis was performed to analyze the protein corona.

Finally, All MUS NP (50 µg) were incubated in 5% FBS (500 µl) for 3 h at 37°C. NP were ultracentrifuged and washed once as previously described to remove free proteins. NP were then added to 15 ml conditioned medium for 3 h at 37°C, ultracentrifuged again, and SDS-PAGE analysis was carried out.

Statistical analysis

Data was expressed as mean ± standard error of the mean (SEM) and analyzed with unpaired one-tailed Student's *t* test. A *P* value of <0.05 was considered statistically significant.

2.4 RESULTS

Characterization of the *in vitro* transwell model of the BBB

The formation of a reliable BBB model was determined using several techniques, indicating the development of relevant biochemical features of the barrier. Trans-endothelial electrical resistance (TEER) was measured and the endothelial permeability (EP) of [^{3}H]-propranolol and [^{14}C]-sucrose through the transwell model was evaluated (Fig. 1 A-B). On day 14 after cell seeding, TEER reached 126.6 ± 5.2 Ω/cm^{2} and the EP of [^{3}H]-propranolol and [^{14}C]-sucrose was 2.55 ± 0.2 x 10^{-5} and 1.88 ± 0.32 x 10^{-5} cm/min respectively, suggesting that tight junctions had formed.[18] The EP of FITC-dextran, with a size (4.5 nm) of the same order as All MUS NP, was very low (7.5 ± 4.3 x 10^{-7} cm/min) on day 14 after culture, thus ruling out paracellular passage of NP (Fig. 1 B).[19] Formation of tight and adherens junctions was confirmed by confocal microscopy (Fig. 1 C-D). Finally, The viability of BBB endothelial cells was evaluated by LDH assay either in the absence or presence of All MUS NP at different concentrations from 0.01 mg/ml to 0.2 mg/ml for 3 h at 37 °C (Fig. 1 E). Since up to 0.1 mg/ml of All MUS NP did not affect cell viability, all experiments were carried out using this concentration. The above described cellular parameters were not affected by the presence of 0.1 mg/ml All MUS NP.

Nanoparticle-BBB interaction and crossing

The core diameter of All MUS NP was 3.5 ± 0.8 nm as measured by TEM and DLS. The zeta potential was -38 ± 5 mV. The EP of All MUS NP (0.1 mg/ml) across the BBB model determined by ICP-OES was 5.3 ± 0.32 x 10^{-6} cm/min, and cellular uptake was 14.5 ± 0.7 % of the loaded amount of gold after 3 h incubation. The percentages of gold (with

respect to the amount loaded) present in the apical and in the basolateral compartments, and in the cell layer after 3 h incubation are shown in Fig. 1 F.

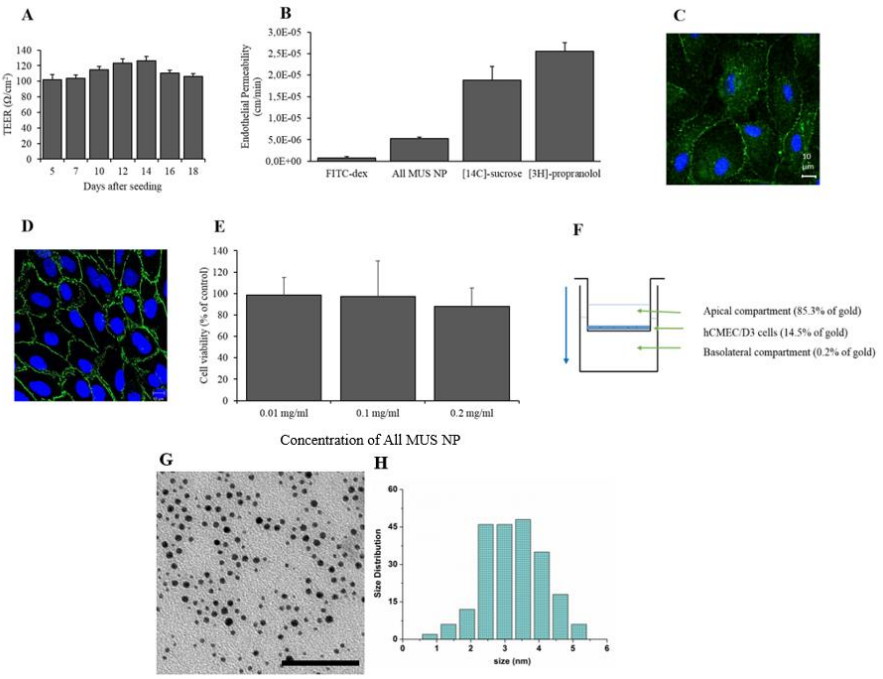

Figure 1: Characterization of the transwell BBB model and and interactions with All MUS NP. (A) TEER reached 126.6 ± 5.2 Ω/cm^2 14 days after cell seeding, and decreased thereafter. Error bars represent standard deviation. **(B)** Endothelial permeability (EP) of FITC-dextran 40kDa (FITC-dex; 7.5 ± 4.3 x 10^{-7} cm/min), All MUS NP (5.3 ± 0.3 x 10^{-6} cm/min), the paracellular probe [^{14}C]-sucrose (1.9 ± 0.3 x 10^{-5} cm/min) and the transcellular probe [^{3}H]-propranolol (2.6 ± 0.2 x 10^{-5} cm/min). Error bars represent SEM. **(C)** Confocal microscopy image showing ZO-1, a tight junction protein and **(D)** β-catenin, an adherens junction protein, formed in the hCMEC/D3 monolayer. Scale bar: 10

μm. **(E)** The effect of All MUS NP on hCMEC/D3 cell viability measured using LDH assay. Up to a concentration of 0.1 mg/ml, NP did not significantly affect the viability of hCMEC/D3 cells after 3 h incubation at 37°C. After incubation with 0.2 mg/ml NP, hCMEC/D3 cell viability was reduced to 88 ± 17 % of control (*p=0.002; Student's 2-tailed *t*-test). Data are expressed as mean of 5 replicates, expressed as percentages relative to controls, and error bars represent SEM. **(F)** The amount of gold present in each part of the transwell model following 3 h incubation is expressed as percentage of the initial amount loaded in the apical compartment. Blue arrow indicates the direction of movement of All MUS NP following addition to the apical compartment. **(G)** Electron micrographs of All MUS NP cores. The scale bar indicates 50 nm. **(H)** Particle size distribution obtained from TEM analysis. The average core diameter was 3.5 ± 0.8 nm.

The ability of All MUS NP to cross the BBB by a transcellular pathway was examined using transmission electron microscopy (TEM). Analysis along the axial plane showed that All MUS NP could be internalized in cytoplasmic vacuoles (Fig. 2 A). Coronal plane sections allowed visualization of the dynamic flow of internalized All MUS NP through the cell layer to the basolateral side where NP were released (Fig. 2 B-C-D).

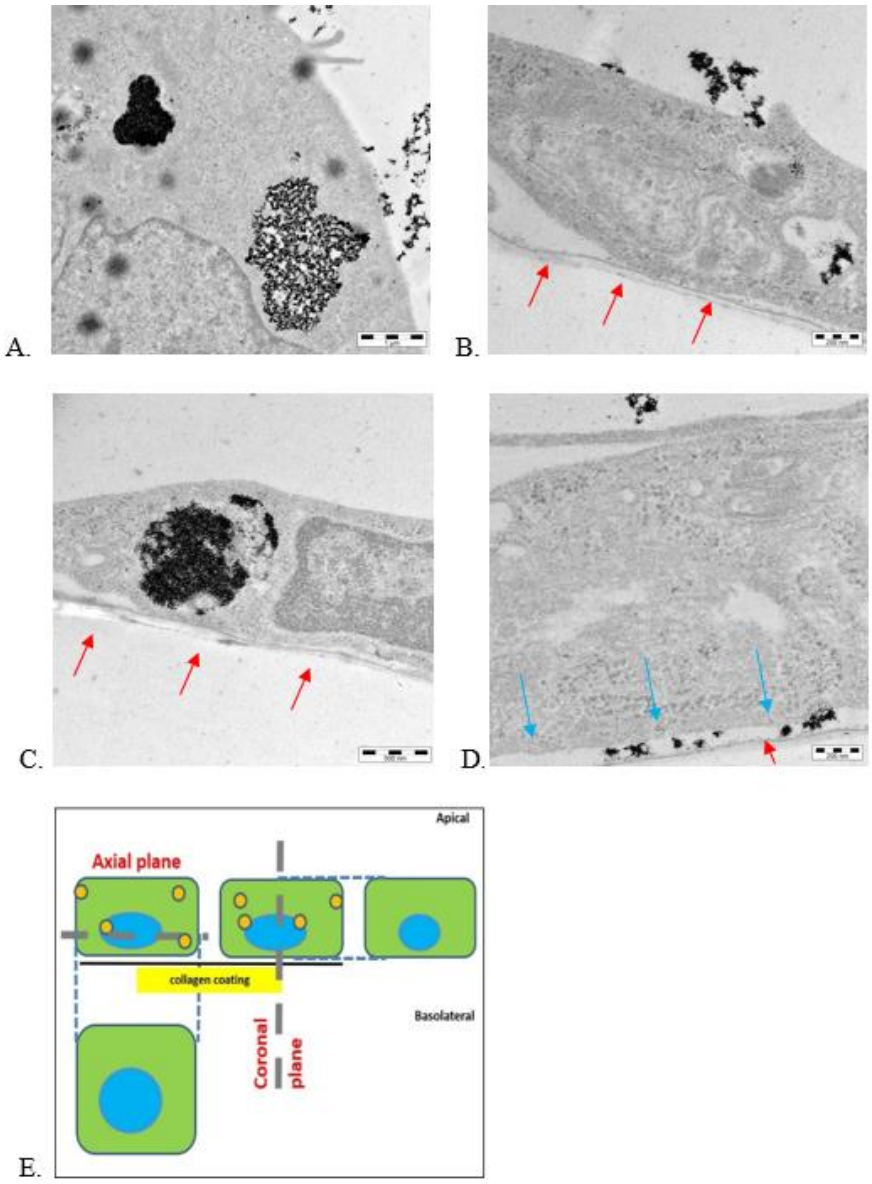

Figure 2: Uptake of All MUS NP by hCMEC/D3 cells in cell medium, visualized by TEM. **(A)** All MUS NP present as agglomerates of different densities in cytoplasmic vacuoles of hCMEC/D3 cells (axial plane). **(B, C, D)** All MUS NP approached the cell membrane (B), were internalized (B and C), and were observed outside the cell in the space between the cell membrane and collagen

coating (D). Red arrows indicate collagen coating and blue arrows indicate cell membrane. **(E)** Scheme depicting axial and coronal cutting planes of hCMEC/D3 cells.

The protein corona on All MUS NP changes qualitatively and quantitatively following passage through the *in vitro* model of the BBB

The evolution of the protein corona was examined by adding All MUS NP suspended in cell medium containing 5% serum to the apical compartment of the transwell system and recovering them from the basolateral compartment, containing medium without serum, after 3 h incubation. NP incubated in cell medium for 3 h bound 1.2 ± 0.1 µg protein/µg Au (n=3).

SDS-PAGE analysis of the corona formed on All MUS NP in the presence of complete cell medium showed ostensible differences before and after passage through the *in vitro* BBB (Fig. 3 A). Selected proteins (highlighted in red in Fig. 3 A) present in the protein corona in the apical compartment hardly crossed the BBB, as indicated by fainter or undetectable bands of corresponding molecular weight after passage. Other proteins (highlighted in blue in Fig. 3 A) were apparently enriched after BBB passage, indicating that they cross the BBB *in vitro*.

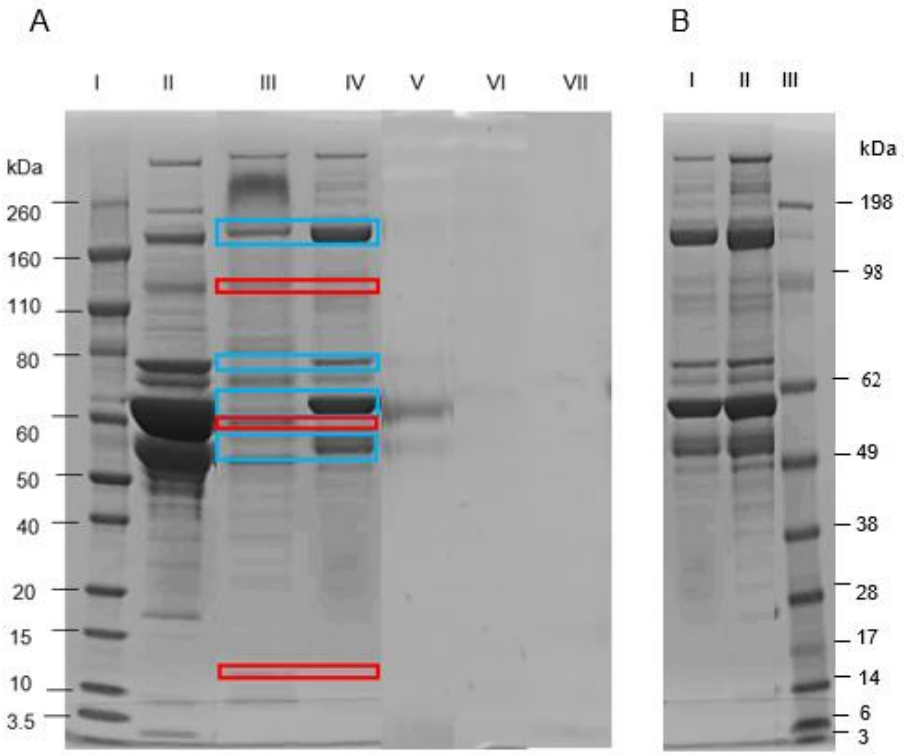

Figure 3: SDS-PAGE analysis of All MUS NP (0.1 mg/ml) before and after passage through the *in vitro* BBB following incubation with cell medium, and the stability of the protein corona after passage through the BBB. **(A)** Lane (I) is the protein standard, (II) is hCMEC/D3 medium, (III) is the apical compartment of the transwell model after 3 h incubation, containing NP that did not cross the cell monolayer, (IV) is the basolateral compartment after 3 h incubation, containing NP that crossed the *in vitro* BBB. Red bands indicate proteins that are excluded following passage through the BBB, *i.e.* protein bands that are visibly darker and larger in the apical compartment compared to the basolateral compartment. Blue bands highlight proteins that are able to pass through the *in vitro* BBB, as indicated by their enrichment in the basolateral compartment. Figure is

representative, and experiment was repeated 3 times. Lane (V) shows the proteins that pass through the cell monolayer to the basolateral compartment, in the absence of NP, after 3 h ("conditioned medium"). Lane (VI) is the corona formed on All MUS NP in conditioned medium. The corona is almost non-existent compared to the corona that is maintained in the same medium following passage from the apical compartment through the hCMEC/D3 monolayer. Lane (VII) is the corona formed in 5% serum and subsequently incubated in conditioned cell medium for 3 h. Proteins become detached from NP following incubation in the conditioned medium. **(B)** Lane (I) is All MUS NP corona after passage with 0% serum in the basolateral compartment, (II) is NP corona after passage with 5% serum in the basolateral compartment, and (III) is a protein standard.

Based on MS analysis, the qualitative and quantitative composition of the corona before and after passage through the BBB was assessed (Table 1). A diverse array of proteins were present in the corona, varying in molecular mass (11 - 272 kDa) and function. The full list of proteins identified in each compartment is presented in Supplementary Table 1. Based on densitometry analysis, 96.8% and 98.1% of proteins in the apical and basolateral compartments respectively were analyzed. In Table 1, a list of the 20 most abundant proteins in the corona before (A) and after (B) passage across the BBB is reported. For reference, the 20 most abundant proteins found in FBS are presented in Supplementary Table 2. The relative abundance of different proteins in the corona changed dramatically following passage. Only 9 of the 20 most abundant proteins in the corona before

traversing the BBB were still in the top 20 most abundant proteins after the passage, serum albumin and α2-macroglobulin being the major ones. On the contrary, the other 11 most abundant proteins were different before and upon the passage.

Table 1: Mass spectrometry analysis of the protein corona before and after passage through the BBB. A: The 20 most abundant proteins in the apical compartment of the transwell model *i.e.* the main components of the protein corona before passage through the *in vitro* BBB. Molecular mass is listed and varies from 11 – 272 kDa.

Proteins in Protein Corona Before BBB Passage (Apical Compartment)	**Composition of corona (%)**	**Mass (kDa)**
α2-macroglobulin	8.42	168
Serum albumin	7.20	70
Hemoglobin fetal subunit β	3.10	16
Fibronectin	2.48	272
α2-HS-glycoprotein	2.23	39
β-2-glycoprotein 1	1.84	38
α1-antiproteinase	1.73	46
Ferritin Light Chain	1.49	20
Complement C3	1.43	187
αS1-casein	1.40	25
Prothrombin	1.18	70
Complement factor H	0.99	140
Plasminogen	0.86	92
Antithrombin-III	0.85	52
C4b-binding protein α chain	0.80	69
Inter-α-trypsin inhibitor heavy chain H4	0.79	101
Hemoglobin subunit α	0.63	15
Histone H4	0.60	11
Serotransferrin	0.53	78
Lumican	0.47	39

B: The 20 most abundant proteins in the basolateral compartment *i.e.* the main components of the protein corona after passage through the *in vitro* BBB.

Proteins in Protein Corona after BBB Passage (Basolateral Compartment)	**Composition of Corona (%)**	**Mass (kDa)**
Serum albumin	25.60	70
α2-macroglobulin	18.43	168
α2-HS-glycoprotein	5.27	39
Serotransferrin	3.78	78
α1-antiproteinase	1.61	46
Vitamin D-binding protein	0.88	54
Fetuin-B	0.61	43
α1B-glycoprotein	0.47	53
Complement C3	0.44	187
Antithrombin-III	0.37	52
α-fetoprotein	0.35	68
Kininogen-1	0.27	69
αS1-casein	0.27	25
Hemopexin	0.24	52
Fibronectin	0.22	272
Transthyretin	0.21	15
Prothrombin	0.19	70
Protein AMBP	0.19	39
Serpin A3-1	0.18	46
Kappa-casein	0.16	21

Thirteen corona proteins were identified by MS as enriched in the basolateral compartment when compared to the apical side (Table 2). The relative abundance of these proteins in the protein corona increased from 1.8 to 9-fold following passage through the *in vitro* BBB. Complement component C9 is the most dramatically enriched following passage, increasing 9-fold following passage to the "brain" side. The amount of protein (in μg) bound to gold NP is presented in Supplementary Table 3.

Table 2: **Thirteen proteins were enriched in the basolateral "brain" compartment when compared to the apical "blood" compartment, indicating their ability to pass through an *in vitro* model of the BBB**.

Proteins in Protein Corona	% of corona in the apical "blood" side	% of corona in the basolateral "brain" side	Mass (kDa)	Fold increase in abundance following passage
Complement component C9	0.01	0.09	62	9.0
Serotransferrin	0.53	3.78	78	7.2
α-1B-glycoprotein	0.08	0.47	53	5.9
Hemopexin	0.05	0.24	52	4.8
Kininogen-1	0.06	0.27	69	4.5
Serum albumin	7.20	25.60	70	3.6
Heat shock cognate 71 kDa protein	0.02	0.07	71	3.5
α-fetoprotein	0.11	0.35	68	3.2
Vitamin D-binding protein	0.33	0.88	54	2.7
Serpin A3-1	0.07	0.18	46	2.6
α2-HS-glycoprotein	2.23	5.27	39	2.4
α2-macroglobulin	8.42	18.43	168	2.2
Fetuin-B	0.33	0.61	43	1.8

Values are the percentage of the total protein corona that is comprised of each protein, as measured by mass spectrometry.

The mechanisms underlying the evolution of the corona from the apical to the basolateral compartment were then investigated. Initially, the passage of proteins through the cell monolayer in the absence of NP was evaluated: serum (5%) was added to the upper chamber and medium with no serum to the lower chamber. A small

proportion of proteins (4.7%), mostly confined to a band in the SDS-PAGE corresponding to albumin, was found in the basolateral medium - from here on called “conditioned medium” - after 3 h incubation (Fig. 3 A).

Two sets of experiments were then designed to assess whether the corona in the basolateral side can be formed *in situ* by: i) NP without corona crossing from the apical side and interacting with proteins in the conditioned medium in the basolateral compartment, or ii) NP crossing with an intact corona from the apical side and interacting with proteins in the conditioned medium. The first possibility was ruled out when 0.1 mg/ml NP were incubated in 15 ml of conditioned medium for 3 h. Analysis of the protein corona by SDS-PAGE did not produce a visible pattern (Fig. 3 A, VI). The second possibility was excluded by incubating corona-coated NP, formed in 5% serum, with conditioned medium for 3 h. The corona detached, and most proteins were not visible by SDS-PAGE (Fig. 3 A, VII). This latter result suggests that the NP corona formed in the apical compartment before passing across the BBB is an unstable entity. Therefore, we investigated the stability of NP corona that crosses the barrier. The experiment reported above, describing the evolution of the NP corona recovered from the basolateral compartment containing medium without serum, was repeated with 5% serum in the basolateral compartment. The composition of NP-corona, examined by SDS-PAGE, either in the presence or in the absence of serum in the “brain” side was comparable (Fig. 3 B), suggesting enhanced stability after barrier crossing.

2.5 DISCUSSION

For a variety of diseases, effective therapy is severely limited or rendered impossible due to an inability to deliver medications to the intended sites of action. Multiple barriers exist throughout the body that have evolved to limit the migration of foreign compounds to tissues. In particular, multiple transporters, metabolic enzymes, and complex junctional structures prevent the paracellular diffusion of hydrophilic blood-borne drugs larger than 0.6 kDa across the BBB.[13]

Nanomedicine offers the chance to improve drug transport and delivery through biological barriers.[21] A vast amount of research and resources are continually invested in innovative design features, resulting in the creation of multifunctional nanoparticles.[22] These features include incorporation of active targeting moieties for enhanced uptake by specific cells.[23-25] Although these modifications highlight the impressive versatility and preclinical potential of nanomedicine, very few nanoparticles progress to the clinical stage.[26, 27] A non-exhaustive list of obstacles includes opsonization and subsequent sequestration by the mononuclear phagocyte system, nonspecific distribution, haematological or blood vessel flow limitations, pressure gradients, cellular internalization, escape from endosomal and lysosomal compartments, and drug efflux pumps.[28-30] It is now firmly established that the nanoparticle protein corona plays a role in these issues, affecting biological interactions and thus nanoparticle fate, and inhibiting the achievement of successful results.[31] Given its intrinsic cellular nature, it is likely that the crossing of the BBB by nanoparticles is also governed by the corona.

Although the features of the corona in the blood are relatively clear[32] and it is known to change upon cellular internalization,[6] its evolution upon passage through the BBB is not understood: what of the original corona is retained, gathered, or lost during this passage is unknown. This information is important within the context of nanoparticles designed for brain targeting and drug delivery to treat central nervous system diseases. Significantly, the stability of the brain internal environment is a prerequisite for its function, and the arrival of normally non-permeant proteins attached to nanoparticles represents a possibly insurmountable challenge.

Understanding the evolution of the corona during the passage across the BBB is challenging, due to the small amount of material that crosses the barrier, and because nanoparticles taken up by cells are usually trafficked along degradative pathways.[33] To overcome these problems, we chose to follow the evolution of the corona across a commonly used cellular model of the BBB, used frequently by our and other groups,[4, 5, 8, 14, 34, 35] obtained by growing a monolayer of cerebral microvascular endothelial cells (hCMEC/D3) on a transwell system separating an apical ("blood" side) from a basolateral ("brain" side) compartment, where the assessment of these features is relatively simple. It should be noted that BBB models, including the present one, do not perfectly mimic the human BBB.[8] However, it is widely agreed that tight junctions are the prime regulators of the BBB permeability. For this reason, our model was always used within the time frame when tight junction formation was assured to be maximal.

We used All MUS NP as a model to study protein corona formation.[15-17, 36] Initially, we showed that All MUS NP have a higher

EP than FITC-dextran (a hydrophilic compound of similar size that is minimally permeable across the transwell model used here) excluding the possibility that All MUS NP pass through the BBB *via* paracellular pathway. Moreover, the TEER values, permeability of paracellular and transcellular probes, and visualization of junctional proteins by confocal microscopy are all comparable to those reported in the literature,[5, 18, 37] indicating the correct formation of the BBB. These features and the viability of hCMEC/D3 cells were not affected by the presence of All MUS NP.

Strikingly, the protein corona of All MUS NP that have traversed the BBB is qualitatively completely different from the initial one. Only 9 of the 20 most abundant proteins present in the initial corona remain in the list after passage, while others are discharged. Thirteen proteins were found to be enriched in the corona after passage, when compared to the initial corona. None of these proteins are derived from the endothelial cell line.

It is noteworthy that serum albumin and α2-macroglobulin are the most abundant proteins in the corona and are greatly enriched after BBB passage. The significance of such enrichment could be questioned in the context of NP crossing the BBB *in vivo*. Both proteins are able to cross the BBB *in vivo*,[38, 39] but in very different amounts (CSF albumin 20 mg/dl; CSF α2-macroglobulin 0.05 mg/dl in healthy individuals), reflecting either their vastly different MW, or their abundance in serum. Thus, it is possible that, *in vivo*, NP carry much more α2-macroglobulin to the brain, compared to physiological conditions. Hypothetically, as α2-macroglobulin is a broad spectrum anti-proteinase, this NP-

mediated transfer could be taken into account to devise therapeutic strategies focused on the CNS.

The enrichment of specific proteins in the basolateral corona suggests that the selection of a subset of NP-protein complexes occurs during BBB crossing. This process likely reflects differences in the efficiency of cell uptake of specific NP-protein complexes, as well as potential protein exchange mechanisms. The precise assessment of these issues will require further investigation. Moreover, the enrichment of specific proteins in the basolateral corona suggests that the proteomic composition may play a major role in the rate/efficiency of BBB cell traversal by NP complexes. Further investigation may lead to the design of nano-devices for efficient brain targeting with therapeutic or diagnostic molecules, the passage of which are normally severely restricted by the BBB. For example, the creation of an artificial corona-NP complex with elevated levels of α2-macroglobulin (or only α 2-macroglobulin), may encourage NP crossing. Additionally, comparing NP with different chemical compositions, but carrying the same artificial corona, could shed light on the role of the bio-nano interface when the NP-corona interacts with biological barriers.

Finally, we demonstrated that the corona present on NP in the "brain" compartment after BBB passage is apparently more stable when compared to the corona in the "blood" compartment. Our hypothesis is that this higher stability is conferred thanks to the removal of specific proteins from the "blood-side" corona during BBB passage. When these hampering proteins are removed, new interactions among proteins of the "brain" corona are permitted, conferring higher stability. Since the removal of specific proteins, occurring during the "physiological"

process of BBB crossing, does not occur when the "blood" corona is directly incubated with conditioned medium, this preliminary hypothesis may explain the dramatic difference in stability.

It should be noted that a limitation of the present investigation is that the stability was assessed at only one final time point. However, the brain corona could evolve over time, and different dynamically evolving corona populations may coexist. Further studies should be carried out to address these possibilities.

Future work could involve the use of more complex *in vitro* BBB models that are closer to the physiological condition, for example including other cell types such as astrocytes and/or pericytes,[8, 40] to give a broader picture of the corona during BBB passage.[41] Importantly, further investigation of these issues should be carried out *in vivo*. While *in vivo* studies have previously evaluated the formation of the protein corona in the bloodstream,[42] the study of corona reaching the brain poses obvious technical problems due to the difficulty of recovering NP from the brain and avoiding contamination/artefacts. We believe that an investigation focused on studying the corona in CSF after systemic administration could represent a first approach to investigate this problem.

2.6 CONCLUSIONS

It has already been established that the protein corona is a dynamic entity, and its composition depends on the environment in which it is formed. Our findings demonstrate that the corona is dramatically affected by interaction with the BBB, and is more stable after it crosses the barrier, emphasizing the role of the protein corona in defining

nanoparticle-cell interactions, and the importance of using carefully designed biological models when testing nanoparticles for biomedical purposes.

Acknowledgements

This work received funding from the European Union's HORIZON 2020 Program for research, technological development and demonstration under grant agreement no. 642028 H2020-MSCA-ITN-2014 to Prof. Massimo Masserini, and the Joint Programme-Neurodegenerative Disease Research (JPND Research 2015) to Dr. Francesca Re (CUP B42F160000900008). We thank P. Couraud of INSERM (Paris, France) for the hCMEC/D3 cells.

Supporting Information Available: Supplementary Information files are available free of charge *via* the Internet at http://pubs.acs.org. Additional data includes a full list of the proteins identified in the protein corona before and after passage through the BBB (Excel file).

Author Contributions

A.Cox and P.A. performed most experiments. C.C., F.R. and F.M. performed the mass spectrometry measurements and analysis of results. R.D. performed immunofluorescence experiments and confocal microscopy. M.T. performed ICP-OES analysis. L.T. performed *in vitro* TEM, and F.F. and A. Corbelli performed TEM analysis. S.K., F.S., F.R., and M.M. discussed the results and gave critical comments

on the manuscript. F.R. and M.M. designed the research and provided funding. A.Cox, F.R., and M.M. wrote the manuscript.

References

1. Hudlikar, M.S.; Li, X.; Gagarinov, I. A.; Kolishetti, N.; Wolfert, M. A.; Boons, G-J. Controlled Multi-functionalization Facilitates Targeted Delivery of Nanoparticles to Cancer Cells. *Chem. Eur. J.* **2016,** *22,* 1415-1423.
2. Latorre, A.; Couleaud, P.; Aires, A.; Cortajarena, A.; Somoza, A. Multifunctionalization of Magnetic Nanoparticles for Controlled Drug Release: A General Approach. *Eur. J. Med. Chem.* **2014,** *82,* 355-362.
3. Yuan, X.; Kang, C-S.; Zhao, Y-H.; Gu, M-Q.; Pu, P-Y.; Tian, N-J.; Sheng, J. Surface Multi-functionalization of Poly(lactic acid) Nanoparticles and C6 Glioma Cell Targeting *In Vivo*. *Chinese J. Polym. Sci.* **2009,** *27,* 231-239.
4. Balducci, C.; Mancini, S.; Minniti, S.; La Vitola, P.; Zotti, M.; Sancini, G.; Mauri, M.; Cagnotto, A.; Colombo, L.; Fiordaliso, F.; Grigoli, E.; Salmona, M.; Snellman, A.; Haaparanta-Solin, M.; Forloni, G.; Masserini, M.; Re, F. Multifunctional Liposomes Reduce Brain β-amyloid Burden and Ameliorate Memory Impairment in Alzheimer's Disease Mouse Models. *J. Neurosci.* **2014,** *34,* 14022-14031.
5. Mancini, S.; Minniti, S.; Gregori, M.; Sancini, G.; Cagnotto, A.; Couraud, P-O.; Ordonez-Gutierrez, L.; Wandosell, F.; Salmona, M.; Re, F. The Hunt for Brain Aβ Oligomers by Peripherally Circulating Multi-functional Nanoparticles: Potential Therapeutic Approach for Alzheimer Disease. *Nanomedicine.* **2016,** *12,* 43-52.
6. Bertoli, F.; Garry, D.; Monopoli, M. P.; Salvati, A.; Dawson, K. A. The Intracellular Destiny of the Protein Corona: a Study on

its Cellular Internalization and Evolution. *ACS Nano.* **2016,** *10*, 10471-10479.

7. Tenzer, S.; Docter, D.; Kuharev, J.; Musyanovych, A.; Fetz, V.; Hecht, R.; Schlenk, F.; Fischer, D.; Kiouptsi, K.; Reinhardt, C.; Landfester, K.; Schild, H.; Maskos, M.; Knauer, S. K.; Stauber, R. H. Rapid Formation of Plasma Protein Corona Critically Affects Nanoparticle Pathophysiology. *Nat. Nanotechnol.* **2013,** *8*, 772-781.
8. Singh, A. V., Hosseinidoust, Z., Park, B. W., Yasa, O., Sitti, M. Microemulsion-based Soft Bacteria-driven Microswimmers for Active Cargo Delivery. *ACS Nano*. **2017**, *11*, 9759-9769.
9. Singh, A. V., Batuwangala, M., Mundra, R., Mehta, K., Patke, S., Falletta, E., Patil, R., Gade, W. N. Biomineralized Anisotropic Gold Microplate-macrophage Interactions Reveal Frustrated Phagocytosis-like Phenomenon: A Novel Paclitaxel Drug Delivery Vehicle. *ACS Appl. Mater. Interfaces.* **2014**, *6*, 14679-14689.
10. Hassan, S., Singh, A. V. Biophysicochemical Perspective of Nanoparticle Compatibility: A Critically Ignored Parameter in Nanomedicine. *J. Nanosci. Nanotechnol.* **2014,** *14*, 402-414.
11. Gidwani, M., Singh, A. V. Nanoparticle Enabled Drug Delivery Across the Blood Brain Barrier: *In Vivo* and *In Vitro* Models, Opportunities and Challenges. *Curr. Pharm. Biotechnol.* **2014**, *14*, 1201-1212.
12. Cipolla, M. J. *The Cerebral Circulation*. San Rafael (CA): Morgan & Claypool Life Sciences **2009**.

13. Pardridge, W. M. Drug Transport across the Blood-Brain Barrier. *J. Cereb. Blood Flow Metab.* **2012,** *32*, 1959-1972.
14. Salvati, E.; Re, F.; Sesana, S.; Cambianica, I.; Sancini, G.; Masserini, M.; Gregori, M. Liposomes Functionalized to Overcome the Blood-Brain Barrier and to Target Amyloid-β Peptide: the Chemical Design Affects the Permeability across an *in vitro* Model. *Int. J. Nanomedicine.* **2013,** *8*, 1749-1758.
15. Verma, A.; Uzun, O.; Hu, Y.; Han, H. S.; Watson, N.; Chen, S.; Irvine, D. J.; Stellacci, F. Surface Structure-regulated Cell Membrane Penetration by Monolayer Protected Nanoparticles. *Nat. Mater.* **2008,** *7*, 588-595.
16. Van Lehn, R. C.; Ricci, M.; Jacob Silva, P. H.; Andreozzi, P.; Reguera, J.; Voichovsky, K.; Stellacci, F.; Alexander-Katz, A. Lipid Tail Protrusions Mediate the Insertion of Nanoparticles into Model Cell Membranes. *Nat. Commun.* **2014**, *5*, 4482.
17. Cagno, V.; Andreozzi, P.; D'Alicarnasso, M.; Jacob Silva, P.; Mueller, M.; Galloux, M.; Le Goffic, R.; Jones, S. T.; Vallino, M.; Hodek, J.; Weber, J.; Sen, S.; Janecek, E. R.; Bekdemir, A.; Sanavio, B.; Martinelli, C.; Donalisio, M.; Rameix Welti, M. A., Eleouet, J. F.; Han, Y.; *et al.* Broad-spectrum Non-toxic Antiviral Nanoparticles with a Virucidal Inhibition Mechanism. *Nat. Mater.* **2018,** *17*, 195-203.
18. Omidi, Y.; Campbell, L.; Barar, J.; Connell, D.; Akhtar, S.; Gumbleton, M. Evaluation of the Immortalised Mouse Brain Capillary Endothelial Cell Line, b.End3, As an *In Vitro* Blood-Brain Barrier Model for Drug Uptake and Transport Studies. *Brain Res* **2003,** *990*, 95-112.

19. Gaillard, P. J.; de Boer, A. G. Relationship between Permeability Status of the Blood-Brain Barrier and *In Vitro* Permeability Coefficient of a Drug. *Eur. J. Pharm. Sci.* **2000,** *12*, 95-102.
20. Zheng, X.; Baker, H.; Hancock, W. S.; Fawaz, F.; McCaman, M.; Pungor, E. Jr. Proteomic Analysis for the Assessment of Different Lots of Fetal Bovine Serum as a Raw Material for Cell Culture. Part IV. Application of Proteomics to the Manufacture of Biological Drugs. *Biotechnol. Prog.* **2006**, *22*, 1294-1300.
21. Upadhyay, R. K. Drug Delivery Systems, CNS Protection, and the Blood Brain Barrier. *Biomed. Res. Int.* **2014**, *2014*, 869269.
22. Cheng, Z.; Al Zaki, A.; Hui, J. Z.; Muzykantov, V. R.; Tsourkas, A. Multifunctional Nanoparticles: Cost *Versus* Benefit of Adding Targeting and Imaging Capabilities. *Science.* **2012,** *338*, 903-910.
23. Deshpande, P. P.; Biswas, S.; Torchilin, V. P. Current Trends in the Use of Liposomes for Tumor Targeting. *Nanomedicine (Lond.)* **2013,** *8*, 1509-1528.
24. Accardo, A.; Aloj, L.; Aurilio, M.; Morelli, G.; Tesauro, D. Receptor Binding Peptides for Target-Selective Delivery of Nanoparticles Encapsulated Drugs. *Int. J. Nanomedicine.* **2014,** *9*, 1537-1557.
25. Steichen, S. D.; Caldorera-Moore, M.; Peppas, N. A. A Review of Current Nanoparticle and Targeting Moieties for the Delivery of Cancer Therapeutics. *Eur. J. Pharm. Sci.* **2013,** *48*, 416-427.
26. Korsmeyer, R. Critical Questions in Development of Targeted Nanoparticle Therapeutics. *Regen. Biomater.* **2016,** *3*, 143-147.

27. Anselmo, A. C.; Mitragotri, S. Nanoparticles in the Clinic. *Bioengineering & Transla. Med.* **2016,** *1*, 10-29.
28. Sanhai, W. R.; Sakamoto, J. H.; Canady, R.; Ferrari, M. Seven Challenges for Nanomedicine. *Nat. Nanotechnol.* **2008,** *3*, 242-244.
29. Shi, J.; Kantoff, P. W.; Wooster, R.; Farokhzad, O. C. Cancer Nanomedicine: Progress, Challenges and Opportunities. *Nat. Rev. Cancer*. **2017,** *17*, 20-37.
30. Bosetti, R.; Vereeck, L. Future of Nanomedicine: Obstacles and Remedies. *Nanomedicine (Lond).* **2011,** *6*, 747-755**.**
31. Nguyen, V. H.; Lee, B-J. Protein Corona: a New Approach for Nanomedicine Design. *Int. J. Nanomedicine.* **2017,** *12*, 3137-3151.
32. Lundqvist, M.; Augustsson, C.; Lilja, M.; Lundkvist, K.; Dahlback, B.; Linse, S.; Cedervall, T. The Nanoparticle Corona Formed in Human Blood or Human Blood Fractions. *PLoS ONE.* **2017,** *12*, e0175871.
33. Yameen, B.; Choi, W. I.; Vilos, C.; Swami, A.; Shi, J.; Farokhzad, O. C. Insight into Nanoparticle Cellular Uptake and Intracellular Targeting. *J. Control. Release.* **2014,** *190*, 485-499.
34. Weksler, B.; Romero, I. A.; Couraud, P-O. The hCMEC/D3 Cell Line as a Model of the Human Blood Brain Barrier. *Fluids Barriers CNS.* **2013, *10***, 16.
35. Magro, R. D., Cox, A., Zambelli, V., Mancini, S., Masserini, M., Re, F. The Ability of Liposomes, Tailored for Blood-brain Barrier Targeting, to Reach the Brain is Dramatically Affected by the Disease State. *Nanomedicine (Lond).* **2018,** *13*, 585-594.

36. Bekdemir, A., Stellacci, F. A centrifugation-based physicochemical characterization method for the interaction between proteins and nanoparticles. *Nat. Commun.* **2016**, *7*, 13121.
37. Cho, C.; Wolfe, J. M.; Fadzen, C. M.; Calligaris, D.; Hornburg, K.; Chiocca, E. A.; Agar, N. Y. R.; Pentelute, B. L.; Lawler, S. E. Blood-Brain-Barrier Spheroids As an *In Vitro* Screening Platform for Brain-penetrating Agents. *Nat. Commun.* **2017,** *8*, 15623.
38. Kanoh, Y., Ohara, T., Kanoh, M., Akahoshi, T. Serum Matrix Metalloproteinase-2 Levels Indicate Blood-CSF Barrier Damage in Patients with Infectious Meningitis. *Inflammation*. **2008**, *31*, 99-104.
39. Asano, T.; Ito, H.; Kariya, Y.; Hoshi, K.; Yoshihara, A.; Ugawa, Y.; Sekine, H.; Hirohata, S.; Yamaguchi, Y.; Sato, S.; Kobayashi, H.; Migita, K.; Ohira, H.; Hashimoto, Y.; Watanabe, H. Evaluation of Blood-Brain Barrier Function by Quotient Alpha2 Macroglobulin and its Relationship with Interleukin-6 and Complement Component 3 Levels in Neuropsychiatric Systemic Lupus Erythematosus. *PLoS One.* **2017,** *12*, e0186414.
40. Nakagawa, S.; Deli, M. A.; Kawaguchi, H.; Shimizudani, T.; Shimono, T.; Kittel, A.; Tanaka, K.; Niwa, M. A New Blood-brain Barrier Model using Primary Rat Brain Endothelial Cells, Pericytes and Astrocytes. *Neurochem. Int.* **2009,** *54*, 253-263.
41. Bertrand, N.; Grenier, P.; Mahmoudi, M.; Lima, E. M.; Appel, E. A.; Dormont, F.; Lim, J-M.; Karnik, R.; Langer, R.;

Farokhzad, O. C. Mechanistic Understanding of *in vivo* Protein Corona Formation on Polymeric Nanoparticles and Impact on Pharmacokinetics. *Nat. Commun.* **2017,** *8*, 777.

42. Strojan, K.; Leonardi, A.; Bregar, V. B.; Krizaj, I.; Svete, J.; Pavlin, M. Dispersion of Nanoparticles in Different Media Importantly Determines the Composition of their Protein Corona. *PLoS One.* **2017,** *12*, e0169552.
43. Gregori, M.; Orlando, A.; Re, F.; Sesana, S.; Nardo, L.; Salerno, D.; Mantegazza, F.; Salvati, E.; Zito, A.; Malavasi, F.; Masserini, M.; Cazzaniga, E. Novel Antitransferrin Receptor Antibodies Improve the Blood-Brain Barrier Crossing Efficacy of Immunoliposomes. *J. Pharm. Sci.* **2016,** *105*, 276-283.
44. Cecchelli, R.; Dehouck, B.; Descamps, L.; Fenart, L.; Buee-Scherrer, V. V.; Duhem, C.; Lundquist, S.; Rentfel, M.; Torpier, G.; Dehouck, M. P. *In Vitro* Model for Evaluating Drug Transport across the Blood-Brain Barrier. *Adv. Drug. Deliv. Rev.* **1999,** *36*, 165-178.
45. Orlando, A.; Cazzaniga, E.; Tringali, M.; Gullo, F.; Becchetti, A.; Minniti, S.; Taraballi, F.; Tasciotti, E.; Re, F. Mesoporous Silica Nanoparticles Trigger Mitophagy in Endothelial Cells and Perturb Neuronal Network Activity in a Size- and Time-Dependent Manner. *Int. J. Nanomed.* **2017,** *12*, 3547-3559.
46. Liu, X.; Chinello, C.; Musante, L.; Cazzaniga, M.; Tataruch, D.; Calzaferri, G.; James Smith, A.; De Sio, G.; Magni, F.; Zou, H.; Holthofer, H. Intraluminal Proteome and Peptidome of Human Urinary Extracellular Vesicles. *Proteomics Clin. Appl.* **2015,** *9*, 568-573.

SUPPLEMENTARY INFORMATION

Supplementary Table 1 is available as an excel file online at http://pubs.acs.org.

Supplementary Table 2: The most abundant proteins in FBS gathered from previously published data[20] and personal data (not shown).

Proteins	Mass (kDa)
Serum albumin	70
Cone cGMP-specific 3',5'-cyclic phosphodiesterase α-subunit	99
α-1-antiproteinase	46
Plasminogen	92
Lactoperoxidase	81
Kininogen, LMW II	48
NADH-ubiquinone oxido-reductase 75	79
α-2-HS-glycoprotein	39
Hemiferrin	78
Prothrombin	70
α2-macroglobulin	168
α-1-1-microglobulin and inter-α-trypsin inhibitor light chain	39
Antithrombin-III	52
Integrin β-1	88
β-2-glycoprotein I	38
Fibronectin	272
Hemoglobin β fetal chain	16
Complement factor H	140
Hemoglobin α chain	15
Complement C3	187

Supplementary Table 3: Thirteen proteins were enriched in the basolateral "brain" compartment when compared to the apical "blood" compartment, indicating their ability to pass through an *in vitro* model of the BBB. There were a total of 1 µg protein per µg NP in the apical compartment, and 11 µg protein per µg NP in the basolateral compartment.

Proteins in Protein Corona	µg proteins per µg NP in apical "blood" side	µg proteins per µg NP in basolateral "brain" side
Complement Component C9	0.0001	0.0013
Serotransferrin	0.0053	0.0581
α-1B-glycoprotein	0.0008	0.0089
Hemopexin	0.0005	0.0052
Kininogen-1	0.0006	0.0068
Serum albumin	0.0720	0.7897
Heat shock cognate 71 kDa protein	0.0002	0.0025
α-fetoprotein	0.0011	0.0121
Vitamin D-binding protein	0.0033	0.0359
Serpin A3-1	0.0007	0.0082
α2-HS-glycoprotein	0.0223	0.2446
α2–macroglobulin	0.0842	0.9235
Fetuin-B	0.0033	0.0362

CHAPTER 3

The extent of human apolipoprotein A-I lipidation strongly affects β-amyloid efflux across the blood-brain barrier *in vitro*

Roberta Dal Magro, Sara Simonelli, Alysia Cox**,** Beatrice Formicola, Roberta Corti, Valeria Cassina, Luca Nardo, Francesco Mantegazza, Gianvito Grasso, Marco Agostino Deriu, Andrea Danani, Laura Calabresi, Francesca Re

Submitted

Highlights

A large body of evidence has established that physiological nanoparticles present in human plasma, i.e. high-density lipoproteins (HDL), are able to cross the BBB and reach the brain. Until now, no data has identified the key features of these particles that determine their ability to traverse the BBB. These features could be important in the pathogenesis of Alzheimer's disease (AD). In this chapter, the ability of different HDL subclasses to cross the BBB and interact with Aβ was investigated for the first time. Focusing on brain Aβ as the target, the possible role of HDL and/or apolipoprotein A-I (apoAI) in the "sink effect" theory for AD treatment is examined. The identification of specific HDL subclasses and/or apoAI conformations that can possibly alter AD pathogenesis could be useful in designing new nanodevices for disease treatment.

3.1 ABSTRACT

Much evidence suggests a protective role of high-density lipoprotein (HDL), and its major apolipoprotein apoAI, in Alzheimer's disease (AD). The biogenesis of nascent HDL is derived from an initial lipidation of apoAI, which is synthesized by the liver and intestine but not in the brain, in a process mediated by ABCA1. The maturation of nascent HDL in mature spherical HDL is due to a second lipidation step, mediated by LCAT, and the change of apoAI conformation. Therefore, different subclasses of apoAI-HDL simultaneously exist in the blood. The ability of apoAI-HDL to target and modulate cerebral β-amyloid (Aβ) content from the periphery is not yet clear. To this purpose, we investigate if and how the lipidation state of apoAI is involved in AD. In particular, we analyse *in vitro* the ability of different subclasses of HDL purified from human plasma, each with different apoAI lipidation states, to cross the blood-brain barrier (BBB), to interact with Aβ aggregates and to affect Aβ efflux across the BBB using a transwell system. The results showed that lipid-free apoAI had a superior ability to enhance *in vitro* Aβ efflux (+30 ± 3%) across the BBB, compared to the other Aβ-binding plasma proteins tested. Interestingly, this effect was amplified by the lipidation of apoAI, reaching maximal Aβ efflux (9×10^{-5} cm/min) when apoAI is adjusted in discoidal HDL. Contrarily, no effect on Aβ efflux was detected when apoAI is in mature spherical HDL, suggesting that the apoAI conformation could be involved in promoting Aβ clearance from the brain, rather than the lipid composition. Finally, when apoAI adjusted its structure in discoidal HDL, rather than in spherical ones, it is able to cross the BBB *in vitro*

and to strongly destabilize the conformation of Aβ fibrils by decreasing the order of the fibril structure (-24%) and the β-sheet content (-14%). These data suggest that the extent of apoAI lipidation, and consequently its conformation, may represent crucial characteristics that influence their protective role in AD pathogenesis.

3.2 INTRODUCTION

ApoAI is a 28 kDa protein synthesized by the liver and small intestine which plays a key role in the biogenesis and metabolism of high-density lipoproteins (HDL). Lipidation of apoAI by the ATP-binding cassette transporter A1 (ABCA1) is essential for the formation of plasma HDL particles. Lipid-free or lipid-poor apoAI acquire small amounts of phospholipid and cholesterol from membrane-bound ABCA1, generating several classes of nascent HDL particles, discoidal ones included. Subsequently, a second lipidation step, mediated by LCAT, is required for maturation of nascent HDL into mature spherical lipid-rich HDL. During the HDL maturation process the secondary structure of apoAI slightly changes. Therefore, in humans, HDL consist of heterogeneous subclasses, which can be identified based on their density, charge, size, and protein/lipid composition. HDL are involved in the removal of excess cholesterol from peripheral tissues including the arterial wall, and its transport to the liver for secretion by reverse cholesterol transport. HDL can exert other protective effects, including anti-oxidative, anti-inflammatory, anti-apoptotic, and anti-infective activities[1].

It is well established that plasma levels of HDL cholesterol (HDL-c) and apolipoprotein A-I (apoAI), the major protein component of plasma HDL, inversely correlate with the development of many disorders, including cardiovascular diseases, diabetes, obesity, cancer, and infectious diseases. Dysregulated HDL metabolism has also been linked to brain disorders: a decrease in plasma levels of HDL-c and/or apoAI are risk factors for memory decline and lipid-related neurodegenerative diseases, such as Alzheimer's disease (AD)[2].

AD is the most common type of dementia and affects tens of millions of people worldwide. The amyloid hypothesis[3-5] proposes that β-amyloid peptide (Aβ), the main component of senile plaques, is the key player in AD pathogenesis. Aβ monomers, derived from the proteolytic cleavage of a larger glycoprotein named amyloid precursor protein, aggregate into different forms of oligomers, which can then deposit in regular fibrils and plaques.

New evidence suggests that apoAI might be involved in the pathogenesis of AD, but its role has not yet been elucidated. Epidemiological studies indicate that AD risk may be attenuated by high levels of circulating HDL and apoAI. Specifically, levels of apoAI positively correlate with Mini-Mental State Examination (MMSE) and Cognitive Ability Screening Instrument (CASI) scores[6], and high HDL levels (>55 mg/dl) in cognitively normal elderly individuals are associated with a significantly reduced risk of developing AD. In symptomatic AD patients, plasma apoAI levels negatively correlate with hippocampal and whole brain volume and mean entorhinal cortical thickness[7]. Decreased levels of serum apoA-I can discriminate AD from non-demented age-matched control subjects[8]. It has been found that apoAI levels are significantly decreased in brain homogenates[9] and the cerebrospinal fluid (CSF)[10] of AD patients compared to controls. *In vivo* studies show that overexpression of apoA-I prevents cognitive deficits, limits brain plaque deposition, and increases soluble Aβ clearance from the brain when administered to AD mouse models. This suggests that apoAI could play a role in the pathogenesis of AD, but more research is needed to clarify its implications.

ApoAI is present in the cerebrospinal fluid (CSF), but its mRNA has not been detected in brain cells[11-13]. Thus, brain apoAI is believed to be plasma derived. The mechanisms by which apoAI reaches the brain have not been fully elucidated, but limited preliminary studies support the hypothesis that peripheral HDL crosses the blood-brain barrier (BBB) and the blood-CSF barrier[14,15].

In this study, we investigate *in vitro* how the extent of apoAI lipidation affects the ability of distinct subclasses of human HDL to cross the BBB, to interact with Aβ aggregates and to affect the Aβ efflux across the BBB using a transwell system.

3.3 MATERIALS AND METHODS

Human samples

Human plasma samples from healthy donors were provided by the Immunohematology and Transfusion Medicine Service (SIMT) of ASST Grande Ospedale Metropolitano Niguarda, Milan. All experimental protocols were approved by license 446-092014 CE from Ospedale Niguarda Ca' Granda and carried out in accordance with these guidelines and regulations. Informed consent was obtained from all donors. Plasma was prepared by low speed centrifugation at 4°C, and lipoprotein isolation started within 6 h from blood collection.

Purification of apoAI-HDL from human plasma

HDL (d=1.063-1.21 g/mL) were purified from human plasma of healthy blood donors by sequential ultracentrifugation. Purified lipoproteins were dialyzed against saline immediately before use and were used to represent the total apoAI-HDL pool of human plasma. This sample was treated with chymase to obtain spherical apoAI-HDL[42], destroying the discoidal ones. Briefly, apoAI-HDL plasma pool was incubated with granule remnants isolated from rat mast cells (30 µg/ml of granule remnant total protein, equal to 40 BTEE Units/ml) for 2 h at 37°C. After incubation, tubes were placed on ice and centrifuged at 4°C, 12000 rpm, for 5 min to remove the granule remnant-bound chymase, and the chymase-free supernatants were collected. The lack of discoidal apoAI-HDL was verified by non-denaturing two-dimensional (2-D) electrophoresis, in which agarose gel electrophoresis was followed by non-denaturing gradient gel electrophoresis (GGE)

and immunoblotting against apoAI. Spherical apoAI-HDL were characterized by AFM, as described below.

Preparation of discoidal HDL

ApoAI was purified from human plasma by gel-filtration chromatography[43] and its purity (> 95%) was confirmed by SDS-polyacrylamide gel electrophoresis (SDS-PAGE) using Coomassie protein staining. This sample represents lipid-poor apoAI. Discoidal apoAI-HDL were prepared by the cholate dialysis method using palmitoyl-oleoyl-phosphatidylcholine (POPC) and apoAI in the weight ratio of 2.5:1[44]. Their size was estimated by non-denaturing GGE using precast 4-30% gels and the Pharmacia Phast System[45]. Phospholipid content of discoidal HDL was measured by an enzymatic method and apoAI concentration was measured by Lowry method. Discoidal HDL were characterized by AFM, as described below.

Atomic Force Microscopy imaging of apoAI-HDL

Atomic Force Microscopy (AFM) imaging was performed using a Nanowizard II (JPK Instruments, Berlin) scanning probe microscope operating in tapping and contact mode in air. In tapping mode imaging of $A\beta_{1-42}$ fibrils, RTESP-300 (Bruker, USA) cantilevers were used with a nominal force constant of 40 N/m, a resonance frequency of 300 kHz, and a nominal tip radius 8 nm. For contact mode imaging of HDL subtypes, DNPS-10 (Bruker, USA) cantilevers were used with a nominal force constant of 0.06 N/m, and a nominal tip radius 10 nm. The detailed protocol used for HDL characterization is supplied as Supplementary Information. A wide range of areas of AFM images were analyzed using the commercial JPK image processing software

and a customized image-analysis software (Matlab, MathWorks Inc, USA).

Preparation and characterization of Aβ aggregates

$A\beta_{1-42}$ (Sigma–Aldrich, Milan, Italy) oligomers or fibrils were prepared as described[16,47,48]. Briefly, the peptide (1 mg/ml) was solubilized in 1,1,3,3,3-hexafluoro-2-propanol (HFIP; Sigma–Aldrich, Milan, Italy), dried, resuspended in DMSO at a concentration of 5 mM, and bath sonicated for 10 min. To obtain an oligomer-enriched preparation, samples were diluted to 100 μM in hCMEC/D3 cell culture medium and incubated for 24 h at 4 °C. To obtain a fibril-enriched preparation, samples were diluted to 200 μM in 10 mM HCl and incubated at 37 °C for 72 h. Aβ oligomers and fibrils were characterized by AFM[47]. For the fibrillation process, samples were diluted to 100 μM in 10 mM HCl and incubated at 37 °C. In the reported images, Aβ was diluted to a final concentration of 10 μM in 10 mM HCl, and deposited on freshly cleaved mica. Images were acquired in air in tapping mode.

Preparation and characterization of the *in vitro* model of the BBB

The *in vitro* BBB model was prepared and characterized as previously described[16], using human brain endothelial cells (hCMEC/D3; from Institut National de la Sante et de la Recherche Medicale, Paris, France). Briefly, hCMEC/D3 were seeded (60, 000 cells/cm^2) onto collagen-coated (8 μg/cm^2 rat tail collagen type 1; Gibco, ThermoFisher Scientific) transwell filters (polycarbonate 12-well, pore size 0.4 μm, translucent membrane insert 1.12 cm^2; Costar) to establish a polarized monolayer. The cell monolayer separates two compartments, an apical

one (0.5 ml) representing the blood and a basolateral one (1 ml) representing the brain. Trans-endothelial electrical resistance (TEER) was monitored with STX2 electrode Epithelial Volt-Ohm meter (World Precision Instruments, Sarasota, Florida). The formation of junctions was evaluated by confocal microscopy and by measuring the endothelial permeability (EP) of [^{14}C-sucrose] (50 μM) and [^{3}H]-propranolol (76 nM; 0.5 μCi). Cell viability was assessed by MTT assay[48].

Effect of apoAI lipidation on *in vitro* Aβ efflux across the BBB

500 nM of Aβ fibrils dissolved in 1 ml of culture medium without serum were placed in the basolateral compartment of the transwell system and the impact of this treatment on cell monolayer was evaluated by monitoring TEER, EP to radiolabelled probes and cell viability, following the procedure described above. 5 nmol/ml of apoAI in discoidal HDL, spherical HDL, or total HDL plasma pool dissolved in 500 μl of PBS were added to the apical compartment of the transwell. After different incubation times (up to 3 h) at 37°C, aliquots from the apical compartment were collected and the Aβ content was measured by ELISA assay (IBL international, Italy). The Aβ endothelial permeability (EP) across the cell monolayer from the basolateral to the apical compartment (defined as Aβ efflux) was calculated as described[16,48]. As controls, 5 nmol/ml of commercially available lipid-free apoAI, α2-macroglobulin, apolipoprotein E or human albumin (all from Sigma, Milano, Italy) dissolved in PBS were added to the apical compartment and Aβ efflux was determined as previously described.

Effect of lipidation of apoAI on its ability to cross the BBB *in vitro*

5 nmol/ml of apoAI in discoidal HDL, spherical HDL, or total HDL plasma pool dissolved in 500 μl of PBS were added to the apical compartment of the transwell and incubated at 37°C. After different times (up to 3 h) of incubation, the amount of apoAI in the basolateral compartment was measured by ELISA assay (IBL International, Italy) and EP was calculated as described[16,48].

Effect of apoAI lipidation on preformed Aβ fibrils

50 μM $A\beta_{1-42}$ fibrils were incubated with 5 μg/ml of apoAI in discoidal HDL, spherical HDL, or apoAI-HDL plasma pool at 37°C in buffer B (PBS 15 mM and NaCl 20mM, pH 7.4). After different incubation times an aliquot from each sample was immobilized on a freshly cleaved mica substrate, rinsed with Milli-Q water, dried under a gentle stream of nitrogen and analyzed by AFM.

The effect of apoAI lipidation on preformed Aβ fibrils was also monitored by ThT assay[24]. Briefly, 2 μM of Aβ fibrils were incubated with 5 μM ThT (Sigma-Aldrich, Milan, Italy), 10mM glycine buffer pH 8.5 in 1 x 1 cm^2 fluorimeter quartz cuvettes equipped with hermetic tips to prevent evaporation. 0.1 mg/ml of apoAI in discoidal HDL, spherical HDL, or total HDL plasma pool were added to the sample and the ThT fluorescence (ex. 450 nm; em. 485 nm) was monitored at 37°C under stirring with a FP8500 fluorimeter (Jasco) equipped with a 4-cells peltier-thermostated sample holder.

Molecular modelling of apoAI

The recently obtained discoidal HDL with apolipoprotein A-I[49] was considered the starting point for this work (PDB ID: 2N5E). One hundred 1,2-dimyristoyl-sn-glycero-3-phosphocholine (DMPC) lipid molecules were inserted as previously described[49]. This model was solvated and neutralized by adding 0.15 M Na and Cl ions. CHARMM36 force field[50] was used to define protein and lipids topologies, and TIP3P model[51] was used for the water molecules. The obtained system was minimized by applying 1,000 steps of steepest descent energy minimization algorithm, followed by preliminary NVT of 200 ps. V-rescale thermostat was applied to maintain the temperature at 300 K with a time constant of 0.1 ps[52]. An NPT of 200 ps was carried out at 300 K (τ=1 ps) and 1 atm (τ=5 ps). V-rescale[52] and Berendsen[53] coupling methods were used as temperature and pressure coupling. Finally, Molecular Dynamics (MD) equilibration of 100 ns was performed to optimize the DMPC/apoAI complex.

Computational docking and MD of apoA-I in complex with Aβ fibril

To determine the initial orientation of Aβ fibrils on apoA-I, a pentamer of $A\beta_{17-42}$ was extracted from the PDB model 2BEG[54] and considered for docking experiments[55]. In detail, the $A\beta_{17-42}$ model was first docked on apoA-I using Patchdock[56]. The top-scored 100 conformations were subjected to Firedock[57,58] to refine and rescore docking solutions. The top ranked molecular system was solvated in a cubic box of 13X11X8 nm^3 and neutralized by counterions. Each system consisted of approximately 120,000 interacting particles. CHARMM36 force field[50]

was used to define protein and lipids topologies, while TIP3P model[51] was used for water molecules. The system was first minimized by applying the steepest descent energy minimization algorithm. Three different replicas of the same system were generated with different initial velocities to increase the statistics of MD data. A preliminary MD simulation of 100 ps was performed in NPT ensemble at 300 K (τ=1 ps) and 1 atm (τ=5 ps) by applying position-restraints on the heavy atoms of the solute. V-rescale[52] and Berendsen[53] coupling methods were used for temperature and pressure coupling. Finally, three production simulations were performed at 300K for 100 ns. For comparison, $A\beta_{17-42}$ alone in water was also simulated. Principal Component Analysis (PCA) was applied to reduce the dimensionality of the system[19,21], elucidating large-scale and low-frequency modes, thus yielding collective motions related to the destabilization of the $A\beta_{17-42}$ fibril[59]. After the alignment of $A\beta_{17-42}$ C-α Cartesian coordinates, the covariance matrix was calculated and diagonalized. To estimate the structural order of the $A\beta_{17-42}$ model and to what extent fibrils chains are aligned, an order parameter was calculated for each MD snapshot using equation (1):

$$(1) ordP = \frac{1}{N_r}\sum_{r=17}^{42}\frac{\langle v_r, z\rangle}{\|v_r\|\cdot\|z\|} = \frac{1}{N_r}\sum_{r=17}^{42}\cos\alpha$$

where N is the number of residues along the peptide chain; v_r is the vector joining each of the Cα-atoms pertaining to chain A with the corresponding Cα-atom (same residue number) of chain E; and z is the fibril axis. Values of ordP close to 1 indicate the amyloid-like shape

alignment, whereas values of ordP < 1 are typical of a distorted structure.

Statistical analysis

Data analysis was performed in Microsoft Excel and Origin Pro 8 software from Origin Lab. Values are expressed as the mean ± s.e.m. or s.d. measured in triplicate. *P*-values <0.05 (calculated by two-tailed unpaired Student's *t* test) are considered statistically significant.

3.4 RESULTS

Characterization of apoAI-HDL

The purification of apoAI-HDL pool from human plasma was verified by 2D-GGE (Fig. 1A). ApoAI-HDL subclasses with different sizes were identified and their concentrations were quantified by densitometry. The left smear (Fig. 1A) represents discoidal apoAI-HDL and right smear represents spherical apoAI-HDL. Discoidal apoAI-HDL was treated with chymase in order to selectively degrade discoidal apoAI-HDL obtaining a preparation enriched in mature, spherical apoAI-HDL. Fig. 1B shows the complete degradation of discoidal particles, indicated by the disappearance of their smear.

A

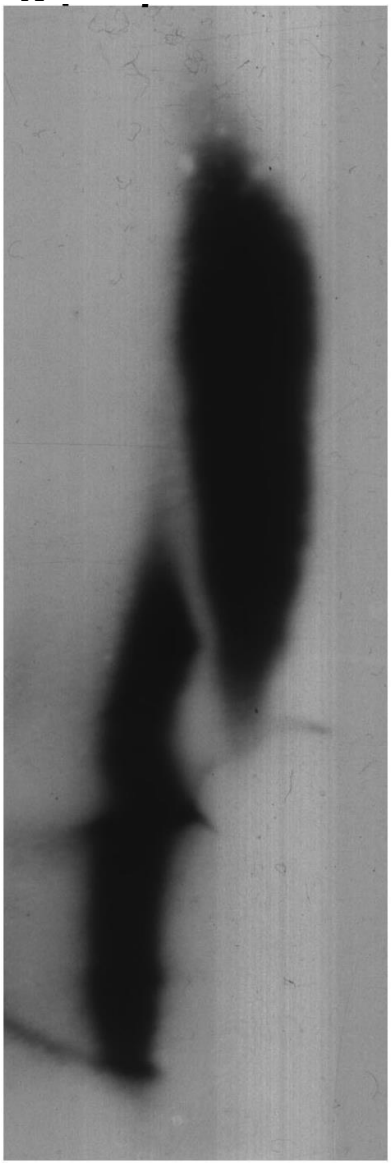

Discoidal apoAI-HDL

Spherical apoAI-HDL

B

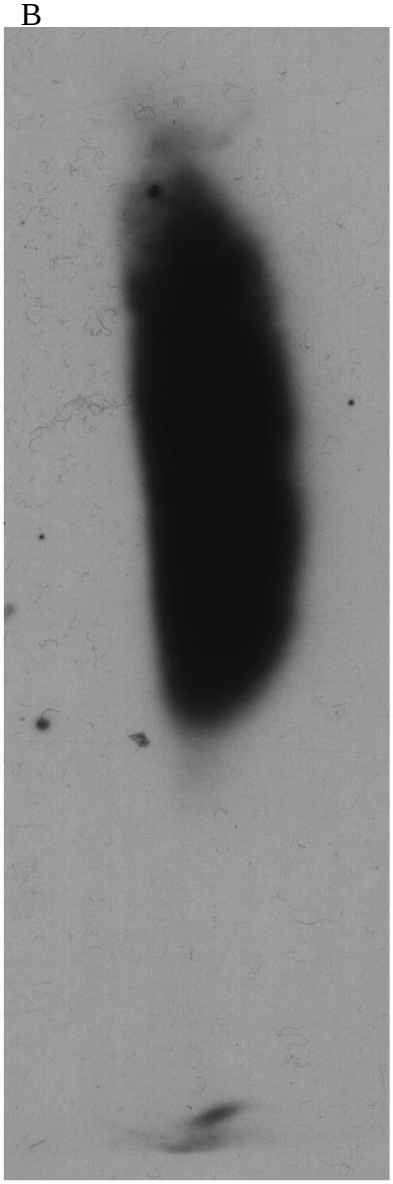

Spherical apoAI-HDL

Figure 1. Effect of chymase treatment on HDL subclasses. HDL preparation was incubated for 2 h at 37°C with chymase-containing granule remnants. HDL subclasses were then separated by two-dimensional electrophoresis and transferred onto a nitrocellulose membrane, on which lipoproteins were detected with a rabbit anti-human apoA-I antibody.

Spherical and discoidal HDL were also characterized by atomic force microscopy (AFM) measurements. The results showed that both HDL subclasses display visual homogeneity in size distribution and morphology (Fig. 2). The statistical distributions of the height measurements taken using AFM imaging allowed discrimination between the spherical and discoidal shapes and showed that the average dimensions of the two HDL subclasses were comparable (spherical HDL radius 12.7 nm, discoidal HDL height 12.9 nm).

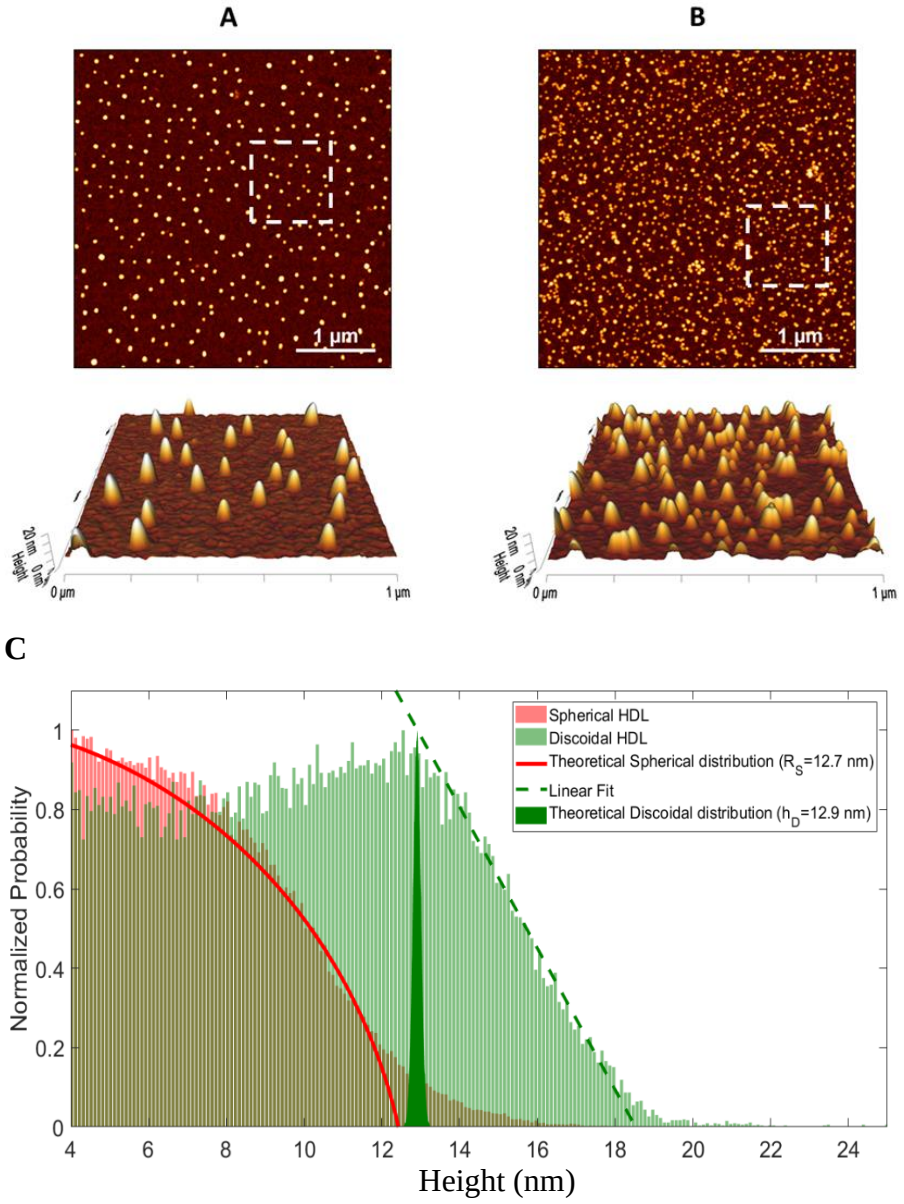

Figure 2. Representative images of the morphology of HDL subclasses obtained by AFM imaging and statistical distributions of the measured heights for spherical and discoidal HDL. (A) Discoidal and (B) spherical HDL on APTES functionalized mica (4 x 4 μm^2, 1024 x 1024 pixel, Z-scale 20 nm), with 3-dimensional projections

of a 1 x 1 μm^2 region (white squares in the images). (C) The histograms represent the normalized height statistical distributions for the spherical (red) and discoidal (green) HDL in the range 4-25 nm. The red continuous line represents the best fit of the histogram to the theoretical distribution for a sphere (R_S=12.7 nm), the green filled area represents the δ-function (h_D = 12.9 nm), and the green dotted line is the linear regression for the final part of the distribution.

Characterization of Aβ fibrillation

The aggregation process of Aβ from monomers to fibrils was monitored and characterized by AFM imaging. Several images were acquired at the beginning of the fibrillation (t = 0 h) and at successive fixed times up to 48 h. Representative images in Fig. 3A show that long unbranched fibrils were formed over time.

The process of fibril growth can be quantitatively evaluated by considering the time evolution of the number of pixels above a fixed height threshold in the AFM images of fibril morphology. Fig. 3B shows AFM images of Aβ fibrils at different incubation times with a height threshold of 1.5 nm. The percentage of pixels above a certain threshold increases with fibril extension and density, and can be considered as a quantitative index of the aggregation process. Threshold pixel percentages over time are shown in Fig. 3C. The results showed that there is continuous Aβ fibril growth in length up to 48h.

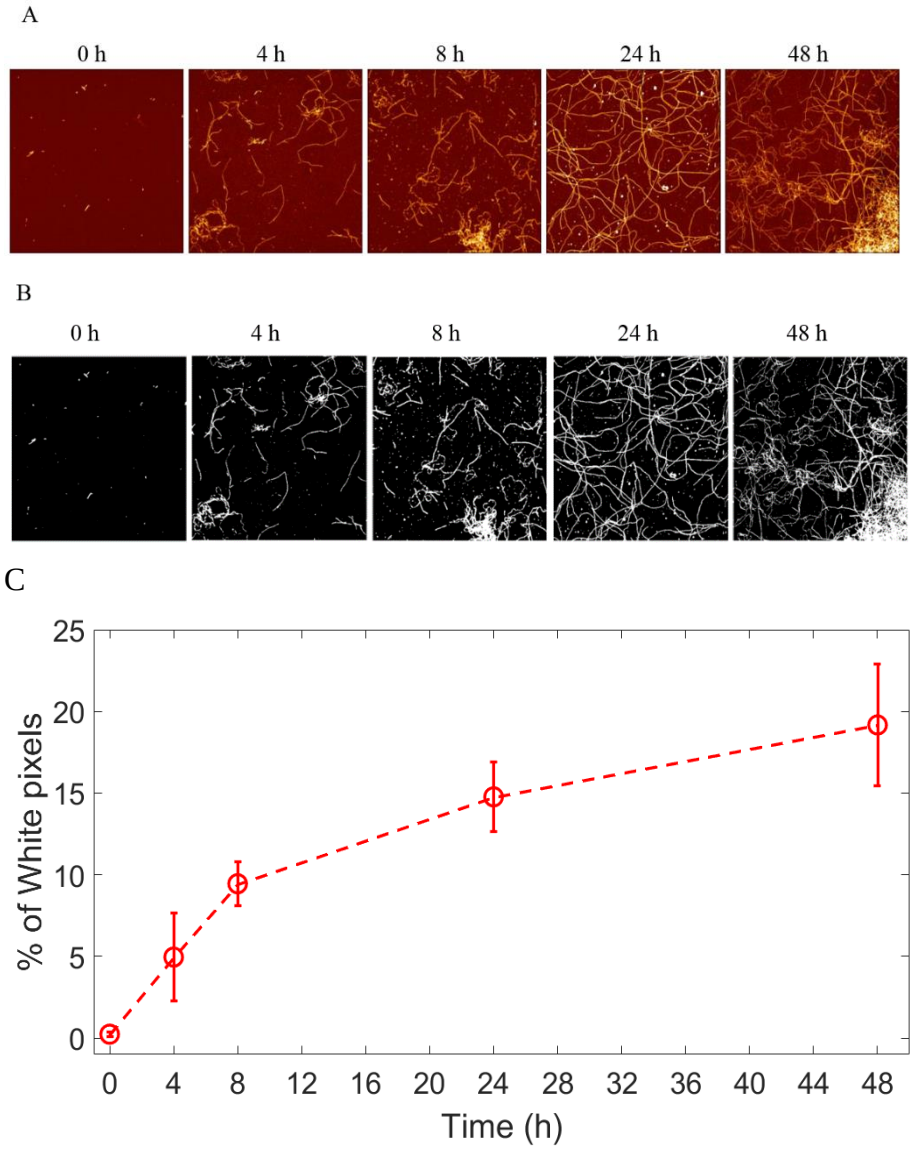

Figure 3. Aggregation process of Aβ from monomers to fibrils studied by AFM and quantification of fibrillation. A) Representative images of Aβ at different fibrillation stages up to 48 h when incubated at 37 °C. 4 x 4 μm^2, 1024 x 1024 pixels, Z-scale 10 nm. B) A fixed height threshold (1.5 nm) was applied to the AFM images, and the

number of pixels above this threshold were quantified and expressed in terms of percentage of total number of pixels. The number of pixels is proportional to the total length of the fibril i.e. to the sum of the lengths of all the deposited fibrils. In this way, it is possible to quantify the fibril growth. C) Percentage of pixels above a height threshold (1.5 nm) obtained from AFM images, and plotted as a function of the incubation time at 37 °C.

Characterization of *in vitro* BBB model

The *in vitro* BBB model was prepared and characterized as described above and results are shown in Fig. 4. TEER was monitored over time and the results showed that the maximum value (116.37 ± 4.37 Ω/cm^2) occurred 6 days after seeding (Fig. 4B). At this time point, the formation of junctions was checked by confocal microscopy and by measuring the paracellular and transcellular EP of radiolabelled sucrose and propranolol, respectively. The results showed that claudin-5 (Fig. 4C, stained in green) and VE-cadherin (Fig. 4C, stained in red), two key components of tight and adherens endothelial junctions, are formed in the hCMEC/D3 monolayer 6 days after seeding. The EP of [^{3}H]-propranolol and [^{14}C]-sucrose was (1.56 ± 0.13) $\times 10^{-5}$ and (3.83 ± 0.84) $\times 10^{-5}$ cm/min, respectively, suggesting that tight junctions had formed (Fig. 4D). At 6 days after seeding, 500 nM of Aβ fibrils (characterized by AFM images, see Fig. 3) were added to the basolateral compartment of the transwell system and the impact of fibrils on cell monolayer properties was checked. The results showed that after 3h exposure of hCMEC/D3 monolayer to fibrils, neither the TEER (114.10 ± 4.82 Ω/cm^2) nor EP of trans- and para-cellular probes changed (Fig. 4D).

Moreover, the treatment did not affect cell viability (>95% cells viability respect to untreated cells), as assessed by MTT assay.

A

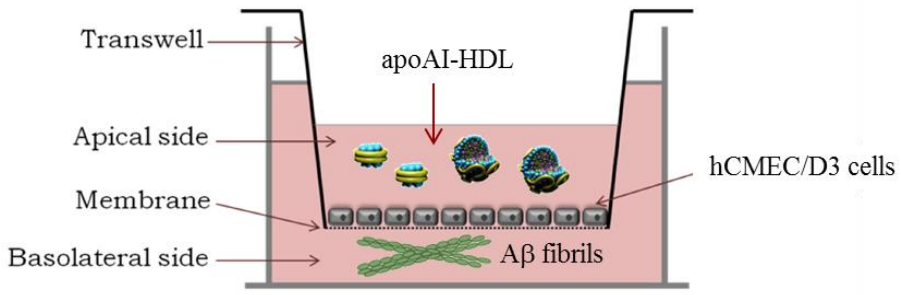

B

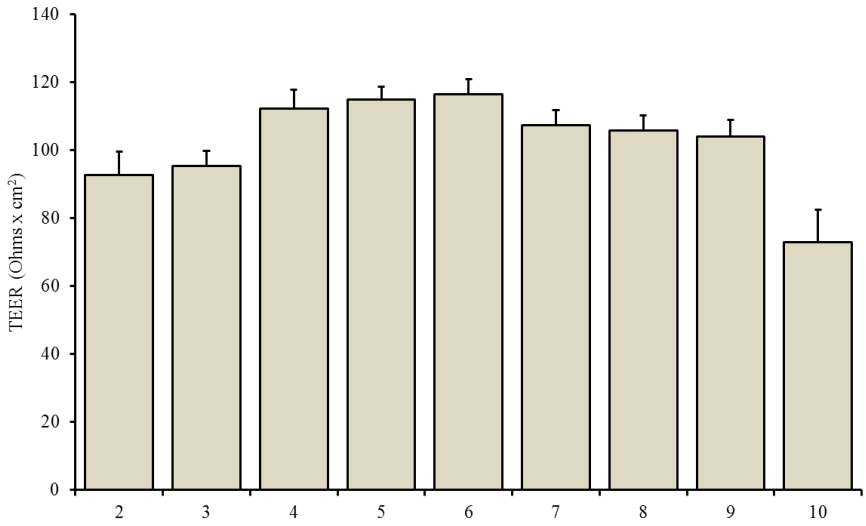

C

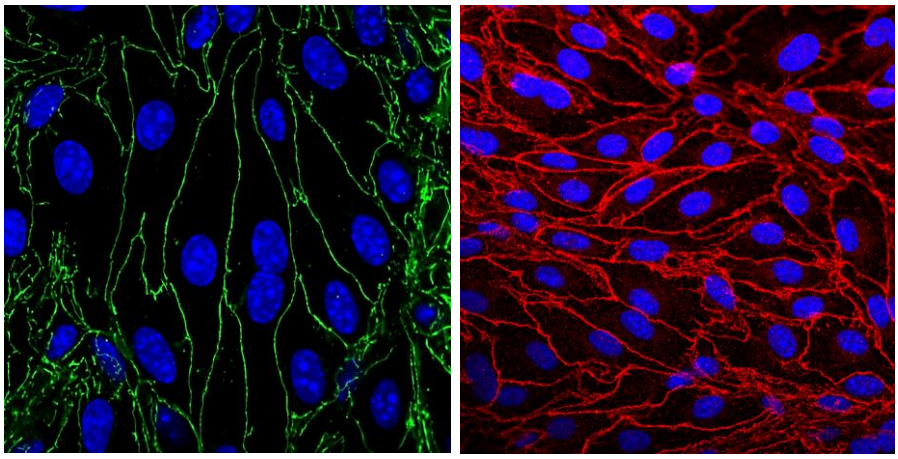

D

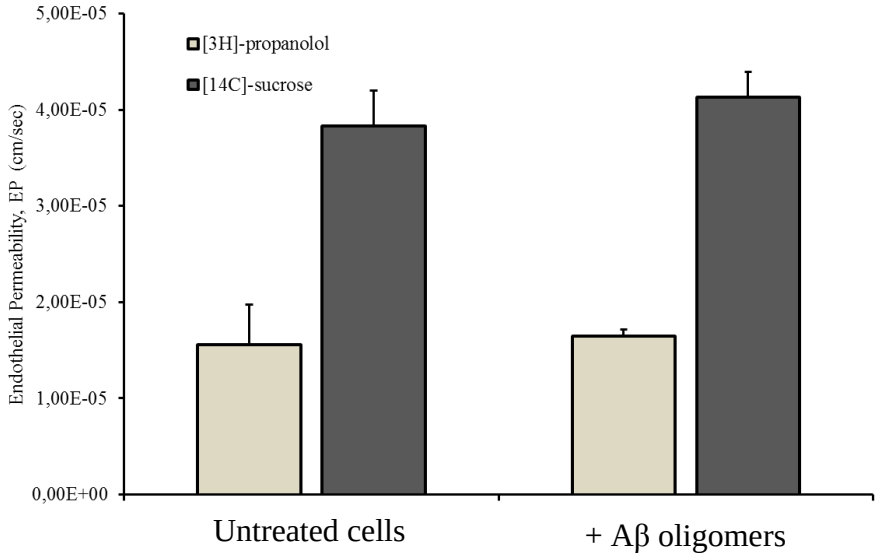

Fig. 4. Characterization of *in vitro* model of the BBB. (A) Schematic representation of the transwell model of the BBB, consisting of an apical "blood" compartment containing apoAI-HDL, and a basolateral "brain" compartment containing Aβ fibrils, separated by a membrane on which hCMEC/D3 cells are seeded. (B) TEER values of hCMEC/D3

cells seeded in transwells measured every day up to 10 days. TEER peaked on day 6 after cell seeding. (C) Staining of the tight junction protein claudin-5 (green) and the adherens junction protein VE-cadherin (red) in hCMEC/D3 cells. Nuclei are stained blue. (D) Passage of the paracellular probe [^{3}H]-propanolol and transcellular probe [^{14}C]-sucrose across the hCMEC/D3 cell monolayer. Endothelial permeability does not change in the presence of Aβ oligomers.

Effect of apoAI lipidation on *in vitro* Aβ efflux across the BBB

The Aβ efflux from the basolateral compartment of the transwell in the presence of apoAI in different lipidation states (in the apical compartment) was measured by ELISA assay. The results showed that the presence of apoAI in the apical compartment significantly increases Aβ efflux from the basolateral side of the BBB model (Fig. 5A). In particular, the ability of apoAI to enhance the Aβ efflux increases with the an increase in its lipidation state, reaching the maximum Aβ efflux when discoidal apoAI-HDL are present in the apical compartment of the transwell system.

The discoidal apoAI-HDL significantly increases Aβ efflux from the basolateral side of the BBB model, compared to the apoAI-HDL plasma pool (p=0.0016) and spherical apoAI-HDL (p=0.011) (Fig. 5B).

Comparing the capability of apoAI to enhance Aβ efflux with other plasma Aβ-binding proteins, i.e. α2-macroglobulin, apolipoprotein E or albumin, the results showed that the strongest increase of Aβ efflux across the BBB was detected with apoAI in the apical compartment (p=0.046) (Fig. 5C).

A

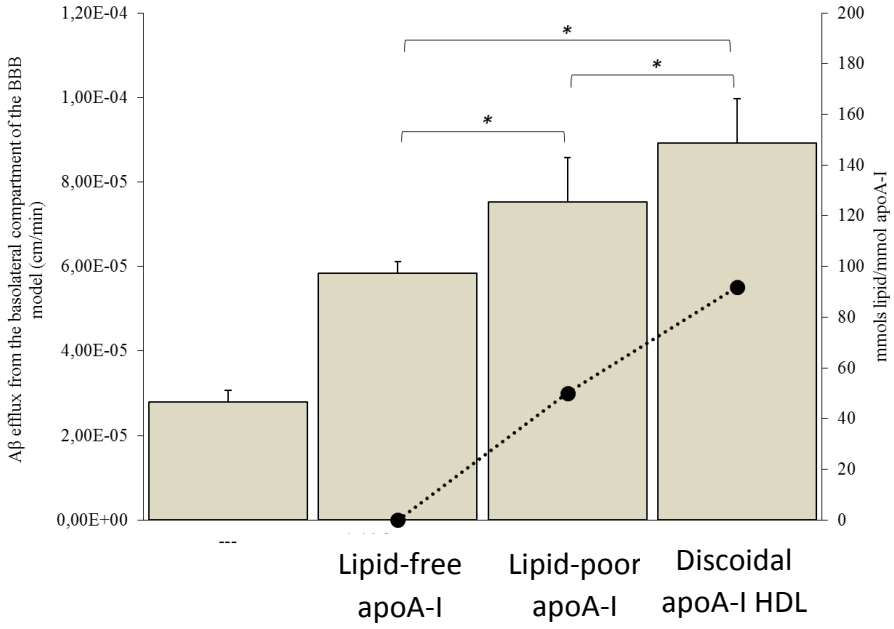
Aβ efflux from the basolateral compartment of the BBB model (cm/min)
1,20E-04
1,00E-04
8,00E-05
6,00E-05
4,00E-05
2,00E-05
0,00E+00
mmols lipid/mmol apoA-I
200
180
160
140
120
100
80
60
40
20
0
*
*
*

Lipid-free apoA-I
Lipid-poor apoA-I
Discoidal apoA-I HDL

B

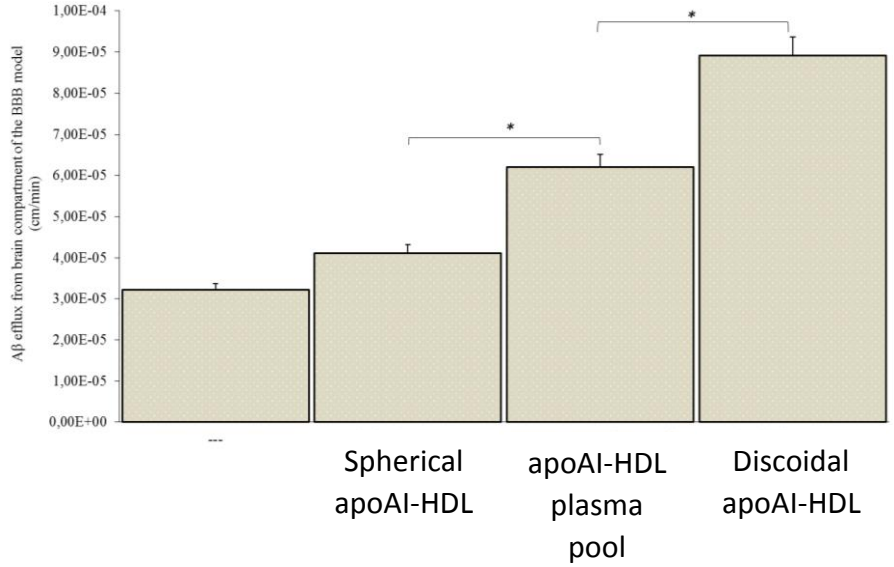
Aβ efflux from brain compartment of the BBB model (cm/min)
1,00E-04
9,00E-05
8,00E-05
7,00E-05
6,00E-05
5,00E-05
4,00E-05
3,00E-05
2,00E-05
1,00E-05
0,00E+00
*
*

Spherical apoAI-HDL
apoAI-HDL plasma pool
Discoidal apoAI-HDL

C

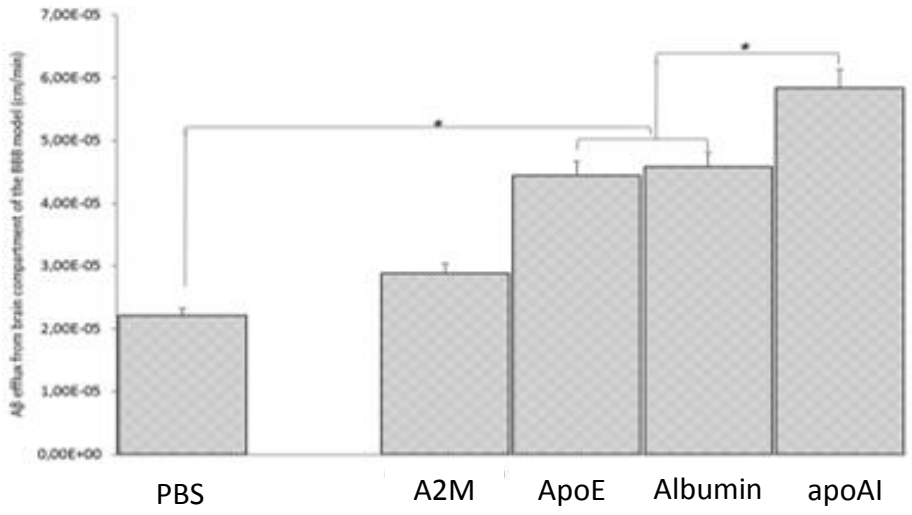

Figure 5. Aβ efflux across the BBB model in the presence of human plasma-derived HDL. hCMEC/D3 cells were cultured on a transwell system and 500 nM of oligomer-enriched Aβ sample was added to the medium in the basolateral compartment. Different subclasses of HDL or Aβ-binding proteins were added to the apical compartment and the Aβ efflux from the basolateral compartment was measured by ELISA assay. (A) Endothelial permeability (EP) of Aβ in the presence of lipid-free, lipid-poor or discoidal apoA-I-HDL. PBS (---) in the apical compartment was used as a control. (B) EP of Aβ in the presence of different HDL subclasses purified from human plasma. PBS (---) in the apical compartment was used as a control. (C) EP of Aβ in the presence of different Aβ-binding proteins (α2-macroglobulin (A2M), ApoE, albumin or apoAI). PBS alone in the apical compartment was used as a control. The data are reported as the mean ± s.e.m. of triplicate experiments and compared by Student t-test, *$p < 0.05$.

***In vitro* BBB crossing of apoAI-HDL**

Different subclasses of apoAI-HDL were added to the apical compartment of the transwell system and their EP across the cell monolayer was estimated by measuring the apoAI content in the bottom compartment by ELISA assay for up to 3h. The results (Fig. 6) showed that discoidal HDL displayed higher EP values, compared to spherical ones (p=0.004) and to lipid-free apoAI (p=0.048).

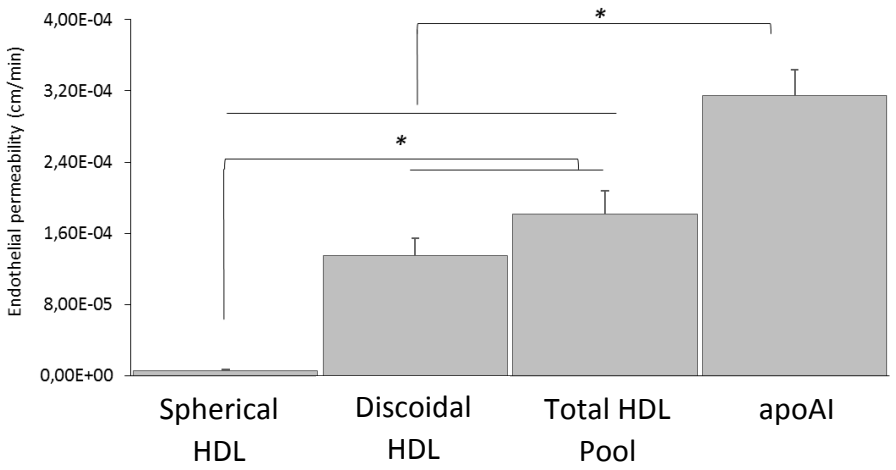

Figure 6. *In vitro* BBB crossing of different subclasses of human plasma HDL. The passage of different HDL subclasses across the hCMEC/D3 monolayer was estimated by quantifying apoA-I in the basolateral compartment of the transwell system at different incubation times (up to 3 h) by ELISA assay. Data were expressed as endothelial permeability (EP), calculated as described in the text. Lipid-free apoA-I was used as control. The data are reported as the mean ± s.e.m. of triplicate experiments and compared by Student's t-test, *= $p<0.01$.

Effect of apoAI lipidation on preformed Aβ fibrils

The effect of apoAI lipidation on the disaggregation of preformed Aβ fibrils was assessed by AFM and thioflavine T (ThT) assay[24]. Aβ fibrils were incubated with apoAI in different lipidation state for up to 24 h and changes in the morphology of fibrils were followed by AFM imaging (Fig. 7). The results showed that, starting from mature Aβ fibrils of comparable length (Fig. 7A, row 1), the incubation with spherical apoAI HDL did not induce significant changes in fibril morphology and concentration (Fig. 7A, column 2) compared to Aβ fibrils alone (Fig. 7A, column 1). On the contrary, incubation with both the apoAI-HDL plasma pool (Fig. 7, column 3) and discoidal apoAI-HDL (Fig. 7A, column 4) induces a strong time-dependent reduction of fibril concentration and extension.

The percentage of pixels above the 1.5 nm threshold (determined as reported in Supplementary Fig. S1 and S2) normalized with respect to the starting point (value at t = 0 h) is reported for each sample at different times to obtain a quantitative analysis of AFM images. The results (Fig. 7B) demonstrate the superior capability of discoidal apoAI-HDL in disassembling preformed Aβ fibrils compared to spherical apoAI-HDL.

The β-sheet content of Aβ fibril samples were analyzed using a ThT fluorescence assay and the results (Fig. 7C) showed that when fibrils are incubated alone, or with spherical apoAI-HDL, their β-sheet content did not significantly change. On the contrary, the presence of apoAI-HDL plasma pool induces a 40% reduction of β-sheet content in 18 h, and there is an almost complete disruption of β-sheet structures within 4 h in the presence of discoidal apoAI-HDL.

A

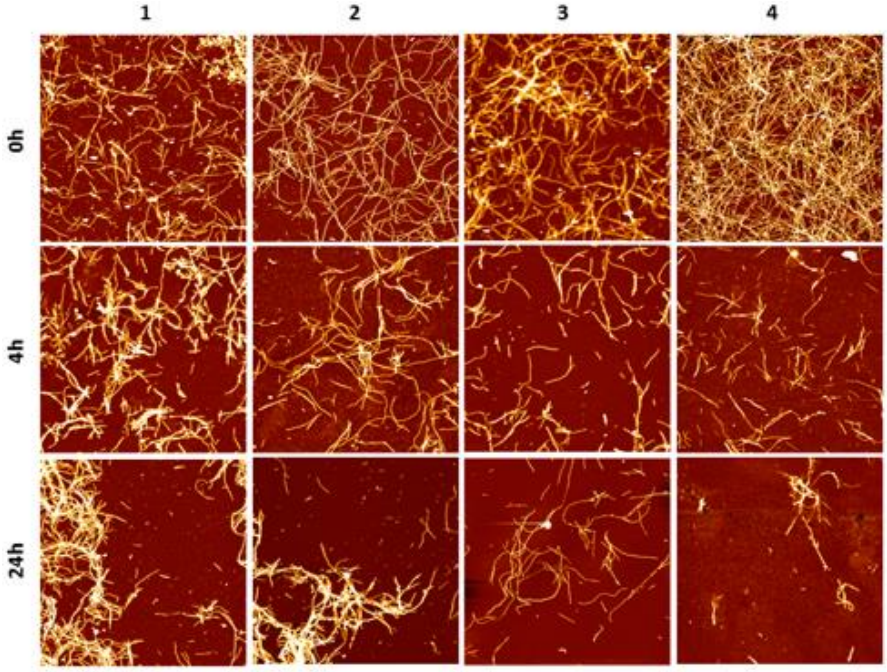
1
2
3
4
0h
4h
24h

B

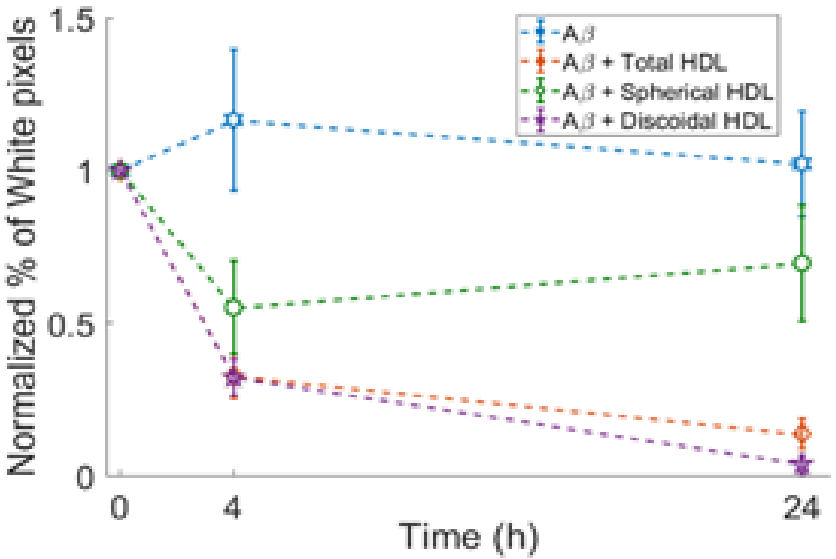
Normalized % of White pixels
1.5
1
0.5
0
0
4
24
Time (h)
Aβ
Aβ + Total HDL
Aβ + Spherical HDL
Aβ + Discoidal HDL

C

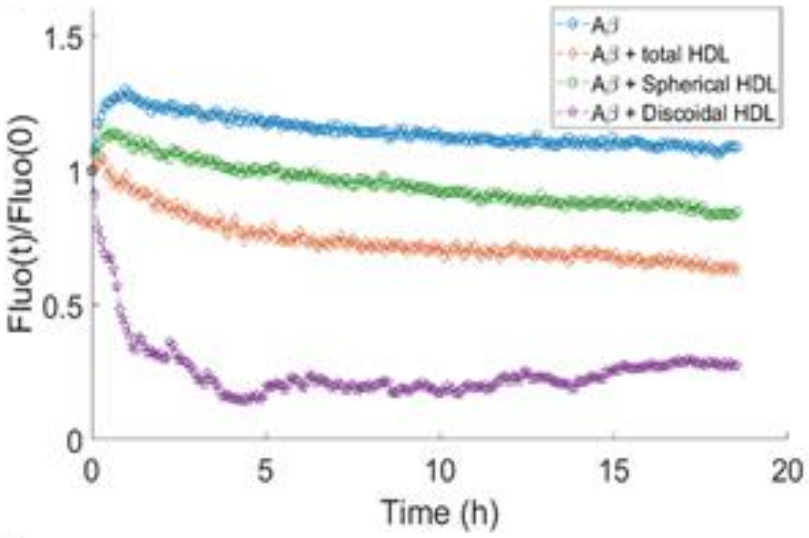

Figure 7. Disaggregation of preformed Aβ fibrils in the presence of HDL. (A) Representative AFM images of Aβ fibrils over time, incubated at 37°C either alone (column 1) or with different HDL subclasses: spherical HDL (column 2), total HDL plasma pool (column 3), discoidal HDL (column 4). Images are 4 x 4 μm^2, 1024 x 1024 pixel, Z-scale 10 nm. (B) The normalized percentage of pixels with a height above a threshold of 1.5 nm (white pixel percentage) is reported for Aβ in the presence of the different HDL subclasses at different incubation times. Values are the average of pixels higher than the threshold over several images acquired on the same sample. Error bars represent s.d. Each sample is normalized to its respective starting point (value at t = 0 h). (C) Thioflavine T fluorescence as a function of time in samples containing 2 μM Aβ fibrils alone (blue) or incubated with spherical HDL (green), total HDL pool (orange) or discoidal HDL (purple). The intensities were normalized to the respective zero-time intensity.

Discoidal apoAI-HDL induce a structural destabilization of Aβ

The interaction between discoidal apoAI-HDL and $A\beta_{17-42}$ was evaluated using molecular dynamics (MD) simulations. Protein structural stability was analyzed by monitoring the time evolution of the Root Mean Square Deviation (RMSD) of $A\beta_{17-42}$ in water and $A\beta_{17-42}$ in complex with apoAI. Three different replicas of the $A\beta_{17-42}$ alone in water and in complex with apoAI were examined to increase the statistics of the MD data. It was observed that protein conformational stability was reasonably reached in the last 20 ns of the simulations (Supplementary Fig. S2). The apoAI-$A\beta_{17-42}$ contact surface, characterized by protein-lipid (Aβ-1,2-dimyristoyl-sn-glycero-3-phosphocholine) and protein-protein (Aβ-apoAI) interactions, covers 6.3 ± 2 nm^2 of solvent accessible surface. The hydrophobic interaction plays a pivotal role in the contact area (Fig. S3). The visual inspection of the apoAI-$A\beta_{17-42}$ complex through the MD simulation is reported in Fig. 8A and highlights the conformational destabilization of the $A\beta_{17-42}$ due to the interaction with apoAI.

The previously highlighted conformational instability can be quantified by analyzing the fibril order parameter (*ordP*), as reported in Fig. 8B. A significantly decreased *ordP* value (ordP < 1 are typical of a distorted structure) was found in the case of apoAI-$A\beta_{17-42}$ (*ordP* = 0.60 ± 0.02) compared to $A\beta_{17-42}$ alone in water (*ordP* = 0.79 ± 0.02). The Principal Component Analysis (PCA) provides another image, which highlights the large-scale and low frequency modes mainly related to the distortion of the Aβ fibril. After the alignment of the Aβ C-α atoms, the covariance matrix was calculated and diagonalized for each simulated system ($A\beta_{17-42}$ in water and $A\beta_{17-42}$ in complex with apoAI).

The amplitude of the first Principal Component Vector, which takes into account more than 50% of the total variance of the protein motion, is reported in Fig. 8C, highlighting a marked increase in conformational fluctuations when $A\beta_{17-42}$ is in complex with apoAI ($eigval_{PCA1}$ = 17) compared to $A\beta_{17-42}$ alone in water ($eigval_{PCA1}$ = 5). Finally, a decreased β-sheet content was observed by computing the secondary structures probabilities (Fig. 8D) along the Aβ fibril chains at the equilibrium, as previously described[17-23].

A

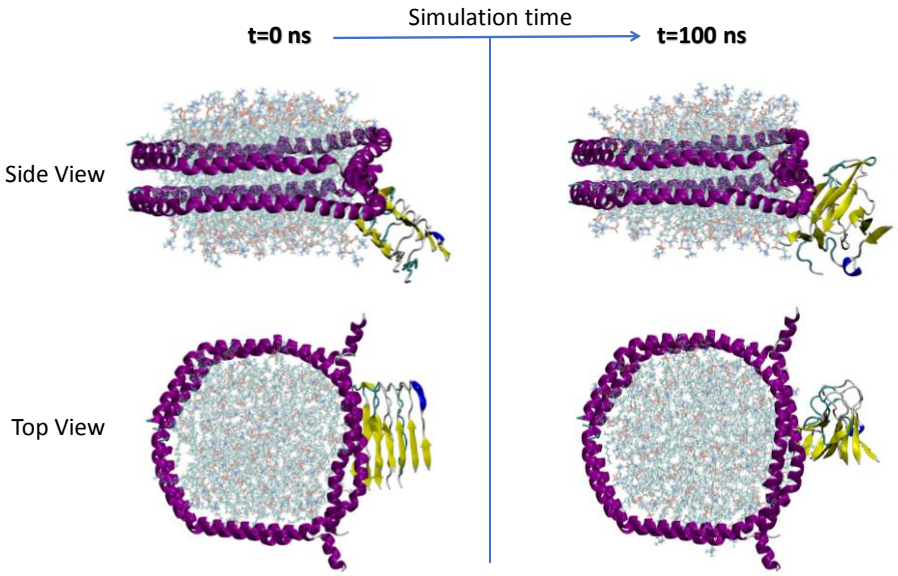

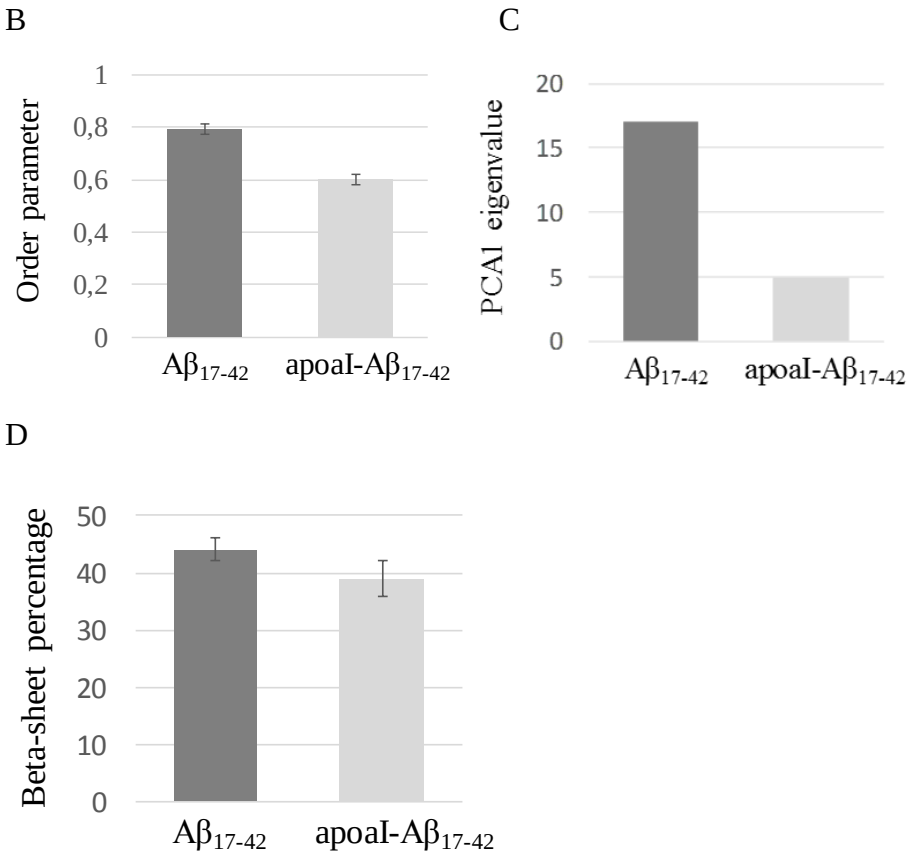

Figure 8. Analysis of Aβ destabilization by discoidal apoA-I HDL obtained by MD simulations. (A) Visual inspection of the apoAI interaction with Aβ fibril at the beginning (t = 0 ns) and at the end (t = 100 ns) of the MD simulation. The side-view and top-view representations are reported in the upper and lower panels respectively. Yellow represents $A\beta_{17-42}$ and magenta represents apoA-I. The destabilization of Aβ fibril is described, reporting (B) the order parameter calculated at the equilibrium, (C) the eigenvalue of the first PCA vector, and (D) the β-sheet content of Aβ fibril alone in water and in complex with apoA-I.

3.5 DISCUSSION

Considerable evidence suggests that plasma HDL, as well as having vasoprotective functions, could exert a protective role in AD[1,2], but the mechanisms involved have not been thoroughly investigated. Since Aβ clearance from the brain, a way to possibly counteract the onset or progression of AD, partially occurs across the brain vasculature[25], an important goal is to understand if and how plasma-derived circulating HDL might affect Aβ passage across the BBB.

Considering previously published data about the ability of HDL and apoA-I to bind Aβ *in vitro*[8,26,27] and reduce Aβ levels in the brains of AD animal models[28], we hypothesized that plasma-derived HDL acts by accelerating the Aβ egress from the brain to the blood *via* the "sink effect", as already speculated for different Aβ binding molecules or particles[29]. To investigate this issue, a simple BBB model was used, consisting of an hCMEC/D3 monolayer that separates a basolateral compartment (containing Aβ to mimic the AD brain[16]) from an apical one (containing different human HDL subclasses to mimic the blood).

The results showed that the presence of apoAI in the apical compartment of the transwell system strongly enhanced the Aβ egress from the basolateral one. This effect is amplified by the lipidation state of apoAI, reaching the maximum Aβ efflux when apoAI is adjusted in discoidal HDL. Contrarily, no effect on Aβ efflux was detected when apoAI is in mature spherical HDL. These results suggest that the 'sink effect' is not due to the lipid portion of HDL, but is boosted by the conformation that apoAI takes, which depends on its lipidation state. In fact, the flexible apoA-I molecule has been previously shown to adapt its structural motif to stabilize the different HDL subclasses. Therefore,

we theorize that the plasma profile of HDL subclasses could differ between healthy and AD patients, thus affecting Aβ clearance from the brain. A recent study showed that HDL from AD patients were less functional compared to HDL from healthy subjects[30], supporting this idea. Moreover, the ability of apoAI to enhance the Aβ efflux from the basolateral compartment was superior respect to the other Aβ-binding plasma proteins tested (α2-macroglobulin, ApoE, albumin). This result is in agreement with the high binding affinity of apoAI for Aβ (kd = 6 nM), compared to the other proteins tested (40 < kd < 400 nM)[26,31,32]. The determination of Aβ binding affinity towards apoAI arranged in different HDL subclasses deserves further investigation.

Since only small soluble Aβ assemblies, and not fibrils, are able to cross the endothelial monolayer and as apoAI is not synthetized in the brain[35,36], the ability of apoAI-HDL to promote the Aβ clearance from the brain should indicate their ability to cross the BBB and to disaggregate fibrils. Our results showed that when apoAI adjusted its structure in discoidal HDL, rather than in spherical ones, it is able to cross the BBB *in vitro*, probably *via* SR-BI receptor present at the BBB level, and expressed on hCMEC/D3 cells[38]. However, this is in contrast with the reported greater (50-fold) affinity of binding to SR-BI by the larger HDL particles compared to the smaller (discoidal HDL) ones[39] which exists due to the apoAI conformation. Nevertheless, our data together with data recently published using apoJ nanodiscs[40] support the hypothesis that the affinity of apoAI to SR-BI is not enough to cross the BBB, and that the shape and size of HDL are additional determining factors. To the best of our knowledge, there are no data about the ability of different HDL subclasses to cross the BBB.

Finally, we investigate the effect of different apoAI-HDL subclasses on pre-formed Aβ fibrils by AFM imaging, ThT assay and MD simulation. AFM imaging showed that the presence of discoidal apoAI-HDL strongly reduces the amount and concentration of long fibrils. This was confirmed by ThT assay, where a strong and rapid reduction of the β-sheet content of fibrils was detected. The molecular modelling results highlighted the conformational destabilization of Aβ upon its interaction with apoAI when associated to discoidal HDL. A significant distortion of the fibril order and a decrease in the β-sheet content was identified, clearly suggesting a key role played by discoidal apoAI-HDL in destabilizing the Aβ fibrils.

Concerning the disaggregating ability of the total HDL plasma pool, it is worth noting that physiologically circulating HDL are composed of 15% discoidal nascent HDL, which is probably enough to maintain Aβ in its soluble form.

In summary, we can speculate that at earliest stages of AD, plasma apoAI-HDL may be involved in synergic activity with brain apoAI-HDL pool, whereby the central HDL pool maintains Aβ in a soluble form, while the peripheral HDL pool enhances its efflux from the brain. These results contribute to previously published knowledge[28,38,41] that could decipher the mechanism by which apoAI-HDL exert their protective role in AD.

Acknowledgements

This work was partly supported by the Grant ATE-Project awarded by University of Milano-Bicocca, 2015-ATE-0510 to F.R.

Conflict of Interest Statement

The authors declare that they have no competing interests.

Author Contributions Statement

R.D. performed *in vitro* experiments on the blood-brain barrier model. S.S. purified, prepared and characterized the different subtypes of HDL from human plasma. A.C. performed *in vitro* experiments with beta-amyloid peptide. B.F. prepared and characterized beta-amyloid aggregates. R.C. and V.C. performed AFM imaging experiments. L.N. performed ThT fluorescence assays. G.G., M.A.D. and A.D. performed the molecular modelling analysis. L.C., F.M. and F.R. contributed to the data interpretation and participated in the drafting of the manuscript. F.R. coordinated the study, designed the experiments, analyzed the data and participated in the drafting of the manuscript. All authors contributed to the paper revision, read and approved the submitted version and agree to be accountable for all the aspects of the work.

References

1. Kingwell, B. A., Chapman, M. J., Kontush, A., Miller, N. E. HDL-targeted therapies: progress, failures and future. *Nat. Rev. Drug Discov.* **13**, 445-464 (2014).

2. Vitali, C., Wellington, C. L., Calabresi, L. HDL and cholesterol handling in the brain. *Cardiovasc. Res.* **103**(3), 405-413 (2014).

3. Haass, C., Selkoe, D. J. Cellular processing of beta-amyloid precursor protein and the genesis of amyloid beta-peptide. *Cell.* **75**, 1039–1042 (1993).

4. Glenner, G. G., Wong, C. W. Alzheimer's disease: initial report of the purification and characterization of a novel cerebrovascular amyloid protein. *Biochem. Biophys. Res. Commun.* **425**, 534–539 (2012).

5. Selkoe, D. J., Hardy, J. The amyloid hypothesis of Alzheimer's disease at 25 years. *EMBO Mol. Med.* **8**, 595–608 (2016).

6. Merched, A., Xia, Y., Visvikis, S., Serot, J. M., Siest, G. Decreased high-density lipoprotein cholesterol and serum apolipoprotein AI concentrations are highly correlated with the severity of Alzheimer's disease. *Neurobiol. Aging.* **21**(1), 27-30 (2000).

7. Hye A, *et al.* Plasma proteins predict conversion to dementia from prodromal disease. *Alzheimers Dement.* **10**, 799–807 (2014).

8. Shih, Y. H., *et al*. Apolipoprotein C-III is an amyloid-β-binding protein and an early marker for Alzheimer's disease. *J. Alzheimers Dis.* **41**, 855-865 (2014).

9. Elliott, D. A., Weickert, C. S., Garner, B. Apolipoproteins in the brain: implications for neurological and psychiatric disorders. *Clin. Lipidol.* **51**, 555-573 (2010).

10. Liu, H. C., *et al*. Proteomic identification of lower apolipoprotein A-I in Alzheimer's disease. *Dement. Geriatr. Cogn. Disord.* **21**, 155–161 (2006).

11. Mahley, R. W., Innerarity, T. L., Rall, S. C. Jr., Weisgraber, K. H. Plasma lipoproteins: apolipoprotein structure and function. *J. Lipid Res.* **25**, 1277–1294 (1984).

12. Harr, S. D., Uint, L., Hollister, R., Hyman, B. T., Mendez, A. J. Brain expression of apolipoproteins E, J, A-I in Alzheimer's disease. *J. Neurochem.* **66**, 2429–2435 (1996).

13. Huang, J. T., *et al.* Independent protein-profiling studies show a decrease in apolipoprotein A1 levels in schizophrenia CSF, brain and peripheral tissues. *Mol. Psychiatry.* **13**, 1118–1128 (2008).

14. Roheim, P. S., Carey, M., Forte, T., Vega, G. L. Apolipoproteins in human cerebrospinal fluid. *Proc. Natl. Acad. Sci. USA.* **76**, 4646–4649 (1979).

15. Pitas, R. E., Boyles, J. K., Lee, S. H., Foss, D., Mahley, R. W. Astrocytes synthesize apolipoprotein E and metabolize apolipoprotein E-containing lipoproteins. *Biochim. Biophys. Acta.* **917**, 148–161 (1987).

16. Mancini, S., *et al.* The hunt for brain Aβ oligomers by peripherally circulating multi-functional nanoparticles: Potential therapeutic approach for Alzheimer disease. *Nanomedicine.* **12**, 43-52 (2016).

17. Deriu, M. A., *et al.* Investigation of the Josephin domain protein-protein interaction by molecular dynamics. *PLoS One.* **9**, e108677 (2014).

18. Grasso, G., *et al.* Cell penetrating peptide adsorption on magnetite and silica surfaces: a computational investigation. *J. Phys. Chem. B.* **119**, 8239–8246 (2015).

19. Deriu, M. A., Grasso, G., Tuszynski, J. A., Gallo, D., Morbiducci, U., Danani, A. Josephin domain structural conformations explored by metadynamics in essential coordinates. *PLOS Comput. Biol.* **12**, e1004699 (2016).

20. Deriu, M. A., *et al.* Characterization of the AXH domain of Ataxin-1 using enhanced sampling and functional mode analysis. *Proteins Struct. Funct. Bioinforma.* **84**, 666–673 (2016).

21. Grasso, G., Deriu, M. A., Tuszynski, J. A., Gallo, D., Morbiducci, U., Danani, A. Conformational fluctuations of the AXH monomer of Ataxin-1. *Proteins.* **84**, 52-59 (2016).

22. Grasso, G., Tuszynski, J. A., Morbiducci, U., Licandro, G., Danani, A., Deriu, M. A. Thermodynamic and kinetic stability of the Josephin Domain closed arrangement: evidences from replica exchange molecular dynamics. *Biol. Direct.* **12**, 2 (2017).

23. Janaszewska, A., *et al.* Multivalent interacting glycodendrimer to prevent amyloid-peptide fibril formation induced by Cu(II): A multidisciplinary approach. *Nano Res.* **11**, 1204 (2018).

24. Quan, L., *et al*. Enhanced detection specificity and sensitivity of Alzheimer's disease using amyloid-β-targeted quantum dots. *Bioconjug. Chem.* **27**(3), 809-814 (2016).

25. Bates, K. A., *et al.* Clearance mechanisms of Alzheimer's amyloid-β peptide: implications for therapeutic design and diagnostic tests. *Mol. Psychiatry.* **14**, 469–486 (2009).

26. Koldamova, R. P., Lefterov, I. M., Lefterova, M. I., Lazo, J. S. Apolipoprotein A-I directly interacts with amyloid precursor protein and inhibits A beta aggregation and toxicity. *Biochemistry.* **40**, 3553-3560 (2001).

27. Paula-Lima, A. C., *et al.* Human apolipoprotein A-I binds amyloid-beta and prevents Abeta-induced neurotoxicity. *Int. J. Biochem. Cell Biol.* **41**, 1361-1370 (2009).

28. Robert, J., *et al.* Reconstituted high-density lipoproteins acutely reduce soluble brain Aβ levels in symptomatic APP/PS1 mice. *Biochim. Biophys. Acta.* **1862**, 1027-1036 (2016).

29. Golabek, A., Marques, M. A., Lalowski, M., Wisniewski, T. Amyloid beta binding proteins *in vitro* and in normal human cerebrospinal fluid. *Neurosci. Lett.* **191**(1-2), 79-82 (1995).

30. Camponova, P., *et al.* Alteration of high-density lipoprotein functionality in Alzheimer's disease patients. *Can. J. Physiol. Pharmacol.* **95**, 894-903 (2017).

31. Mettenburg, J. M., Arandjelovic, S., Gonias, S. L. A chemically modified preparation of alpha2-macroglobulin binds beta-amyloid peptide with increased affinity and inhibits Abeta cytotoxicity. *J. Neurochem.* **93**(1), 53-62 (2005).

32. Du, Y., *et al.* Alpha2-Macroglobulin as a beta-amyloid peptide-binding plasma protein. *J. Neurochem.* **69**, 299-305 (1997).

33. Guha, M., Gao, X., Jayaraman, S., Gursky, O. Correlation of structural stability with functional remodeling of high-density lipoproteins: the importance of being disordered. *Biochemistry.* **47**, 11393-11397 (2008).

34. Pourmousa, M., Song, H. D., He, Y., Heinecke, J. W., Segrest, J. P., Pastor, R. W. Tertiary structure of apolipoprotein A-I in nascent high-density lipoproteins. *PNAS.* **115**(20), 5163-5168 (2018).

35. Demeester, N., *et al.* Characterization and functional studies of lipoproteins, lipid transfer proteins, and lecithin:cholesterol acyltransferase in CSF of normal individuals and patients with Alzheimer's disease. *J. Lipid Res.* **41**, 963-974 (2000).

36. Koch, S., *et al.* Characterization of four lipoprotein classes in human cerebrospinal fluid. *J. Lipid Res.* **42**, 1143-1151 (2001).

37. Stukas, S., *et al.* Intravenously injected human apolipoprotein A-I rapidly enters the central nervous system via the choroid plexus. *J. Am. Heart Assoc.* **3**, e001156 (2014).

38. Robert, J., *et al.* High-density lipoproteins suppress Aβ-induced PBMC adhesion to human endothelial cells in bioengineered vessels and in monoculture. *Mol. Neurodegener.* **12**, 60 (2017).

39. de Beer, M. C., Durbin, D. M., Cai, L., Jonas, A., de Beer, F. C., van der Westhuyzen, D. R. Apolipoprotein A-I conformation markedly influences HDL interaction with scavenger receptor BI. *J. Lipid Res.* **42**, 309-313 (2001).

40. Fernández-de-Retana, S., *et al.* Characterization of ApoJ-reconstituted high-density lipoprotein (rHDL) nanodisc for the potential treatment of cerebral β-amyloidosis. *Sci. Rep.* **7**, 14637 (2017).

41. Slot, R. E., *et al.* Apolipoprotein A1 in Cerebrospinal Fluid and Plasma and Progression to Alzheimer's Disease in Non-Demented Elderly. *J. Alzheimers Dis.* **56**, 687-697 (2017).

42. Favari, E., *et al.* Depletion of pre-beta-high density lipoprotein by human chymase impairs ATP-binding Cassette Transporter A1- but not Scavenger Receptor Class B Type I-mediated lipid efflux to high density lipoprotein. *J. Biol. Chem.* **279**, 9930-9936 (2004).

43. Bernini, F., Calabresi, L., Bonfadini, G., Franceschini, G. The molecular structure of apolipoprotein A-II modulates the capacity of HDL to promote cell cholesterol efflux. *Biochim. Biophys. Acta.* **1299**, 103-109 (1996).

44. Calabresi, L., Vecchio, G., Frigerio, F., Vavassori, L., Sirtori, C. R., Franceschini, G. Reconstituted high-density lipoproteins with a disulfide-linked apolipoprotein A-I dimer: evidence for restricted particle size heterogeneity. *Biochemistry.* **36**, 12428-12433 (1997).

45. Franceschini, G., *et al.* Differential effects of fenofibrate and extended-release niacin on high-density lipoprotein particle size distribution and cholesterol efflux capacity in dyslipidemic patients. *J. Clin. Lipidol.* **7**, 414-422 (2013).

46. Oertel, J., *et al.* Anisotropic metal growth on phospholipid nanodiscs via lipid bilayer expansion. *Sci. Rep.* **6**, 26718 (2016).

47. Gregori, M., *et al.* Stability of Aβ(1-42) peptide fibrils as consequence of environmental modifications. *Eur. Biophys. J.* **39**, 1613–1623 (2010).

48. Bana, L., *et al.* Liposomes bi-functionalized with phosphatidic acid and an ApoE-derived peptide affect Aβ aggregation features and cross the blood-brain-barrier: implications for therapy of Alzheimer disease. *Nanomedicine.* **10**, 1583-1590 (2014).

49. Bibow, S., *et al.* Solution structure of discoidal high-density lipoprotein particles with a shortened apolipoprotein A-I. *Nat. Struct. Mol. Biol.* **24**, 187–193 (2016).

50. Huang, J., MacKerell, A. D. CHARMM36 all-atom additive protein force field: Validation based on comparison to NMR data. *J. Comput. Chem.* **76**, 2135–2145 (2013).

51. Jorgensen, W. L., Chandrasekhar, J., Madura, J. D., Impey, R. W., Klein, M. L. Comparison of simple potential functions for simulating liquid water. *J. Chem. Phys.* **79**, 926 (1983).

52. Bussi, G., Donadio, D., Parrinello, M. Canonical sampling through velocity rescaling. *J. Chem. Phys.* **126**, 14101 (2007).

53. Berendsen, H. J. C., Postma, J. P. M., Van Gunsteren, W. F., DiNola, A., Haak, J. R. Molecular dynamics with coupling to an external bath. *J. Chem. Phys.* **81**, 3684–3690 (1984).

54. Luhrs, T., *et al.* 3D structure of Alzheimer's amyloid-(1-42) fibrils. *Proc. Natl. Acad. Sci.* **102**, 17342–17347 (2005).

55. Yu, X., Zheng, J. Cholesterol Promotes the Interaction of Alzheimer β-Amyloid Monomer with Lipid Bilayer. *J. Mol. Biol.* **421**, 561–571 (2012).

56. Schneidman-Duhovny, D., Inbar, Y., Nussinov, R., Wolfson, H. J. PatchDock and SymmDock: servers for rigid and symmetric docking. *Nucleic Acids Res.* **33**, W363–W367 (2005).

57. Andrusier, N., Nussinov, R., Wolfson, H. J. FireDock: Fast interaction refinement in molecular docking. *Proteins Struct. Funct. Bioinforma.* **69**, 139–159 (2007).

58. Mashiach, E., Schneidman-Duhovny, D., Andrusier, N., Nussinov, R., Wolfson, H. J. FireDock: a web server for fast interaction

refinement in molecular docking. *Nucleic Acids Res.* **36**, W229–W232(2008).

59. Maisuradze, G. G., Liwo, A., Scheraga, H. Principal component analysis for protein folding dynamics. *J. Mol. Biol.* **385**, 312–329 (2009).

SUPPLEMENTARY INFORMATION

Characterization of HDL by AFM imaging

AFM measurements allow discrimination of the different geometrical appearances of the HDL subtypes through determination of their morphological characteristics. Considering the intrinsic tip convolution (finite size and specific geometry of the AFM cantilever tip) and the relatively small dimensions of the samples, discoidal and spherical HDL cannot be clearly distinguished by AFM imaging. However, these image limitations can be overcome by considering the shape of the height statistical distributions (Fig. 2C). Through AFM imaging, each (x, y) coordinate of the image is associated with the quantity z, which represents the measured height at the (x, y) coordinate. By analyzing the statistical distribution of heights for discoidal HDL (Fig. 2C, green), the distribution of the height values (4 - 25 nm) is significantly different from the height distribution of spherical HDL (Fig. 2C, red). Only heights > 4 nm are analyzed in order to eliminate the substrate contributions (heights too close to the mica surface i.e. z≈0). In order to quantify the resulting statistical outcomes, the normalized spherical HDL height histograms (Fig. 2C, red) were fitted into the formula theoretically predicted for a sphere:

$$h(x) = n_0\left(R_s + 2\pi\sqrt{{R_s}^2 - x^2}\right).$$

where n_0 is the normalization factor and R_s is the mean radius of the spheres (12.7 nm with a coefficient of determination R^2=0.96).

For discoidal HDL (Fig. 2C, green), assuming deposition only with the disk bases parallel to the mica surface, the theoretical height distribution can be considered a δ-function centered on the disk's average height h_D. The height distribution is influenced by the tip convolution, the polydispersity of the sample, and the possible different deposition orientation of the disks. Since the data cannot be fitted to the δ-function, the maximum height of the distribution is considered as the mean disk's height. To simplify the visualization of the maxima, the linear regression of the final part of the distribution is shown (Fig. 2C). Using this procedure, the average height value for discoidal HDL is 12.9 nm. Height distribution statistical analysis is successful in discriminating between different HDL subtypes, which exhibit comparable radial projections.

Interaction of discoidal HDL with Aβ by computational modelling

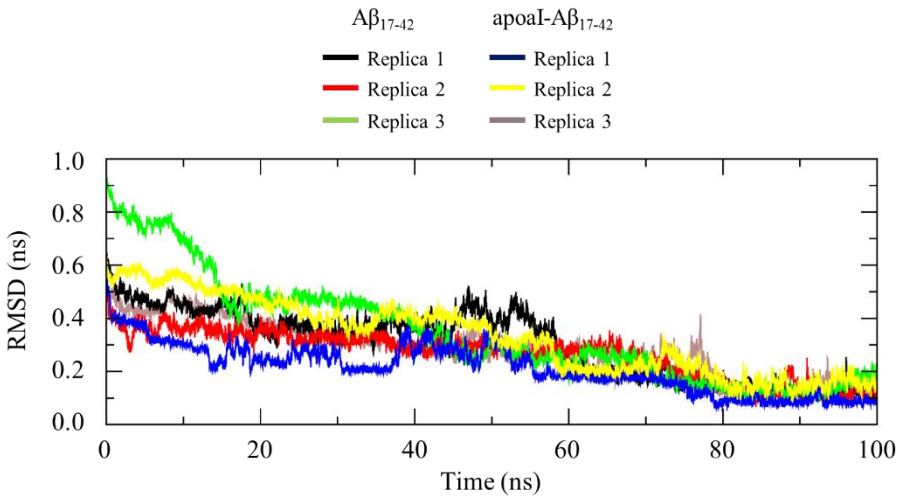

Figure S1. Protein structural stability by MD. C-alpha/C-alpha Root Mean Square Deviation (RMSD) plot computed for each replica of the $A\beta_{17-42}$ and apoA-I-$A\beta_{17-42}$ molecular systems. Protein conformational stability was reasonably reached in the last 20 ns of the simulations.

From images to numbers: quantification by using a height threshold

By applying a threshold to every AFM image, it is possible to measure the number of pixels whose height was above this threshold (white pixels). The number of white pixels is directly proportional to the total quantity of Aβ aggregated in fibrils in the field of view (Fig. S2, which represents Fig. 7 after a threshold application of 1.5 nm).

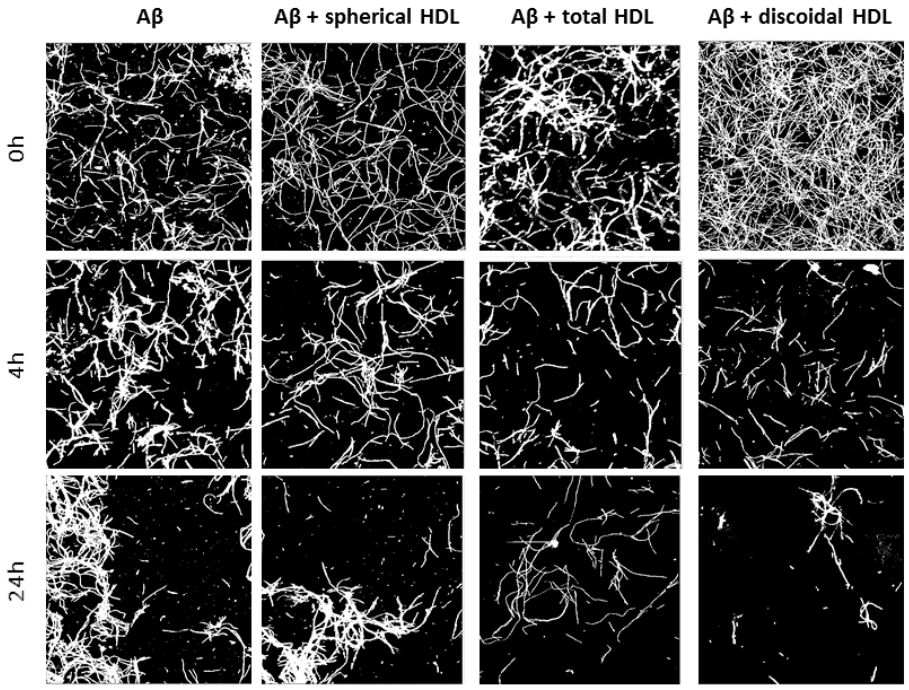

Figure S2. A fixed height threshold (1.5 nm) applied to the representative AFM images in Fig. 7. This process allows quantification of the percentage of white pixels (pixels above a certain threshold), which is correlated to fibril crowding (total length and number).

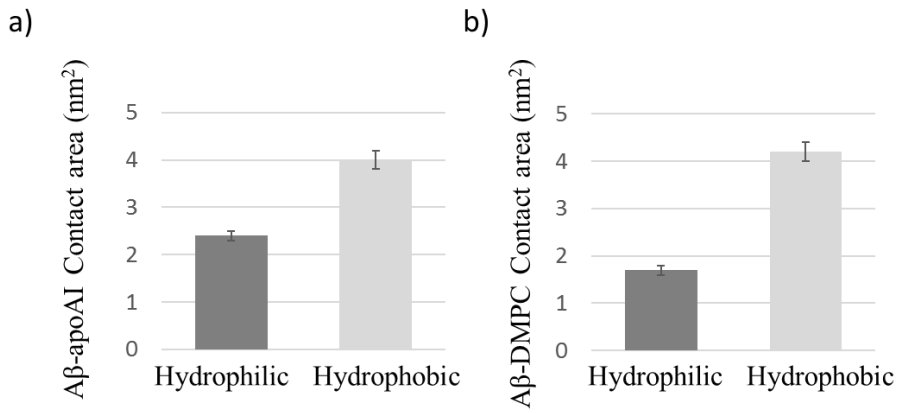

Figure S3. Interaction between $A\beta_{17-42}$ and apoA-I evaluated by MD. Histogram of the apoAI-$A\beta_{17-42}$ contact surface characterized by a) protein-protein, i.e. Aβ-apoAI, and b) protein-lipid, i.e. Aβ-DMPC contact surface. In both cases, the hydrophobic contribution plays a major role in driving the apoAI-$A\beta_{17-42}$ interaction.

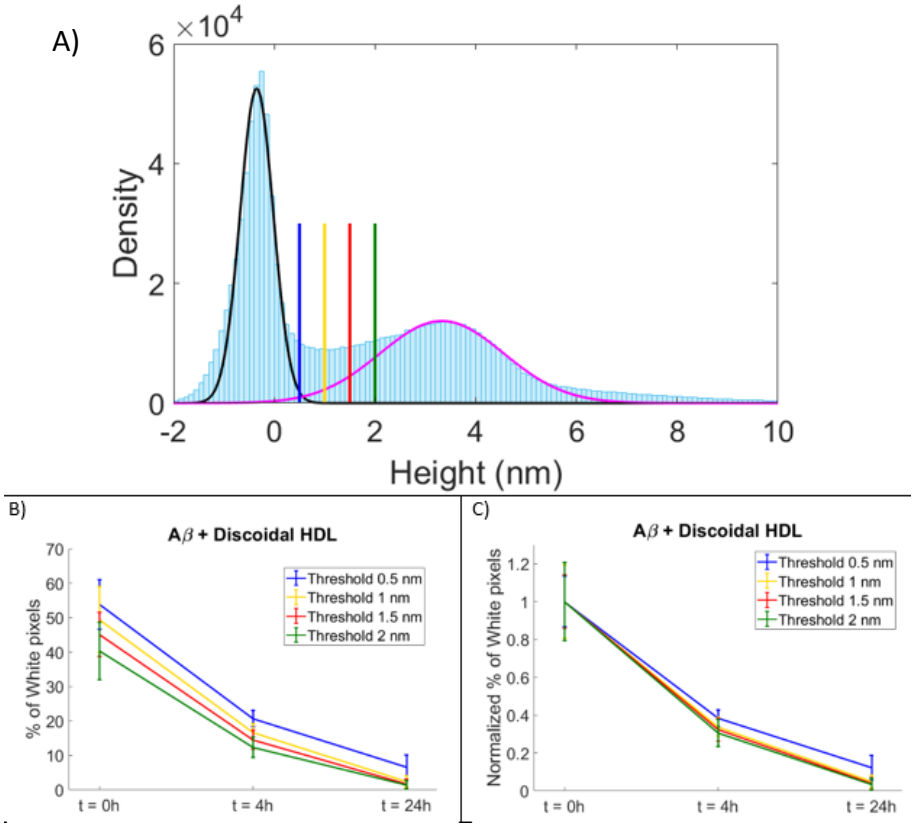

Figure S4. A) Representative height histogram of an AFM image of fibrils. Two peaks are visible, one corresponding to the mica surface (black Gaussian fit), and one corresponding to the fibrils (magenta Gaussian fit). Four possible height threshold values are indicated: 0.5 nm (blue), 1 nm (yellow), 1.5 nm (red), 2 nm (green). B) Percentage of pixels above a fixed height threshold (white pixels) as a function of the incubation time of Aβ with discoidal HDL at 37°C, evaluated using 4 different thresholds (0.5 nm in blue, 1 nm in yellow, 1.5 nm in red, 2 nm in green). C) Normalized percentage of white pixels above a fixed height threshold as a function of the incubation time of Aβ with discoidal HDL at 37°C, evaluated using 4 different thresholds (0.5 nm

in blue, 1 nm in yellow, 1.5 nm in red, 2 nm in green). Normalization is calculated with respect to the t = 0 h sample.

CHAPTER 4

The Ability of Liposomes, Tailored for Blood-Brain Barrier Targeting, to Reach the Brain is Dramatically Affected by the Disease State

Roberta Dal Magro, Alysia Cox, Vanessa Zambelli, Simona Mancini, Massimo Masserini, Francesca Re

Nanomedicine (London), 2018; 13(6):585-594

Highlights

The majority of *in vitro* and *in vivo* models of the BBB represent the healthy state or are not complex enough to accurately match the human pathology of specific diseases. The testing of NPs in such limited models restricts their translational potential. This chapter explores if the ability of nanoparticles, specifically designed for brain targeting, to cross the BBB depends on the disease or age state. This research is important for the thoughtful analysis of NPs *in vitro* and *in vivo* and to maximize their successful application to humans.

4.1 ABSTRACT

Aim: To investigate if and how the ability of liposomes, previously designed for Alzheimer's therapy, to reach the brain changes in aging/pathological conditions with respect to the healthy state. **Methods:** Biodistribution and pharmacokinetics of liposomes in young or aged healthy mice and in an Alzheimer's mouse model were measured by radiochemical techniques. The expression of brain receptors and structural proteins was evaluated by Western blot. **Results:** At equal blood levels, the amount and integrity of liposomes in the brain were dramatically lower in Alzheimer's or aged mice, with respect to young animals. These differences are likely attributable to molecular alterations in the brain vasculature.

Conclusion: Brain alterations in pathology or aging should be considered in the design of drug delivery systems for brain targeting.

4.2 INTRODUCTION

The blood–brain barrier (BBB) is a highly complex multicellular structure that protects the brain from harmful substances and invading organisms from the bloodstream, supplying brain tissue with nutrients and controlling its homeostasis [1]. Diffusion across the BBB is strictly limited by multiple transporters, metabolic enzymes and complex junctional structures, which prevent the paracellular diffusion of hydrophilic blood-borne substances larger than 0.6 kDa [2]. The development of new strategies to treat brain diseases is one of the most challenging research areas, considering the low drug accessibility to the brain due to the presence of the BBB [3].

In several high incidence brain pathologies, such as stroke, brain infections, Alzheimer's (AD) and Parkinson's disease (PD), the BBB is altered [4]. The failure to maintain the specialized BBB components make it more permeable, allowing the entry of molecules that can promote neuroinflammation and neurodegeneration [5]. However, even if damaged and more permeable, the BBB can pose serious challenges to drug delivery into the brain.

Nanoparticles (NPs), liposomes included, are considered one of the most promising and versatile drug delivery systems to inaccessible regions such as the brain, as they can protect therapeutic agents while efficiently delivering them into the damaged areas. Several NP formulations have been effective in crossing the BBB in healthy animals, mainly when they are modified with BBB targeting ligands [3,6]. Nevertheless, it is important to consider that the BBB modifications in pathology could alter the NPs performance in reaching the brain from the periphery. Indeed, the evaluation of the NPs ability

to reach the brain in disease states could give important information in order to design new and innovative formulations capable of successfully targeting damaged areas in the brain [6,7].

Within this frame, we have previously synthesized and fully characterized multifunctional liposomes (modified [m] apolipoprotein E [apoE] receptor-binding domain - phosphatidic acid [PA] liposomes [LIP] – mApoE-PA-LIP) for the treatment of AD. These liposomes are dually functionalized with a synthetic peptide (mApoE; CWGLRKLRKRLLR), containing the receptor-binding domain of apolipoprotein-E for the BBB targeting and crossing, and with phosphatidic acid (PA), as a β-amyloid (Aβ) binding ligand [8,9]. The ability of mApoE-PA-LIP to cross the BBB both *in vitro*, using BBB transwell models, and *in vivo*, in healthy mouse models, has already been shown [10,11]. These liposomes destabilize brain Aβ aggregates, promoting their removal across the BBB via the 'sink' effect, thus ameliorating the memory impairment of aged symptomatic AD mouse models [11]. Moreover, mApoE-PA-LIP delay the phenotype progression and prevent the memory impairment in a presymptomatic stage mouse model of AD [12]. As most research assessing NPs ability to cross the BBB is performed using *in vitro* BBB models or healthy young animals, without considering the BBB status, the aim of this study is to compare the *in vivo* biodistribution of mApoE-PA-LIP in the healthy and diseased state, in other words, AD, raising awareness in the scientific community about its importance.

4.3 MATERIALS AND METHODS

Materials

Sm, Chol, mal-PEG-PE and PA were purchased from Avanti Polar Lipids, Inc. (AL, USA). The Thermobarrel Extruder was from Lipex Biomembranes (BC, Canada). Ultrapure and deionized water were obtained from Direct-Q5n system (Millipore, Italy). mApoE (CWGLRKLRKRLLR-NH_2) was purchased from DBA Italia (Segrate, Italy). [^{3}H] Sphingomyelin, [^{14}C] PA, Ultima Gold scintillation cocktail and Solvable tissue solubilizer were from PerkinElmer (Italy). All other chemicals were of analytical grade and were obtained from either Sigma–Aldrich (Milan, Italy) or Merck (Milan, Italy).

Animals

All procedures involving animals and their care were conducted according to European Union (EEC Council Directive 86/609, OJ L 358, 1; 12 December 1987) and Italian (D.L. n.116, G.U. suppl. 40, 18 February 1992) laws and policies, and in accordance with the United States Department of Agriculture Animal Welfare Act and the National Institutes of Health (MA, USA) policy on Humane Care and Use of Laboratory Animals.

Six to eight week old healthy Balb/c male mice (five mice/group; Charles-River, Italy) were used to mimic young healthy conditions. Twelve-month-old APP/PS1 transgenic (Tg) male mice (five mice/group; B6C3-Tg[APPswe,PSEN1dE9]85Dbo/Mmjax mice; The Jackson Laboratory) were used as an AD-like model. Twelve months old wildtype male littermates from the same colony as the Tg mice (five mice/group; The Jackson Laboratory) were used to mimic

aged healthy conditions. Untreated 6–8 week old healthy Balb/c male mice (Charles-River, Italy) were used as a control (brains were used to measure the basal levels of brain and BBB macromolecules; plasma was used to assess the stability of liposomes).

For biodistribution and pharmacokinetics experiments, 5–10 animals for each of the analyzed variables was considered to be the minimum number necessary to guarantee valid and significant results, taking into account the need to minimize the use of animals. This number of animals was calculated using the site http://www.stat.ubc.ca/~rollin/stats/ssize/ (power 80% e; p =0.05) and a minimum number of animals equal to n=5 for each experimental condition was obtained, in agreement with previous similar studies [13–15].

Liposome preparation and characterization

mApoE-PA-LIP were prepared as described previously [10,11]. Briefly, liposomes composed of sphingomyelin, cholesterol, PA and maleimide-PEG-lipid (46.25:46.25:5:2.5 molar ratio) were prepared in 10 mM phosphate-buffered saline (pH 7.4) by extrusion procedure through polycarbonate membranes with 100 nm diameter pores to obtain unilamellar vesicles. 1.8 × 105 dpm/μl of each radiolabeled tracer, [^{14}C]-PA and [^{3}H]-sphingomyelin was added as tracers to follow the mApoE-PA-LIP biodistribution *in vivo* by radioactivity counting [10]. Liposomes were incubated with mApoE peptide (1.2:1, peptide:lipid molar ratio) in phosphate-buffered saline (pH 7.4) at room temperature o/n, in order to form the thio-ether bond between the cys of the peptide and the maleimide on liposome surface. After incubation,

free mApoE peptide was removed by PD-10 column [8,9]. mApoE attached on the liposomes surface was quantified fluorometrically (λex = 495 nm; λem = 592 nm) [8,9] and phospholipid content was quantified by Stewart Assay [16] or by measuring the radioactive lipids recovery by liquid scintillation counting using a Tri-Carb 2200 CA Liquid scintillation analyzer (Packard).

Size and polydispersity index (PDI) were analyzed by dynamic light scattering (DLS) technique (Brookhaven Instruments Corporation, NY, USA), as described previously [17]. ζ-potential was determined by using an interferometic Doppler velocimetry with the same instrument equipped with ZetaPALS device. Liposome stability was determined by following the size and PDI in physiological buffer by DLS for 7 days, and by measuring the calcein release from liposomes in physiological buffer and in mouse plasma following the procedure already described [18].

Pharmacokinetics & Biodistribution

A total of 100 µl of 15 mM (total lipid concentration) radiolabeled mApoE-PA-LIP or PA-LIP was administered by intraperitoneal injection to mice, as previously described [11]. A total of 3, 6 or 24 h after injection, mice were sacrificed by an overdose of isoflurane, which leads to breathing arrest within 1 min. Blood was collected by cardiac puncture. Brain, liver, spleen and kidney were dissected, rinsed with PBS to wash away blood attached around the organs and weighed. A total of 0.1 g of each tissue or 100 µl of blood, in triplicate, were solubilized by digestion in 1 ml Solvable at 55 °C in a water bath for 2 h and cooled to room temperature, as described [19]. Three aliquots of

300 μl with 30% H_2O_2 were added to samples for decolorization. Radioactivity was measured by liquid scintillation counting [10,11]. Data were expressed as % of injected dose on total organ weight/volume ± SD and analyzed by Student's *t*-test. The possible radioactivity derived from the blood was subtracted from the radioactivity values measured in the brain (-5% of measured radioactivity) [19]. A p-value < 0.05 was considered statistically significant. Experiments were done at least in triplicate.

Western Blot Analysis

Half brains were homogenized in a buffer containing 50 mM Tris-HCl pH 7.4, 150 mM NaCl, 2 mM EDTA, 1% Triton X-100, 0.1% SDS, 1 mM dithiothreitol and 2% protease inhibitor. After centrifugation at 16,000 × *g* for 20 min at 4 °C, the supernatant was retained and total protein content was quantified by bicinchoninic acid assay (Pierce BCA Protein Assay Kit, Thermo Fisher Scientific, Milan, Italy).

SDS-PAGE was carried out on an aliquot of the supernatant containing 100 μg of total proteins using 4–12% NuPAGE Bis-Tris gel (Thermo Fisher Scientific). Proteins were transferred to nitrocellulose membrane. Membranes were blocked with PBS-Tween 20 containing 5% (w/v) bovine serum albumin for 2 h, at RT and then incubated o/n at 4 °C with the primary antibodies: rabbit anti low-density lipoprotein receptor (LDL-R) 1:1000, mouse anti-LDL-R-related protein-1 (LRP-1) 1:1000, rabbit anti-receptor for advanced glycation endproducts (RAGE) 1:1000 and mouse anti-claudin-5 (CLD-5)-Alex Fluor 488 1:200 (Thermo Fisher Scientific). After washing, blots were incubated for 2 h with the appropriate secondary antibody (horseradish

peroxidase-conjugated goat anti-mouse 1:20,000, horseradish peroxidase-conjugated goat anti-rabbit 1:20,000; Thermo Fisher Scientific) diluted in PBS-Tween 20⁄5% bovine serum albumin and proteins were visualized with enhanced chemiluminescence by Amersham Imager 600 (GE Healthcare Srl, Milan, Italy). CLD-5 bands were visualized by fluorescence detection by Amersham Imager 600 (GE Healthcare). Proteins bands were analyzed using NIH Image J software. All the data have been normalized to β-actin (mouse anti-β-actin, 1:1500, Thermo Fisher Scientific).

4.4 RESULTS

Characterization of liposomes

The total lipid recovery (9 ± 1.3 mg lipids/ml) after extrusion was >90%. DLS results showed that, under physiological conditions (pH 7.4; 37°C), the final preparations of liposomes had a size <120 nm, were monodisperse (PDI <1), and negatively charged (Figure 1A). The liposomes size (PA-LIP), which slightly increases (+9%) after surface functionalization with mApoE, remained constant within the experimental error for up to 7 days (data not shown). The release of calcein incorporated in liposomes was 10 ± 3% in 50 h in physiological buffer (pH 7.4; 37°C) and 12 ± 4 in 50 h in mouse plasma.

The blue shift in the emission of mApoE peptide when coupled to liposomes is generally observed when tryptophan is transferred into a less polar environment or becomes motionally restricted. The yield of liposome surface functionalization with mApoE peptide (Figure 1B), determined by following the Trp fluorescence, was 65 ± 12%, according to data already published [8,9]. Considering that ~70,000 lipids are in the outer layer of a 120-nm diameter LIP containing 2.5 mol% of mal-PEG-PE, with a coupling efficiency of ~65%, the mApoE density after incubation is of ~1150 peptide molecules per single liposome, according to previous results [8,9].

Ⓐ

Liposomes (LIP)	Diameter (nm ± SD)	PDI	ζ-potential (mv ± SD)
PA-LIP	109.5 ± 3	0.095	-21.18 ± 1.67
mApoE-PA-LIP	119.2 ± 7	0.099	-18.59 ± 1.69

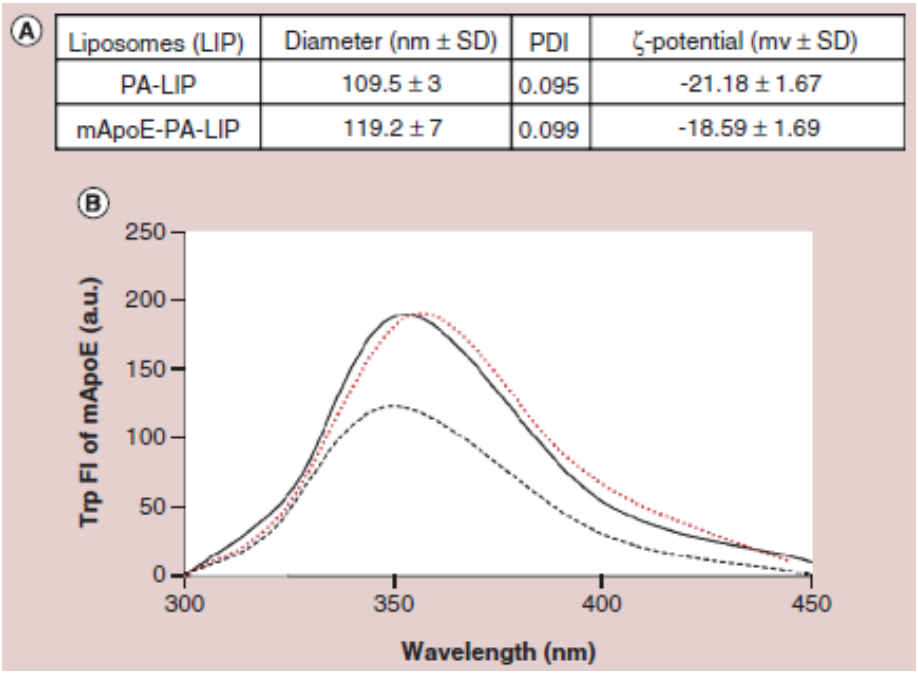

Figure 1. Characterization of liposomes. (A) Size, polydispersity (PDI) and ζ-potential values of PA-LIP and mApoE-PA-LIP determined by dynamic light scattering. **(B)** Fluorescent spectra of Trp-mApoE peptide in solution (red line), after incubation with LIP (dark line), or after mApoE-PA-LIP purification (dark dotted line).

Biodistribution & pharmacokinetics of mApoE-PA-LIP

We investigated the biodistribution and pharmacokinetics of dual radiolabeled mApoE-PA-LIP in young and aged healthy mice and in aged AD-like mice. A total of 3, 6 or 24 h after intraperitoneal injection, the radioactivity in different tissues was measured. The results showed that the distribution of radioactivity was comparable among all the animal groups tested. Six hours after injection the blood contained 25 ±

7% (mean of different animal models) of the injected radioactivity, while liver, spleen and kidneys (taken together) contained 18.5 ± 7.2% (mean of different animal models) of the injected dose (Figure 2A). These data are comparable to those previously obtained [10,11] in healthy young mice. Radioactivity data presented do not reach 100% of administered radioactivity because not all animal organs have been analyzed. Pharmacokinetics of mApoE-PA-LIP in the blood showed that their half-life is about 18 h with a clearance of 1.65 × 10-6 ml/min (Figure 2B), with no significant differences between experimental groups.

Interestingly, comparing the amount of radioactivity in the brains of different animal models, the highest values were detected in the brains of young healthy mice when compared with aged ones, either healthy or diseased ($p < 0.01$) (Figure 2C).

A noteworthy result is that the ratio between the two radiotracers of the injected mApoE-PA-LIP preparation was comparable to the ratio detected in the brains of young healthy mice, suggesting that mApoE-PA-LIP reach the brain in an intact form. On the contrary, the different ratio detected in the brain of aged mice, both healthy and AD-like, suggests that liposomes are only partially intact when they reach the brain under these conditions (Figure 2D). The ratio of the two radiotracers in peripheral tissues was comparable to that of the injected mApoE-PA-LIP ($p < 0.05$).

In healthy young mice, the brain-to-blood ratio of radioactivity, calculated 6 h after injection, was 1.37 ml/g and 5.8 ml/g for PA-LIP and mApoE-PA-LIP respectively. In Tg mice the ratio was 0.75 and 3.1 for PA-LIP and mApoE-PA-LIP, respectively.

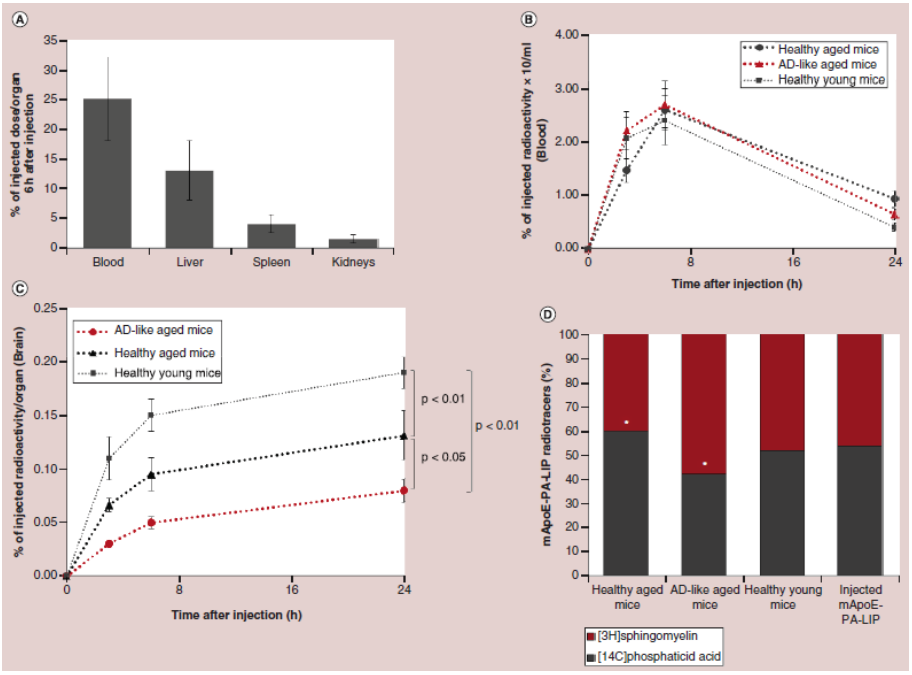

Figure 2. *In vivo* biodistribution and pharmacokinetics of mApoE-PA-LIP. Radiolabeled mApoE-PA-LIP were administered by intraperitoneal injection (100 µl of 15 mM total lipids containing 1.8 × 105 dpm/µl of [^{3}H]-sphingomyelin and 1.8 × 105 dpm/µl of [^{14}C]-phosphatidic acid) in healthy aged mice (10-month old non-transgenic mice), AD aged mice (transgenic APP/PS1 mice), or healthy young mice (6–8 weeks old healthy Balb/c mice). Three, 6, or 24 h after injection mice were sacrificed and the radioactivity in blood, liver, spleen and kidneys was measured by liquid scintillation counting. The results are expressed as % of injected [^{3}H]-sphingomyelin radioactivity/organ weight or volume ± SD measured in different tissues (n = 5 mice/experimental group). **(A)** Biodistribution of mApoE-PA-LIP 6 h after injection in different tissues. Results are expressed as the mean of the different animal models used. **(B)** Pharmacokinetics of mApoE-PA-LIP in the blood at different times after injection. **(C)**

Pharmacokinetics of mApoE-PA-LIP in the brain at different times after injection. **(D)** % of radioactivity of two radiotracers embedded in mApoE-PA-LIP measured before the injection (administered mApoE-PA-LIP) and in the brain of the different animal models 6 h after injection. All the results are expressed as % of injected [3H]-sphingomyelin radioactivity/organ weight (or total blood volume) ± SD measured. Data were analyzed by Student's *t*-test and a p-value < 0.05 was considered significant (n = 5 mice/experimental group). *$p < 0.05$ versus administered mApoE-PA-LIP.

LDL-R, LRP-1, RAGE & CLD-5 expression in the mouse brains

To understand whether the differing ability of liposomes to reach the brain after peripheral injection is attributable to the different brain status, BBB features included, the expression of selected proteins involved in the brain and BBB functionality was measured in the mouse brain homogenates by WB analysis. Untreated Balb/c mice (2 mice) were used representative of the brain and BBB healthiness.

The results (Figure 3A & B) showed that the expression of LDL-R, LRP-1, RAGE and CLD-5 changes with the aging in healthy mice and between the healthy and AD status in aged animals. In particular, the results showed that levels of receptors, which are expressed also at the BBB level, decreased in the case of LRP-1 (-70 ± 3%) and increased in the case of RAGE (+34 ± 4%) in AD mice compared with young and old healthy mice. Levels of LDL-R tend to decrease in healthy aged mice and significantly decrease in AD mice (-38 ± 5%) with respect to young healthy mice. Finally, levels of CLD-5, a protein of endothelial tight junctions, tend to increase with aging, with CLD-5 levels

increasing twofold in aged AD mice compared with healthy young mice. The calculation of correlation index between the levels of brain macromolecules and the amount of liposome-associated radioactivity in the brain of different mouse models used showed that these two variables are strongly correlated. In particular, CLD-5 and RAGE are inversely correlated with the amount of liposomes in the brain ($r = -0.98$; $r = -0.94$), while LDL-R and LRP-1 are directly correlated ($r = +0.99$; $r = +0.91$). No significant differences in the LDL-R, LRP-1, RAGE and CLD-5 levels have been detected between treated and untreated healthy young mice.

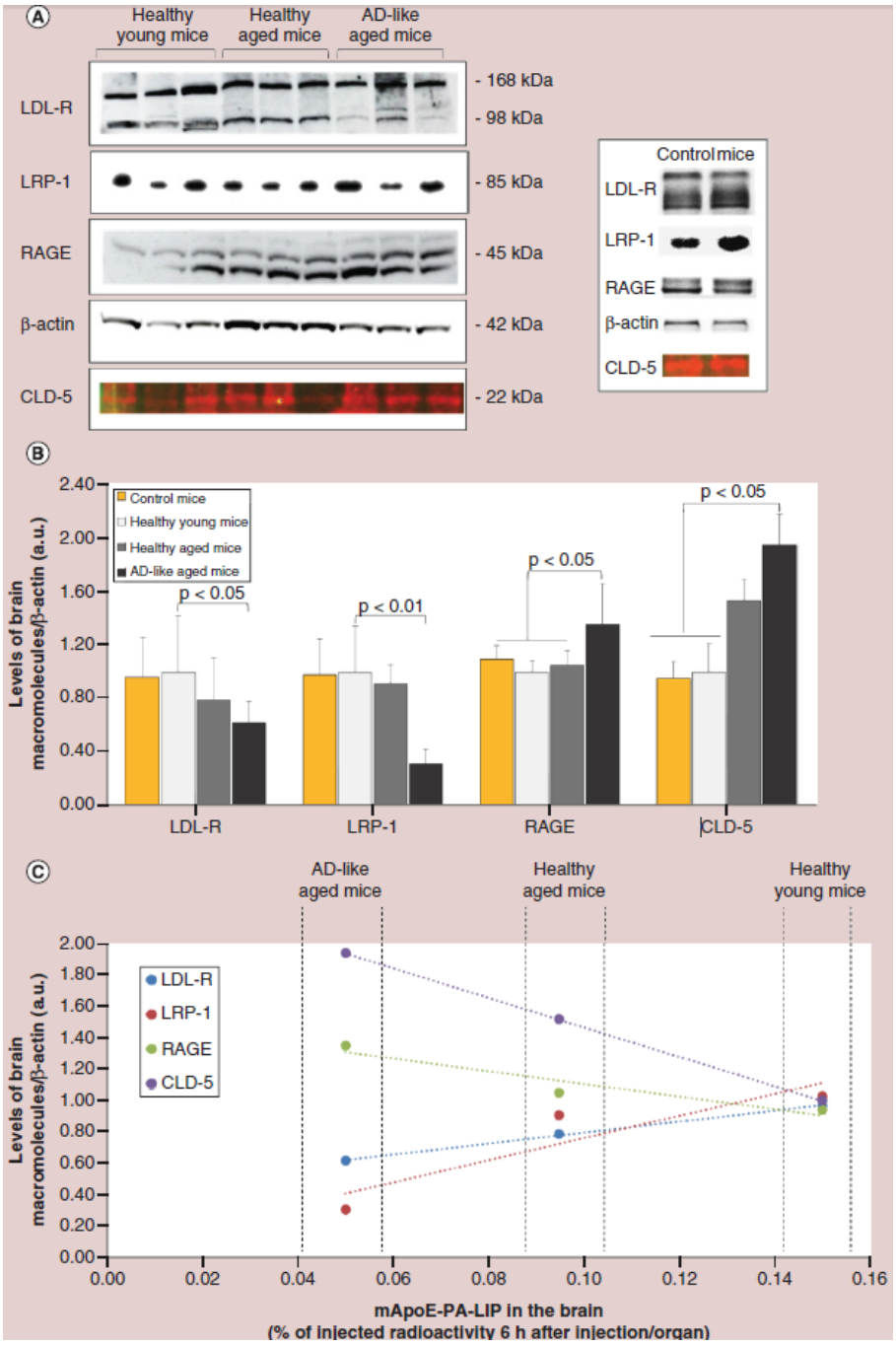

Figure 3. Assessment of the brain transporters, receptors and structural proteins by WB. After treatment with mApoE-PA-LIP,

animals were sacrificed and half brains were homogenized. An aliquot of the total brain homogenate, containing 100 μg of total proteins, was analyzed by SDS-PAGE/WB. LDL-R, LRP-1, RAGE and CLD-5 were analyzed by immunoblotting followed by enhanced chemiluminescence or fluorescence detection. **(A)** Representative blots of macromolecules in the brains of treated mice are shown. In the inset, blots of macromolecules in the brains of untreated Balb/c mice are shown. **(B)** The intensity of chemiluminescent or fluorescent bands was semiquantitatively estimated by Amersham Imager 600 and expressed as the ratio between the intensity of the spot of interest and the intensity of β-actin bands. Data are mean ± SD and compared by Student's *t*-test. **(C)** Correlation between the levels of brain macromolecules and amount of mApoE-PA-LIP in the brain of different mouse models used. CLD-5: Claudin 5; LDL-R: Low-density lipoprotein receptor; LRP-1: LDL-R-related protein-1; RAGE: Receptor for advanced glycation end products; WB: Western blot.

4.5 DISCUSSION

Currently, the BBB status is often not properly considered in the design of drugs or drug delivery systems targeting the brain. Even if drugs are normally tested in relevant animal models of disease for their therapeutic efficacy, preliminary experiments devoted to improve their context-dependent BBB targeting potentiality are often neglected. Within this frame, the present study aimed to compare the extent of liposome mobility across the BBB after peripheral injection, in physiological and pathological (i.e., AD) conditions. For this purpose we utilized multifunctional liposomes that were previously designed and characterized for the treatment of AD [11,12] and are able to reach the brain *in vivo*. These liposomes were functionalized with PA, as an Aβ ligand, and with mApoE, for the BBB targeting, following the procedure previously described [11,12]. These liposomes were characterized and the results showed that the liposomes size increased after mApoE coupling, indicating their successful functionalization. This was also confirmed by the blue shift in the emission of Trp-mApoE peptide, when coupled to liposomes. However, even after liposomes functionalization their average diameter remains below 120 nm. This particle dimension has been shown to be suitable to cross the BBB, since a clear inverse correlation between NP size and BBB penetration has been shown [21,22]. The negative ζ-potential values and the low PDI of liposomes are indicative of liposomes stability due to electrostatic repulsion, reducing the risk of their aggregation [8,9].

It could be questionable the use of liposomes for the purpose of this paper due to their possible instability depending on their environment. The measurement of size by DLS and of calcein release

from liposomes over time in physiological conditions showed that liposomes are stable, making them suitable to be used for the aim of this investigation.

After characterization, these liposomes were administered to healthy (young and aged) or diseased (aged AD APP/PS1 mouse model) mice by intraperitoneal injection. This administration route, largely utilized especially in mice for practical reasons, facilitates the slow introduction of liposomes to the bloodstream, which is an important condition for therapy in AD treatment [12,23]. Moreover, it has been already shown that the amount of liposome-associated radioactivity that reaches the brain 3 h after injection is similar between three different administration routes: intravenous, intraperitoneal or intratracheal [12,24].

The results showed that mApoE-PA-LIP-associated radioactivity reaches the brain of the different animal models tested in different amounts, with the highest values measured in young healthy mice. The amount of radioactivity reaching the brain was dramatically reduced in aged and AD mice, suggesting that the brain and its vasculature could strongly affect the liposomes performance in brain targeting, affecting their therapeutic efficacy. Moreover, the results showed that the liposome-associated radioactivity tends to accumulate in the mouse brains, in agreement with data already reported [11,12,24]. Considering the peripheral toxicity of apoE and its enhancing effect on Aβ aggregation, it could be questionable the use of these device for AD therapy. Therefore, it is important to highlight that mApoE peptide herein used is derived from the receptor-binding domain of apoE (141–150 a.a.), which is not able to bind Aβ, and not from the apoE domain

involved in the interaction with Aβ (200–299 a.a.) [25]. Moreover, already published results showed that the mice treatment with mApoE-PA-LIP has no effect on brain hepatic functions [12].

An indication of mApoE-PA-LIP integrity (or disruption) was obtained by comparing the ratio of the two radiotracers embedded in the original liposome preparation (injected mApoE-PA-LIP) to the radioactivity measured in different organs. Though this approach gives indirect information about the liposome integrity, it is commonly utilized in the literature [10,12,26,27]. The results suggest that mApoE-PA-LIP reach the brain in an intact form only in young healthy mice. Even if the AD-like features are detectable in APP/PS1 Tg mice starting from 8 to 10 months of age, it would be interesting to investigate how the amount of mApoE-PA-LIP that reaches the brain changes in younger AD mice. It has been recently shown that at 4–5-month-old, APP/PS1 Tg mice display microvascular ultrastructural changes [28]. It is possible that these alterations could affect the liposomes passage across the BBB. This issue deserves further investigation.

Altogether, our results suggest that the conventional PK/PD experiments with NPs designed to target the brain can only be reliable when carried out in the correct physiopathological model.

Concerning the reasons for the differences detected, it is likely that age-related physiological or pathological changes in the CNS, BBB included [5,29], could affect the brain-targeting performance of mApoE-PA-LIP. Indeed, our results showed alterations in the brain expression of receptors and structural proteins under the different conditions investigated, which are not attributable to the mice treatment because LDL-R, LRP-1, RAGE and CLD-5 brain levels were

comparable to those of untreated mice. In particular, we found a decrease of LRP-1 and LDL-R in AD mice compared with young and old healthy mice. These receptors are likely involved in the mechanism of BBB crossing by mApoE-PA-LIP, as already suggested [10]. Therefore, the decrease in their brain levels could be responsible for the reduction of mApoE-PA-LIP radioactivity in the brain of AD-like mice. Our previous results about the *in vivo* biodistribution of mApoE-PA-LIP [10,11] in healthy mice showed that the presence of mApoE (as a BBB targeting ligand) on liposomes surface increased their ability to reach the brain. Here, in order to evaluate if this also occurs in Tg mice, where the BBB is altered, we compared the radioactivity in the brain of young and AD-like mice after administration of PA-LIP. The brain-to-blood ratio, an excellent way of evaluating brain-targeting efficiency of neurotherapeutics [30], showed that, to a lesser extent, the presence of mApoE on liposomes surface improves their ability to reach the brain. Therefore, we speculate that the therapeutic effectiveness of these liposomes in AD could be influenced by the brain vasculature status.

Since the alterations of the levels of brain and BBB macromolecules strongly correlates with the ability of liposomes to reach the brain, the identification of the BBB changes in aging and disease conditions is essential to improve the design of drug delivery systems and to deepen the knowledge of the disease pathophysiology. This paper documents partial research resulting from an ongoing study with the aim to study the BBB evolution in a diseased state. To this purpose, our preliminary results showed that the expression level of RAGE, which controls the Aβ influx from the blood to the brain [31], increased in AD-like mice compared with young and old healthy mice,

in agreement with the knowledge that RAGE expression is upregulated by Aβ in AD patients and animal models [32]. Moreover, our results showed that levels of CLD-5, mainly expressed by brain endothelial cells [33], tend to increase with the aging and with AD pathology. It is known that in AD, Aβ peptide might alter the BBB integrity by acting on TJs protein complexes, in particular from the structural point of view. A decrease in occludin and ZO-1 expression and an increase of claudins levels (CLD-1 and CLD-5) has been reported in aging and AD [34], in agreement with the results presented here. Unfortunately, the isolation of the BBB from adult mice is a difficult procedure that requires a lot of animals. It is clear that detailed BBB analysis on both a structural and functional level deserves further investigation.

Financial & competing interests' disclosure

This work was partly supported by the Grant ATE-Project Funded by University of Milano-Bicocca, 2015-ATE-0510 to F Re and by Joint Programme-Neurodegenerative Disease Research (JPND Research 2015) to F Re (CUP B42F16000090008). The authors have no other relevant affiliations or financial involvement with any organization or entity with a financial interest in or financial conflict with the subject matter or materials discussed in the manuscript apart from those disclosed.

4.6 CONCLUSIONS

The evolution of the BBB features connected to aging and/or pathological conditions should be considered for more effective design of nanodelivery systems for brain targeting. Taking advantage of the current knowledge on BBB impairment, for example the higher expression of RAGE in AD or lactoferrin in PD, it is feasible to design a strategy for more effective drug delivery into damaged brain areas. In this context, we are developing an *in vitro* BBB model that reflects alterations in the AD state thanks to the NAB3 project (Development of a Novel multicellular *in vitro* model of AD-like BBB), funded by JPND Research Programme. This will represent a novel and highly valuable tool for drug design and testing.

Author Contributions

R.D. and V.Z. performed *in vivo* experiments and western blot analyses. S.M. and A.C. prepared and characterized liposomes. F.R. and M.M. contributed to the data interpretation and participated in the drafting of the manuscript. F.R. coordinated the study, designed the experiments, and analyzed the data. All authors contributed to the paper revision, read and approved the submitted version and agree to be accountable for all the aspects of the work.

4.7 EXECUTIVE SUMMARY

- The blood–brain barrier protects the brain from harmful substances, but limits drug accessibility to the brain from the blood.
- Nanoparticles represent the most promising drug delivery system to target the brain, but their ability to reach the brain in a disease state should be taken into account.
- Radiolabeled liposomes, designed for brain targeting, were administered to young or aged healthy mice and to an Alzheimer's mouse model to study biodistribution and pharmacokinetics.
- The amount and integrity of liposomes in the brain were dramatically lower in Alzheimer's mice and aged mice with respect to young animals.
- Brain levels of receptors and blood–brain barrier structural proteins are different in aging and pathological conditions when compared with healthy models.

References

Papers of special note have been highlighted as: • of interest; •• of considerable interest

1 Banks WA. From blood–brain barrier to blood–brain interface: new opportunities for CNS drug delivery. *Nat. Rev. Drug Discov.* 15(4), 275–292 (2016).

2 Pardridge WM. Drug transport across the blood–brain barrier. *J. Cereb. Blood Flow Metab.* 32(11), 1959–1972 (2012).

3 Masserini M. Nanoparticles for brain drug delivery. *ISRN Biochem.* 2013, 238428 (2013).

4 Obermeier B, Daneman R, Ransohoff RM. Development, maintenance and disruption of the blood–brain barrier. *Nat. Med.* 19(12), 1584–1596 (2013).

5 Zlokovic BV. Neurovascular pathways to neurodegeneration in Alzheimer's disease and other disorders. *Nat. Rev. Neurosci.* 12(12), 723–738 (2011).

•• Highlights therapeutic opportunities relating to blood–brain barrier (BBB) dysfunction associated with neurodegenerative disorders, such as Alzheimer's disease.

6 Saraiva C, Prac¸a C, Ferreira R, Santos T, Ferreira L, Bernardino L. Nanoparticle-mediated brain drug delivery: overcoming blood–brain barrier to treat neurodegenerative diseases. *J. Control. Release* 235, 34–47 (2016).

7 Zhang TT, Li W, Meng G, Wang P, Liao W. Strategies for transporting nanoparticles across the blood–brain barrier. *Biomater Sci.* 4(2), 219–229 (2016).

8 Re F, Cambianica I, Zona C *et al.* Functionalization of liposomes with ApoE-derived peptides at different density affects cellular uptake and

drug transport across a blood–brain barrier model. *Nanomedicine* 7(5), 551–559 (2011).

9 Re F, Cambianica I, Sesana S *et al.* Functionalization with ApoE-derived peptides enhances the interaction with brain capillary endothelial cells of nanoliposomes binding amyloid-beta peptide. *J. Biotechnol.* 156(4), 341–346 (2011).

10 Bana L, Minniti S, Salvati E *et al.* Liposomes bi-functionalized with phosphatidic acid and an ApoE-derived peptide affect Aβ aggregation features and cross the blood-brain-barrier: implications for therapy of Alzheimer disease. *Nanomedicine* 10(7), 1583–1590 (2014).

11 Balducci C, Mancini S, Minniti S *et al.* Multifunctional liposomes reduce brain β-amyloid burden and ameliorate memory impairment in Alzheimer disease mouse models. *J. Neurosci.* 34(42), 14022–14031 (2014).

• The results reported in this paper about the efficacy of multifunctional liposomes to treat Alzheimer's disease in animal model pave the way to use nanomedicine for the cure of neurodegenerative diseases.

12 Mancini S, Balducci C, Micotti E *et al.* Multifunctional liposomes delay phenotype progression and prevent memory impairment in a presymptomatic stage mouse model of Alzheimer disease. *J. Control. Release* 258, 121–129 (2017).

•• Demonstrates the possibility to prevent Alzheimer's disease, delay phenotype progression and prevent memory impairment in a mouse model by using multifunctional liposomes.

13 Tosi G, Bortot B, Ruozi B *et al.* Potential use of polymeric nanoparticles for drug delivery across the blood–brain barrier. *Curr. Med. Chem.* 20(17), 2212–2225 (2013).

14 Ansciaux E, Burtea C, Laurent S *et al. In vitro* and *in vivo* characterization of several functionalized ultrasmall particles of iron oxide, vectorized against amyloid plaques and potentially able to cross the blood–brain barrier: toward earlier diagnosis of Alzheimer's disease by molecular imaging. *Contrast Media Mol. Imaging* 10(3), 211–224 (2015).

15 Zhang D, Fa HB, Zhou JT, Li S, Diao XW, Yin W. The detection of β-amyloid plaques in an Alzheimer's disease rat model with DDNP-SPIO. *Clin. Radiol.* 70(1), 74–80 (2015).

16 Stewart JC. Colorimetric determination of phospholipids with ammonium ferrothiocyanate. *Anal. Biochem.* 104(1), 10–14 (1980).

17 Gobbi M, Re F, Canovi M *et al.* Lipid-based nanoparticles with high binding affinity for amyloid-beta1–42 peptide. *Biomaterials* 31(25), 6519–6529 (2010).

18 Canovi M, Markoutsa E, Lazar AN, Pampalakis G, Clemente C, Re F *et al.* The binding affinity of anti-Aβ1–42 MAb-decorated nanoliposomes to Aβ1–42 peptides *in vitro* and to amyloid deposits in post-mortem tissue. *Biomaterials* 32(23), 5489–5497 (2011).

19 Wan L, Pooyan S, Hu P, Leibowitz MJ, Stein S, Sinko PJ. Peritoneal macrophage uptake, pharmacokinetics and biodistribution of macrophage-targeted PEG-fMLF (N-formyl-methionyl-leucyl-phenylalanine) nanocarriers for improving HIV drug delivery. *Pharm. Res.* 24(11), 2110–2119 (2007).

20 Huiban M, Coello C, Wu K *et al.* Investigation of the brain biodistribution of the lipoprotein-associated phospholipase A2 (Lp-PLA2) inhibitor [18F]GSK2647544 in healthy male subjects. *Mol. Imaging Biol.* 19(1), 153–161 (2017).

21 Etame AB, Smith CA, Chan WC, Rutka JT. Design and potential application of PEGylated gold nanoparticles with size-dependent permeation through brain microvasculature. *Nanomedicine* 7, 992–1000 (2011).

22 Talamini L, Violatto MB, Cai Q *et al.* Influence of size and shape on the anatomical distribution of endotoxin-free gold nanoparticles. *ACS Nano* 11(6), 5519–5529 (2017).

23 Ord´o˜nez-Guti´errez L, Re F, Bereczki E, Ioja E, Gregori M, Andersen AJ *et al.* Repeated intraperitoneal injections of liposomes containing phosphatidic acid and cardiolipin reduce amyloid-β levels in APP/PS1 transgenic mice. *Nanomedicine* 11(2), 421–430 (2015).

24 Sancini G, Dal Magro R, Ornaghi F *et al.* Pulmonary administration of functionalized nanoparticles significantly reduces beta-amyloid in the brain of an Alzheimer's disease murine model. *Nano Res.* 9(7), 2190–2201 (2016).

25 Pillot T, Goethals M, Najib J *et al.* Beta-amyloid peptide interacts specifically with the carboxy-terminal domain of human apolipoprotein E: relevance to Alzheimer's disease. *J Neurochem.* 72(1):230–7 (1999).

26 Rauscher A, Frindel M, Rajerison H *et al.* Improvement of the targeting of radiolabeled and functionalized liposomes with a two-step system using a bispecific monoclonal antibody (anti-CEA × Anti-DTPA-In). *Front. Med. (Lausanne)* 2, 83 (2015).

27 Rangger C, Helbok A, Sosabowski J *et al.* Tumor targeting and imaging with dual-peptide conjugated multifunctional liposomal nanoparticles. *Int. J. Nanomedicine* 8, 4659–4671 (2013).

28 Kelly P, Denver P, Satchell SC, Ackermann M, Konerding MA, Mitchell CA. Microvascular ultrastructural changes precede cognitive impairment in the murine APPswe/PS1dE9 model of Alzheimer's disease. *Angiogenesis* 20(4):567–580 (2017).

29 Cai W, Zhang K, Li P *et al.* Dysfunction of the neurovascular unit in ischemic stroke and neurodegenerative diseases: an aging effect. *Ageing Res. Rev.* 34, 77–87 (2016).

•• These manuscripts claim that the BBB is altered, both in permeability and structure, in disease conditions.

30 Kulkarni AD, Patel HM, Surana SJ, Belgamwar VS, Pardeshi CV. Brain–blood ratio: implications in brain drug delivery. *Expert Opin. Drug Deliv.* 13(1), 85–92 (2016).

31 Zolezzi JM, Inestrosa NC. Peroxisome proliferator-activated receptors and Alzheimer's disease: hitting the blood–brain barrier. *Mol. Neurobiol.* 48, 438–451 (2013).

32 Bell RD. The imbalance of vascular molecules in Alzheimer's disease. *J. Alzheimers Dis.* 32(3), 699–709 (2012).

•• These manuscripts claim that the BBB is altered, both in permeability and structure, in disease conditions.

33 Huber JD, Witt KA, Hom S, Egleton RD, Mark KS, Davis TP. Inflammatory pain alters blood–brain barrier permeability and tight junctional protein expression. *Am. J. Physiol. Heart Circ. Physiol.* 280, H1241–H1248 (2001).

• **These manuscripts claim that the BBB is altered, in both permeability and structure, in disease conditions.**

34 Marco S, Skaper SD. Amyloid beta-peptide1–42 alters tight junction protein distribution and expression in brain microvessel endothelial cells. *Neurosci. Lett.* 401(3), 219–224 (2006).

CHAPTER 5

Summary, Conclusions and Future Perspectives

Neurodegeneration is the hallmark of an increasingly prevalent group of disorders that generally lack therapeutic and curative options. The high socio-economic burden of neurodegenerative diseases means that it is essential to explore new, dynamic technologies for effective treatment.

The major obstacle to effective pharmacological treatment of neurodegenerative disorders is the blood-brain barrier (BBB), a highly efficient, selectively permeable network of cells and mechanisms to protect the central nervous system (CNS) from toxic substances in the peripheral circulation. Nanomedicine offers a unique and promising role in crossing the BBB to deliver therapeutic and/or diagnostic agents to the brain. Functionalization of nanoparticles (NPs) is postulated to ensure efficient targeting, in order to optimize drug delivery, therapeutic outcomes, and reduce peripheral side effects, particularly of drugs that do not normally penetrate the BBB [1].

Within this frame, the knowledge of the features that influence the passage of NP across the BBB are critical. For instance, the identification of appropriate ligands targeting the BBB is an essential part of NP formulation. Furthermore, the presence of the protein corona, a layer of physiological proteins that bind to NPs upon *in vivo* administration, may affect the NP-BBB interaction. Therefore, knowledge of corona-NP interactions is vital in NP design.

Here, in Chapter 2, the dynamic nature of the protein corona upon crossing a transwell model of the BBB was demonstrated. For the first time it was shown that the protein corona changes quantitatively and qualitatively after passage through the *in vitro* BBB. Furthermore, the BBB-permeant corona is stable after crossing. This information

offers new insight into the biological processes that affect NPs *in vivo*, and should be taken into consideration when designing BBB-targeting nanodevices.

In more detail, thirteen corona proteins were found to be enriched in the "brain-side" with respect to the "blood-side", indicating their preferential ability to enter the *in vitro* brain when bound to NPs. In particular, albumin, α_2-macroglobulin, and α_2-HS-glycoprotein are highly abundant in the blood-side and brain-side corona, and show enrichment. These physiological proteins could theoretically be used as ligands for NP functionalization, forming an "artificial corona" able to increase BBB-penetrating capabilities, a line of research currently under investigation. The use of physiological proteins, particularly those that normally cross the BBB, albeit in small amounts, offers many benefits, including a reduced chance of neurotoxicity or immunogenic side effects that could occur with synthetic materials.

As mentioned, one promising corona protein identified was albumin, the most abundant serum protein, which is known to cross the *in vivo* BBB in healthy conditions [2], and in higher quantities after traumatic brain injury [3], in Huntington disease [4], diabetes and dementia [5]. Another enriched protein is α_2-macroglobulin, a broad spectrum antiprotease that also crosses the healthy BBB [6] and is a biomarker for multiple sclerosis (MS) [7]. In MS patients, an increase in the protein is seen in the cerebro-spinal fluid of patients with relapsing-remitting, secondary progressive, and primary progressive forms of MS when compared to healthy controls, making it a useful tool in effective diagnosis of the disease. Furthermore, the fact that it is able to cross the BBB in this disease state indicates that it may be useful in

promoting targeted drug delivery specifically in MS patients. Its anti-inflammatory effects are also promising in treating neurological conditions that are coupled with increased local or generalized inflammation [8]. Finally, Fetuin A, also known as α_2-HS-glycoprotein, is predominantly found in fetal serum where it prevents tissue calcification [9]. It can cross the BBB during ischemic injury [10]. Though albumin has previously proved useful in helping nanoparticles to cross the BBB [11], the use of α_2-macroglobulin or fetuin A for this purpose has never been investigated, and is a promising strategy for BBB targeting.

It should be noted that protein functionalization of NPs could significantly increase these protein levels in the brain. The risks associated with dramatically altering protein homeostasis in the CNS should be carefully explored *in vivo* using healthy and diseased models of the BBB. Another factor that may influence the future use of such proteins is competition with endogenous proteins. As albumin and α_2-macroglobulin normally pass through the healthy BBB and in certain disease states, and both proteins are highly abundant in the blood, competition with circulating proteins may limit the amount of protein-functionalized NPs that cross the BBB by receptor-mediated pathways.

The contribution of NPs to the effective treatment of neurodegenerative diseases does not necessarily imply the passage of NPs from the blood to the brain. For instance, in the case of beta-amyloid (Aβ) peptide, which plays a pivotal role in AD pathogenesis [12, 13], the "sink effect" theory postulates that removal of Aβ from the peripheral circulation induces efflux of excess Aβ from the brain, decreasing the amyloid burden and ameliorating AD symptoms [14,

15]. Chapter 3 documents a possible way to destabilize Aβ and enhance its efflux from the brain, using a physiological type of NP, namely high-density lipoproteins (HDL). A protective role of plasma HDL and apolipoprotein A-I (apoA-I) has been speculated, and this knowledge was employed to analyze their effect on Aβ efflux from the brain. Here, it was demonstrated that discoidal HDL could strongly enhance efflux of Aβ from the "brain" to the "blood" of an *in vitro* model of the BBB. This efflux effect was stronger than that of other HDL subtypes, possibly due to its high protein:lipid ratio. This research suggests that alterations of HDL levels or its subclass profiles in AD patients could lead to reduced Aβ brain clearance.

The specific role of apoA-I, a major component of HDL, on the sink effect theory was also examined. Aβ efflux from the *in vitro* brain was strongly enhanced by the presence of apoA-I in the "blood", more than α_2-macroglobulin, apoE, or albumin. This may be due to its high binding affinity for Aβ (Kd = 6 nM). Furthermore, the lipidation state of apoA-I affected its ability to clear Aβ across the *in vitro* BBB model. In the discoidal conformation, apoA-I associated to HDL could distort and destabilize Aβ fibrils, reduce β-sheet content and fibril concentration. This activity may allow fibrils, normally too large to cross the BBB, to be cleared from the brain. This data elucidates a role for HDL and apoA-I in AD pathogenesis and treatment. Indeed, the observation that size, shape, and lipidation state of HDL/apoA-I affect BBB crossing and Aβ clearance rates across the BBB model is reminiscent of the extensive data showing that NP size and shape is vital when it comes to brain targeting.

Another vital part of NP development for treatment of neurodegenerative diseases is choosing appropriate experimental models, either *in vitro* cell lines representing the targeted cell of choice, or animal models displaying characteristics of the diseased state. Too often, basic models that are not necessarily suitable for testing targeted NPs are chosen for preliminary *in vitro* or *in vivo* analysis. In Chapter 4, the ability of liposomes designed specifically to cross the BBB and treat Alzheimer's disease (AD), the most common neurodegenerative disorder [16], was shown to be affected either by the diseased state or the age of the mouse model used. Here, the quantity of liposomes that entered the AD-affected or aged brain in mice was significantly lower than the amount found in young healthy mouse brains. This was likely due to molecular alterations in the brain vasculature that limited entry of liposomes normally entering the brain *via* receptor mediated transcytosis. This dramatic change in NP brain delivery depending on disease and age state highlights the need for investigation of all NPs for brain targeting, and indeed all brain-targeting pharmaceuticals, in models mirroring the specific diseased and age state.

In conclusion, a broad range of factors need to be taken into account when designing NPs for therapy and diagnosis of neurodegenerative disorders, including the protein corona, ligands for functionalization, size and shape of targeting agents, and the experimental models being used. The results of this thesis provide further novel knowledge on this issue, and pave the way for new approaches in nanomedicine design.

References

[1] E. Salvati, F. Re, S. Sesana, I. Cambianica, G. Sancini, M. Masserini, M. Gregori, Liposomes functionalized to overcome the blood-brain barrier and to target amyloid-β peptide: the chemical design affects the permeability across an in vitro model, Int J Nanomedicine 8 (2013) 1749-58.

[2] Y. Kanoh, T. Ohara, M. Kanoh, T. Akahoshi, Serum matrix metalloproteinase-2 levels indicate blood-CSF barrier damage in patients with infectious meningitis, Inflammation 31(2) (2008) 99-104.

[3] B.J. Blyth, A. Farhavar, C. Gee, B. Hawthorn, H. He, A. Nayak, V. Stöcklein, J.J. Bazarian, Validation of serum markers for blood-brain barrier disruption in traumatic brain injury, J Neurotrauma 26(9) (2009) 1497-1507.

[4] A. Di Pardo, S. Castaldo, L. Capocci, E. Amico, M. Vittorio, Assessment of Blood-brain Barrier Permeability by Intravenous Infusion of FITC-labeled Albumin in a Mouse Model of Neurodegenerative Disease, J Vis Exp (129) (2017).

[5] S. Janelidze, J. Hertze, K. Nägga, K. Nilsson, C. Nilsson, M. Wennström, D. van Westen, K. Blennow, H. Zetterberg, O. Hansson, S.B.S. Group, Increased blood-brain barrier permeability is associated with dementia and diabetes but not amyloid pathology or APOE genotype, Neurobiol Aging 51 (2017) 104-112.

[6] T. Asano, H. Ito, Y. Kariya, K. Hoshi, A. Yoshihara, Y. Ugawa, H. Sekine, S. Hirohata, Y. Yamaguchi, S. Sato, H. Kobayashi, K. Migita, H. Ohira, Y. Hashimoto, H. Watanabe, Evaluation of blood-brain barrier function by quotient alpha2 macroglobulin and its relationship with interleukin-6 and complement component 3 levels in

neuropsychiatric systemic lupus erythematosus, PLoS One 12(10) (2017) e0186414.
[7] J. Ottervald, B. Franzén, K. Nilsson, L.I. Andersson, M. Khademi, B. Eriksson, S. Kjellström, G. Marko-Varga, A. Végvári, R.A. Harris, T. Laurell, T. Miliotis, D. Matusevicius, H. Salter, M. Ferm, T. Olsson, Multiple sclerosis: Identification and clinical evaluation of novel CSF biomarkers, J Proteomics 73(6) (2010) 1117-32.
[8] L. Cucullo, N. Marchi, M. Marroni, V. Fazio, S. Namura, D. Janigro, Blood-brain barrier damage induces release of alpha2-macroglobulin, Mol Cell Proteomics 2(4) (2003) 234-41.
[9] M. Häusler, C. Schäfer, C. Osterwinter, W. Jahnen-Dechent, The physiologic development of fetuin-a serum concentrations in children, Pediatr Res 66(6) (2009) 660-4.
[10] G.A. Laughlin, L.K. McEvoy, E. Barrett-Connor, L.B. Daniels, J.H. Ix, Fetuin-A, a new vascular biomarker of cognitive decline in older adults, Clin Endocrinol (Oxf) 81(1) (2014) 134-40.
[11] T. Lin, P. Zhao, Y. Jiang, Y. Tang, H. Jin, Z. Pan, H. He, V.C. Yang, Y. Huang, Blood-Brain-Barrier-Penetrating Albumin Nanoparticles for Biomimetic Drug Delivery via Albumin-Binding Protein Pathways for Antiglioma Therapy, ACS Nano 10(11) (2016) 9999-10012.
[12] L.F. Lue, Y.M. Kuo, A.E. Roher, L. Brachova, Y. Shen, L. Sue, T. Beach, J.H. Kurth, R.E. Rydel, J. Rogers, Soluble amyloid beta peptide concentration as a predictor of synaptic change in Alzheimer's disease, Am J Pathol 155(3) (1999) 853-62.
[13] C.A. McLean, R.A. Cherny, F.W. Fraser, S.J. Fuller, M.J. Smith, K. Beyreuther, A.I. Bush, C.L. Masters, Soluble pool of Abeta amyloid

as a determinant of severity of neurodegeneration in Alzheimer's disease, Ann Neurol 46(6) (1999) 860-6.
[14] J.G. Sutcliffe, P.B. Hedlund, E.A. Thomas, F.E. Bloom, B.S. Hilbush, Peripheral reduction of β-amyloid is sufficient to reduce brain β-amyloid: implications for Alzheimer's disease, J Neurosci Res 89(6) (2011) 808-14.
[15] Y. Matsuoka, M. Saito, J. LaFrancois, K. Gaynor, V. Olm, L. Wang, E. Casey, Y. Lu, C. Shiratori, C. Lemere, K. Duff, Novel therapeutic approach for the treatment of Alzheimer's disease by peripheral administration of agents with an affinity to beta-amyloid, J Neurosci 23(1) (2003) 29-33.
[16] D.B. Fraller, State of the science: use of biomarkers and imaging in diagnosis and management of Alzheimer disease, J Neurosci Nurs 45(2) (2013) 63-70.

PUBLICATIONS

Dal Magro RD, Simonelli S, **Cox A**, Formicola B, Corti R, Cassina V, Nardo L, Mantegazza F, Grasso G, Deriu MA, Danani A, Calabresi L, Re F. *HDL shape and apoA-I conformation are crucial features to destabilize β-Amyloid fibrils, promoting its clearance from the brain.* Submitted.

Cox A, Andreozzi P, Dal Magro R, Fiordaliso F, Corbelli A, Talamini L, Chinello C, Raimondo F, Magni F, Tringali M, Krol S, Silva PJ, Stellacci F, Masserini M, Re F. *Evolution of nanoparticle protein corona across the blood-brain barrier.* ACS Nano 2018;12(7): 7292-7300.

Magro RD, **Cox A**, Zambelli V, Mancini S, Masserini M, Re F. *The ability of liposomes, tailored for blood-brain barrier targeting, to reach the brain is dramactically affected by the disease state.* Nanomedicine (Lond.) 2018;13(6):585-594.

ACKNOWLEDGEMENTS

First and foremost, thank you to my supervisor Prof Masserini and co-supervisor Francesca for their endless help, support, suggestions, and teaching over the last 3 years. I have learned so much from both of you and my experience with you has made me more passionate about research.

Thank you to everyone in the lab in Monza, past and present, for their scientific and personal help, including (but not limited to) Simona Mancini, Maria Gregori, Roberta Dal Magro, Beatrice Formicola, Silvia Picciolini, and all of the students who have passed through. I particularly want to thank Silvia Sesana, without whom I probably would not have survived the move to Italy.

Thank you to Rana Edwards, Josu Andrieu, and Geeta for their scientific and personal help, especially in the last year.

Thank you to all of the collaborators I have worked with over the last 3 years, from Milan and beyond, some of whom directly contributed to the work described in this thesis. Thank you to the members of the NABBA consortium, particularly those from Enivroinvest and Prof. Couvreur's group at the University of Paris-Sud, both of which welcomed me with open arms for some incredibly helpful secondments. Thank you also to my tutor, Dr. Mario Salmona, for his guidance.

Thank you to my friends and family, especially my parents for all of their support throughout this PhD. Thank you to Luke for making everything easier.